Energy Education and Research Collaboration EERC

Eleventh Quarterly Report
Phase II
January 1, 2012

Prepared by

Dean Darryll Pines

Principal Investigator and EERC Project Director

Prof. Balakumar Balachandran, Chair

EERC Project Deputy Director

Dr. Azar Nazeri

EERC Research Manager

THE UNIVERSITY OF MARYLAND AND THE PETROLEUM INSTITUTE OF ABU DHABI, UAE

EERC Key Contributors

University of Maryland – College Park, MD, USA

Shapour Azarm
Balakumar Balachandran
David Bigio
H.A. Bruck
Nikil Chopra
Avram Bar-Cohen
Serguei Dessiatoun
Ashwani K. Gupta
Satyandra K. Gupta
Yunho Hwang
P.K. Kannan
Mohammad Modarres
Michael Ohadi
Reinhard Radermacher
Amir Shooshtari

Petroleum Institute – Abu Dhabi, UAE

Youssef Abdel-Majid
Ahmed Al Shoaibi
Ali Almansoori
Mohamed Alshehhi
Ali Elkamel
S.C. Fok
Saleh Al Hashimi
Ebrahim Al-Hajri, Returning ADNOC Scholar
Afshin Goharzadeh
Hamad Karki
Isoroku Kubo
Peter Rodgers
Abdennour Seibi

Table of Contents

Executive Summary

The following is a summary of the major project activities that have taken place over the completed quarter. For more detail, see the individual reports in the last section of this report.

Thrust 1: Energy Recovery and Conversion

Sulfur Recovery from Gas Stream using Flameless and Flame Combustion Reactor
A.K. Gupta, A. Al Shoaibi

- Collected sulfur deposits under different equivalence ratios and from different acid gas compositions (H_2S, CO_2, and N_2) for analysis.
- Analyzed the sulfur deposits captured at different experimental conditions (with CO_2 and N_2) using X-Ray powder diffraction, laser induced breakdown spectroscopy LIBS, and flame spectroscopy. Results did not show substantial differences between the spectra.
- Journal paper, entitled "Fate of sulfur with H_2S injection in methane/air flames," has been accepted for publication in Journal of Applied Energy (November 2011) and is now available online in the journal.

Separate Sensible and Latent Cooling with Solar Energy
R. Radermacher, Y. Hwang, I. Kubo

- Finished the dessicant wheel cycle testing
- Finished the complete cycle (VCC+DWC) testing

Waste Heat Utilization in the Petroleum Industry
R. Radermacher, Y. Hwang, S. Al Hashimi, P. Rodgers

- Used pinch analysis to compare the proposed CCS configuration against the conventional CCS configuration.
- Continued to develop robust optimization technique for solving problems with uncertainty

Thrust 2: Energy-Efficient Transport Process Projects

Multidisciplinary Design and Characterization of Polymer Composite Seawater Heat Exchanger Module
P. Rodgers, A. Bar-Cohen, S.K. Gupta, D. Bigio, H.A. Bruck

- Presented two papers entitled "Polymer Heat Exchangers – An Enabling Technology for Water and Energy Savings" and "Modeling and Validation of Prototype Thermally Enhanced Polymer Heat Exchanger," at the 2011 International Mechanical Engineering Congress & Exposition on November 15th in Denver, Colorado.

- Drafted a press release entitled “3D-Printed Plastic Heat Exchanger” to be distributed by the Department of Mechanical Engineering at the University of Maryland.
- Developed a manufacturability analysis and mold design, through:
- Explicit construction of moldability-based feasibility boundary
- Feature removal for efficient assessment of mold-filling feasibility of finned-plate geometries
- Methodology for measuring fiber orientation.
- Prepared and tested specimens with micro and nanoscale ingredients to study mixing effects in a Twin Screw Extruder to characterize the development of multi-scale structure and associated properties for these novel polymer composites for PHX applications.

Study on Microchannel-Based Absorber/Stripper and Electrostatic Precipitators for CO_2 Separation from Flue Gas

S. Dessiatoun, A. Shooshtari, M. Ohadi, A. Goharzadeh

- Obtained useful kinetic data from batch-scale polymerization with the produced catalyst.
- Initiated experiments in the microchannel reactor.

Microreactors for Oil and Gas Processes Using Microchannel Technologies

S. Dessiatoun, A. Shooshtari, E. Al-Hajri, M. Alshehhi, A. Goharzadeh

- Improved design for large-scale technology demonstrator unit.
- Performed parametric studies and performance characterization of technology demonstrator unit.

Thrust 3: Energy System Management

Integration of Engineering and Business Decisions for Robust Optimization of Petrochemical Systems

S. Azarm, P.K. Kannan, A. Almansoori, A. Elkamel

- Finalized the manuscript for the book chapter in “Multi-Objective Optimization: Techniques and Applications in Chemical Engineering”:
  - Defined and implemented a new objective robustness measure to restrict only downside variation in objective functions
  - Presented two important Robust Multi-Objective Genetic Algorithms (RMOGAs), i.e., a nested approach and a sequential approach
  - Combined an efficient online approximation technique with the two RMOGA approaches and compared them in terms of computational efficiency
- Conducted robust optimization for the newly developed crude oil refinery model and obtained optimal operational variables:
  - Developed a series of crude oil processing modules in Matlab to simulate the crude distillation process.
  - Connected a crude simulation model with a multi-objective optimizer to obtain optimal operational variables
  - Improved the product output and reduced cost in the process in the solutions obtained

Dynamics and Control of Drill Strings

B. Balachandran, H. Karki, Y. Abdelmagid

- Performed experiments on the torsional vibrations of the experimental drill string apparatus. From the Fourier spectra of the torsional vibrations, under whirling conditions, the torsional vibrations occur at the drive speed plus the whirling speed.
- Completed the bottom assembly mechanism on the drill string apparatus.

Studies on Mobile Sensor Platforms

B. Balachandran, N. Chopra, H. Karki, S.C. Fok

- Extended SLAM algorithms to include representation of more complex indoor environments using line based maps.
- Conducted experiment to demonstrate SLAM with a mobile platform by using a laser sensor and encoders for odometry information. Analyzed data.

Development of a Probabilistic Model for Degradation Effects of Corrosion-Fatigue Cracking in Oil and Gas Pipelines

M. Modarres, A. Seibi

Completed the following:

- Classification of the creep models.
- Proposed probabilistic model.
- Development of parameters of the proposed probabilistic model.
- Case study (field application): Estimation of probability of exceedance (PE) on 0.04% strain level.

Introduction

Linda Schmidt Sabbatical at PI

Dr. Linda Schmidt, Associate Professor of Mechanical Engineering at the University of Maryland, has been spending her sabbatical at the Petroleum Institute since September 2011.

Dr. Schmidt originally visited PI in March of 2011 to conduct a series of workshops, including “Enhancing and Assessing Design Project Teamwork,” “Teaching Sketching,” and “Scoping Quality Design Projects.” She also consulted with program administrators and faculty regarding ABET design experience requirements. She was a guest lecturer in several sophomore level design (STEPS) classrooms, where she demonstrated current approaches to brainstorming and sketching and facilitated activities with students.

Because this visit was so successful, Dr. Schmidt was invited to spend a year at PI to help develop curriculum with PI faculty and to lecture in the STEPS course and senior design courses.
Dr. Schmidt spent the fall semester partnering with a STEPS class and senior design class faculty, researching design journaling, and conducting sketching experiments with students in design classes. She also conducted exploratory meetings with PI alumni working at ADNOC companies on activities to bridge student classroom skills with professional workplace tasks.

In the spring semester, Dr. Schmidt is continuing the educational projects she started in the fall, including administering a Senior Design Course survey and co-organizing a “Design Day” at the end of the semester. She is also hoping to conduct an anonymous, online survey of all faculty of senior design teams to determine ways to further fine-tune the design curriculum.

In addition, she is working on several research projects. With Dr. Caroline Brandt, she is researching student attitudes toward thinking and learning. She is also working on a study on peer evaluation with Dr. Jaby Mohammad. This study explores the cultural reasons behind student behavior and the ways students are influenced by their relationships. She also plans to explore new research possibilities with ADNOC operating companies on design and engineering decision-making.

Ben Brooke Jump-starts Petroleum Institute Baja SAE Program

Ben Brooke arrived at the Petroleum Institute (PI) in October 2011 to build a Baja SAE program at PI. In this program, students design, build, and race a small off-road vehicle that can survive rough terrain and environmental conditions. The Baja SAE teams participate in international competitions that simulate the process of bringing a new product to the industrial market.

Ben graduated in 2011 from the honors program of the University of Maryland’s Department of Mechanical Engineering, with a concentration on Vehicle Dynamics. He is the recipient of many awards and honors, including a Northrop Grumman Scholarship, the Society of Automotive Engineers Senior Award, the Department of Mechanical Engineering Chairman’s Award, and the Department of Mechanical Engineering Chair’s Award for Leadership. Ben was involved as a project manager or lead machinist in many projects during his undergraduate years, including as project manager for the University of Maryland's Formula SAE team. In this project, Ben led thirty undergraduate students as they designed, fabricated and raced an open wheel, Formula-style race car for the Formula SAE international competition, against 120 other college teams. Under his leadership, the UMD team took fourth place out of sixty competitors.

The University of Maryland sent the 2007 Terps Baja vehicle to PI in the summer of 2011, to be used in the Baja program at PI. When Ben arrived at PI in October, he was pleased to find that the Mechanical Engineering department at PI, and Dr. Nader Vadani, who is running the Baja SAE program, had already taken significant steps to set up the program and had provided the team with a spacious meeting room as well as access to machining and fabrication equipment. During the past fall semester, Ben taught an introductory course on vehicle fundamentals to fifteen students and assigned the students the task of analyzing the strengths and weaknesses of the 2007 Terps Racing Baja vehicle and identifying areas for improvement. He also started working with the students on an individual basis to develop the fabrication skills necessary to build a Baja SAE vehicle. Meanwhile, he has been engaged in procuring the specialized equipment needed for this project as well as the material needed to complete the Baja SAE vehicle itself.

This semester Ben will train the students to become self-sufficient and drive each other to make informed design decisions that will help them complete their project on time and independently. During the spring semester of 2012 he will task the students with the design of individual components on the Baja SAE vehicle and fabrication of these parts in order to complete the vehicle by the end of the semester. His meetings with students will begin to trend away from lessons on vehicle dynamics towards lessons on running design meetings themselves and setting specific deadlines for goals that have to be met in order to complete their inaugural vehicle.

Ben and Dr. Vahdati plan to travel to the United States with a team of PI students to attend a Baja SAE competition in June.

Individual Project Reports

Thrust 1
Energy Recovery and Conversion Projects

Sulfur Recovery from Gas Stream using Flameless and Flame Combustion Reactor

UMD Investigators: **Ashwani K. Gupta**
GRA: **Hatem Selim**
PI Investigators: **Ahmed Al Shoaibi**
Start Date: **October 2006**

1. Objectives / Abstract

The main objective is to obtain fundamental information on the thermal process of sulfur recovery from sour gas by conventional flame combustion as well as flameless combustion, using numerical and experimental studies. Our ultimate goal is to determine optimal operating conditions for enhanced sulfur conversion. Therefore, an experimental study of the flameless combustion processes of the Claus furnace is proposed so that the results can be used in the normal flame process for determining improved performance. In this study we explored different operating conditions and performed in-flame and exhaust gas analyses under both flame and flameless modes of reactor operation. This will provide better understanding of the process with the goal of attaining enhanced sulfur capture efficiency.

Specific objectives are to provide:

- A comprehensive literature review of the existing flame combustion process for sulfur removal with special reference to sulfur chemistry
- Near isothermal reactor conditions and how such conditions assist in the enhanced sulfur recovery process
- CFD simulation of the flame and flameless combustion in the furnace.
- Determination of the chemical kinetics and the major reaction pathways to seek for high performance
- Design of a reactor for experimental verification of the numerical results
- Measurements and characterization of the combustion furnace under various conditions, including the conditions that utilize high temperature air combustion principles for flameless combustion
- Experiments with different sulfur content gas streams using the flame and flameless combustion furnace modes of operation.
- Installation of the appropriate diagnostics for quantification of stable and intermediate sulfur compounds in the process and exit stream
- Flow, thermal and chemical speciation characteristics of the reactor
- Product gas stream characteristics and evaluation of sulfur recovery and performance in the process

2. Deliverables

- Collect sulfur deposits under different equivalence ratios and from different acid gas compositions (H_2S, CO_2, and N_2) for analysis

- Analyze the sulfur deposits captured at different experimental conditions (with CO_2 and N_2) using x-ray powder diffraction, laser induced breakdown spectroscopy LIBS, and flame spectroscopy
- Journal paper "Fate of sulfur with H_2S injection in methane/air flames," has been accepted for publication in Journal of Applied Energy (November 2011) and is now available online in the journal

3. Executive Summary

During the reported quarter, progress continued with major focus on the experimental part of the project. Sulfur deposits formed during experiments were collected at different equivalence ratios under different acid gas compositions (H_2S, CO_2, and N_2).

The collected samples were analyzed using different techniques. The techniques used were x-ray powder diffraction, laser induced breakdown spectroscopy (LIBS), and flame spectroscopy. The experimental setup was modified to examine sulfur deposits using the flame spectroscopy. Sulfur deposits were burned using combustion products of hydrogen/air flame. A honeycomb was used to introduce the hot combustion products of H_2/air flame onto the sulfur chunks. Excited species emissions were introduced into a spectrometer using a fiber optic cable. A seven-channel spectrometer was used to implement LIBS experiments on the sulfur deposits. This provided higher resolution than otherwise could be achieved.

A journal paper entitled "Fate of sulfur with H_2S injection in methane/air flames" was submitted to The Journal of Applied Energy. This paper has been accepted for publication (November 2011) and is now available online at the journal website.

4. Progress

4.1 Formation of sulfur deposits

Sulfur deposits were formed from different gas compositions. Reactor housing was used as the sulfur collector. Figure 1 shows how sulfur deposits were formed and collected into the reactor housing.

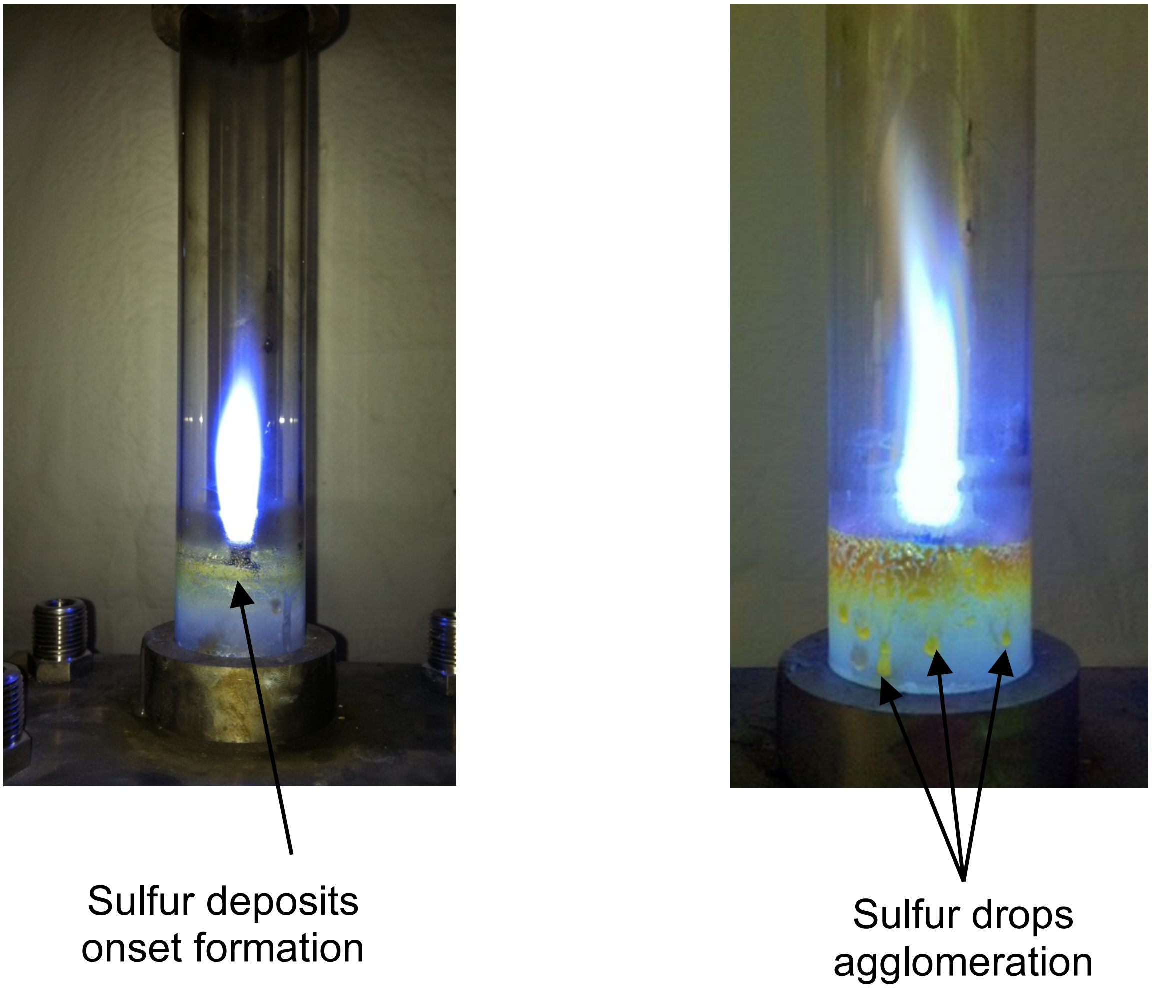

Figure 1. Formation of sulfur deposits and precipitation in reactor housing.

4.1.1 Sulfur deposits formed under different equivalence ratios

Sulfur deposits were collected under Claus conditions as well as stoichiometric combustion conditions. Reaction conditions were as follows:

Claus conditions

H_2S flow rate: 0.7 lit/min
O_2 flow rate: 0.35 lit/min

Stoichiometric conditions

H_2S flow rate: 0.7 lit/min
O_2 flow rate: 1.05 lit/min

Figures 2 and 3 show the captured sulfur deposits under stoichiometric conditions and Claus conditions, respectively. The experiment lasted for 125 minutes under stoichiometric conditions. However, the Claus conditions experiments lasted for 50 minutes. This is attributed to the depletion of sulfur formed under stoichiometric conditions as compared to Claus conditions.

Figure 2. Collected sulfur deposits Stoichiometric conditions Experiment time: 2 hr, 5 min.

Figure 3. Collected sulfur deposits Claus conditions Experiment time: 50min.

An x-ray powder diffraction experiment was conducted on both the sulfur samples collected. The results revealed that both the sulfur deposits samples gave nearly the same diffractograms. Therefore it can be inferred that sulfur deposits formed were not affected significantly by the equivalence ratios. Figure 4 shows diffractograms of both the samples as well as diffractogram of sulfur (S_8) obtained from the literature.

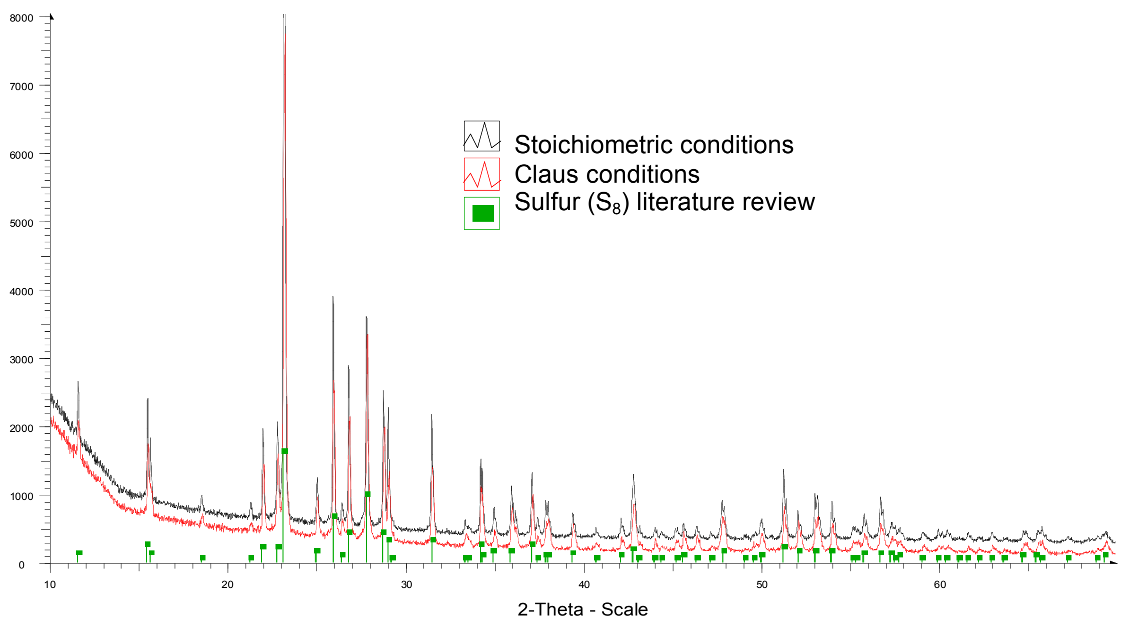

Figure 4. Diffractogram of different sulfur samples and that from the literature on S_8.

Laser breakdown induced spectroscopy (LIBS) was also conducted on the captured sulfur deposits. Figure 5 shows the seven-channel spectrometer used for the LIBS experiments. The results obtained did not show any significant differences between the obtained spectra. Figures 6 and 7 show the LIBS spectra of sulfur deposits collected under stoichiometric conditions and Claus conditions, respectively.

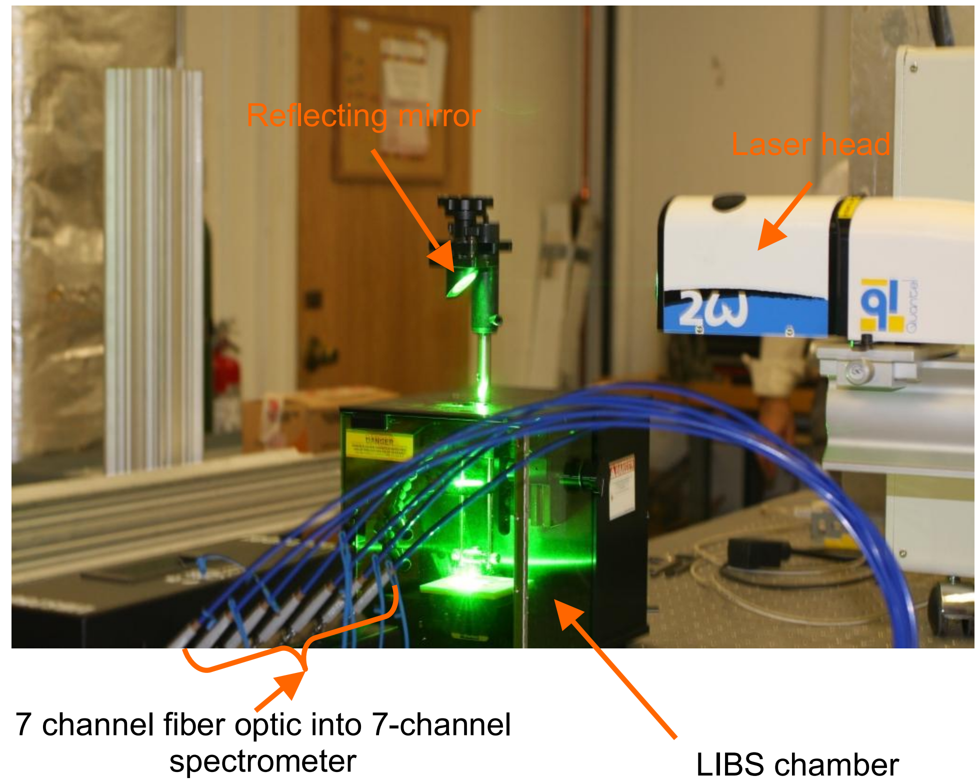

Figure 5. Seven-channel spectrometer used for laser induced breakdown spectroscopy (LIBS).

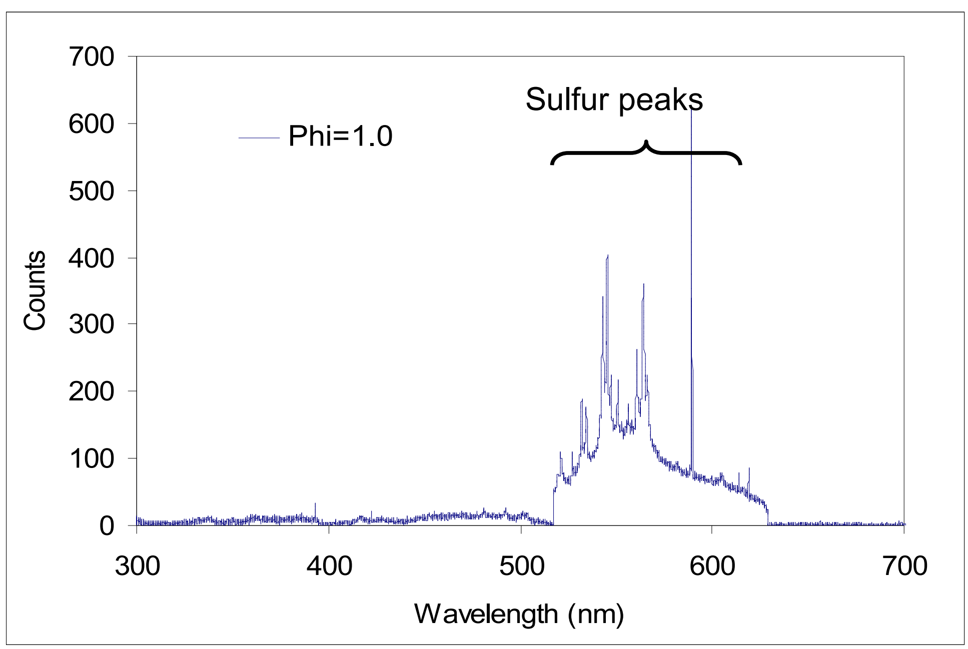

Figure 6. Emission spectra of sulfur deposits collected at stoichiometric conditions.

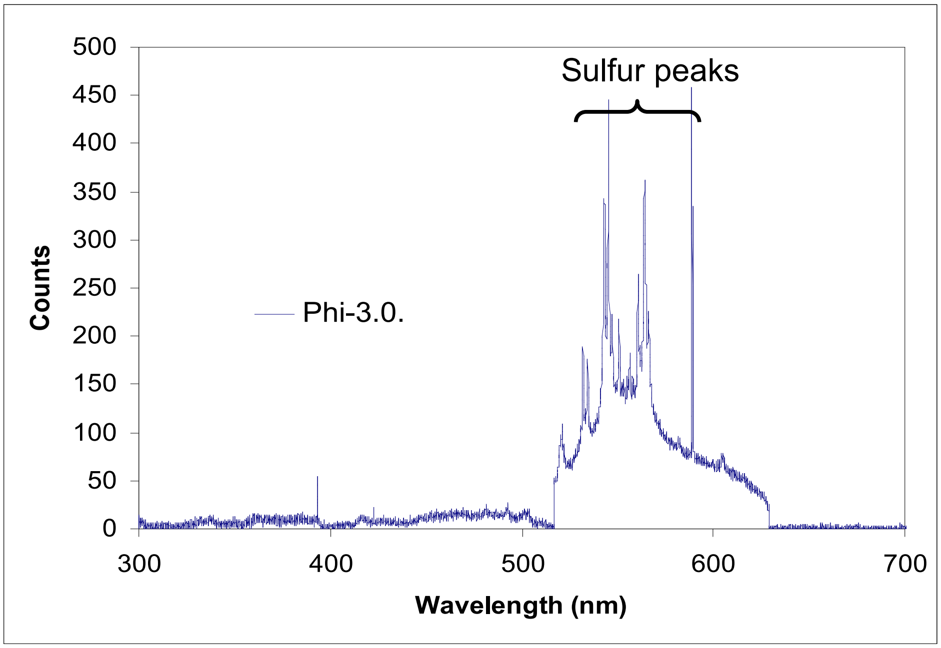

Figure 7. Emission spectra of sulfur deposits collected at Claus conditions.

4.1.2 Sulfur deposits formed from different acid gas compositions

Investigations on the sulfur deposits collected from different acid gas compositions were conducted using flame spectroscopy. Acid gas composition varied as 100% H_2S, 70% H_2S+30% CO_2, and 70% H_2S+30% N_2. Sulfur deposits were combusted using hot combustion products of H_2/air flame. A honeycomb was used to channel the hot gases onto the sulfur deposits. Excited species emissions were introduced into spectrometer using a fiber optic cable. Figure 8 shows a schematic of the experimental setup. Figure 9 shows a photograph of the hot gas of H_2/air flame introduced into the honeycomb as well as the subsequent flame color produced from the burning of sulfur. Results revealed that emission spectra are indeed from excited sulfur emissions (S_2). In addition, the spectra did not show distinct peaks of any other contaminants including carbon or nitrogen. These results do not decisively support that sulfur deposits do not include other contaminants. Figures 10 to 18 show the emissions spectra of sulfur deposits obtained from different acid gas compositions. This requires further examination using some other diagnostics.

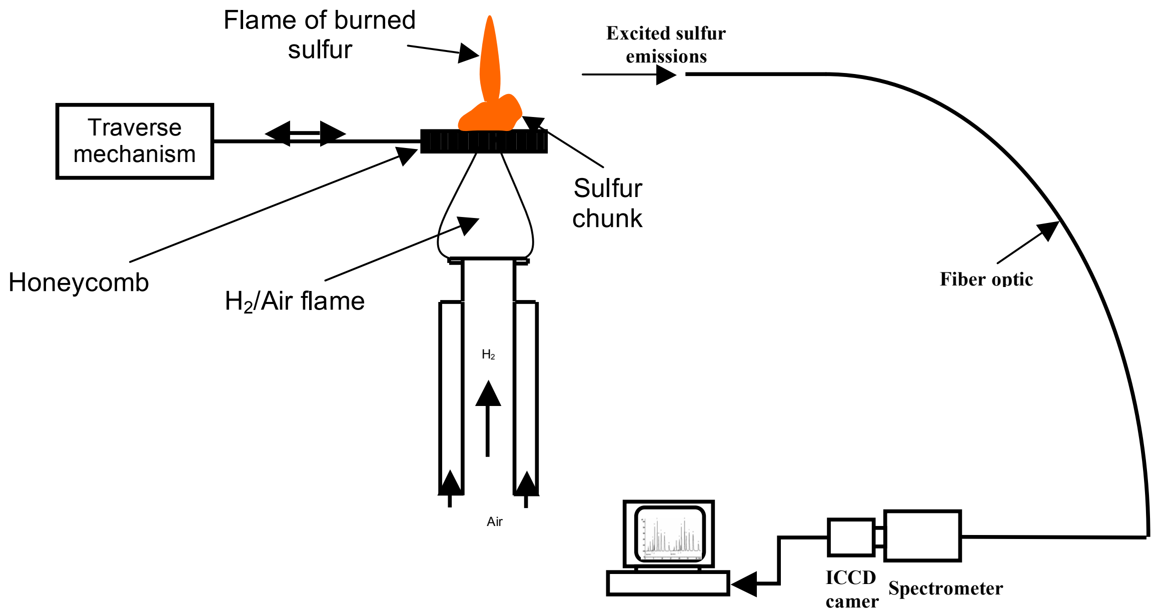

Figure 8. A schematic diagram of the experimental setup used for flame spectroscopy experiments.

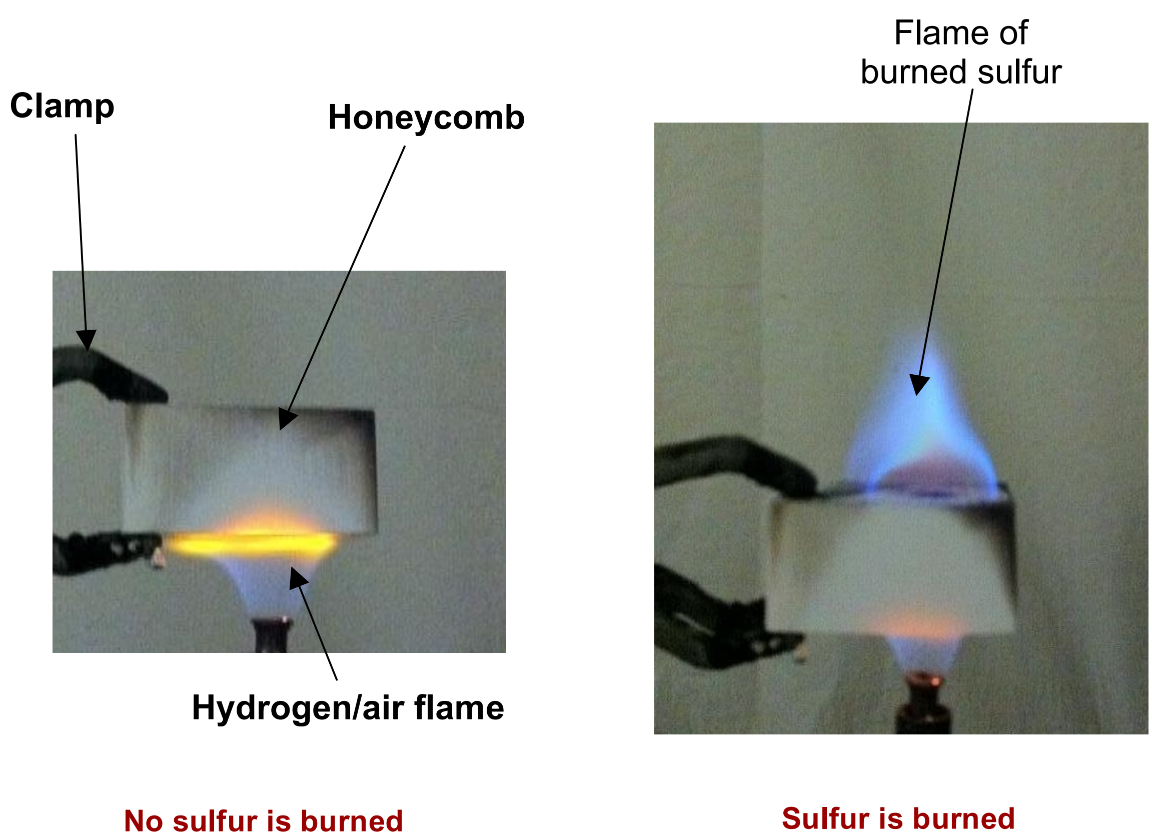

Figure 9. Photograph of hydrogen air flame and combustion of sulfur on a honeycomb placed in the flow path of hot gases.

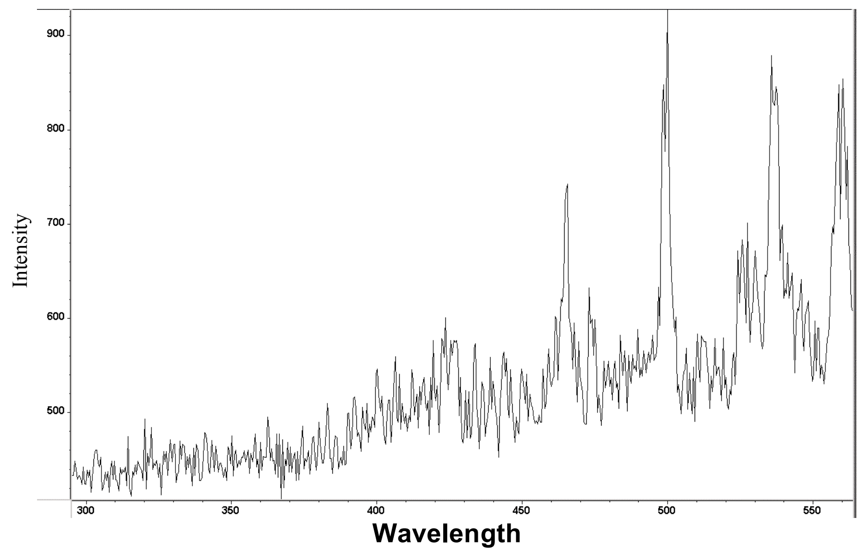

Figure 10. Emission spectra of sulfur deposits, acid gas stream (H_2S), wavelength (300-560 nm).

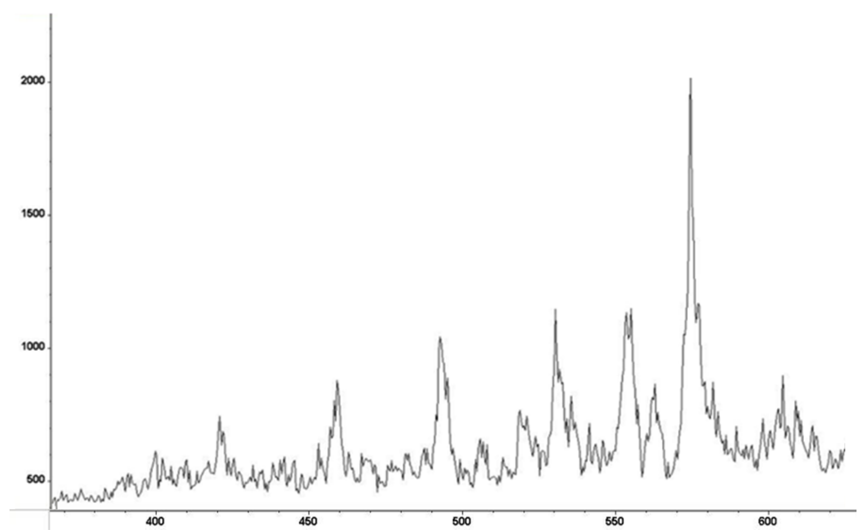

Figure 11. Emission spectra of sulfur deposits, acid gas stream (H_2S), wavelength (370-630 nm).

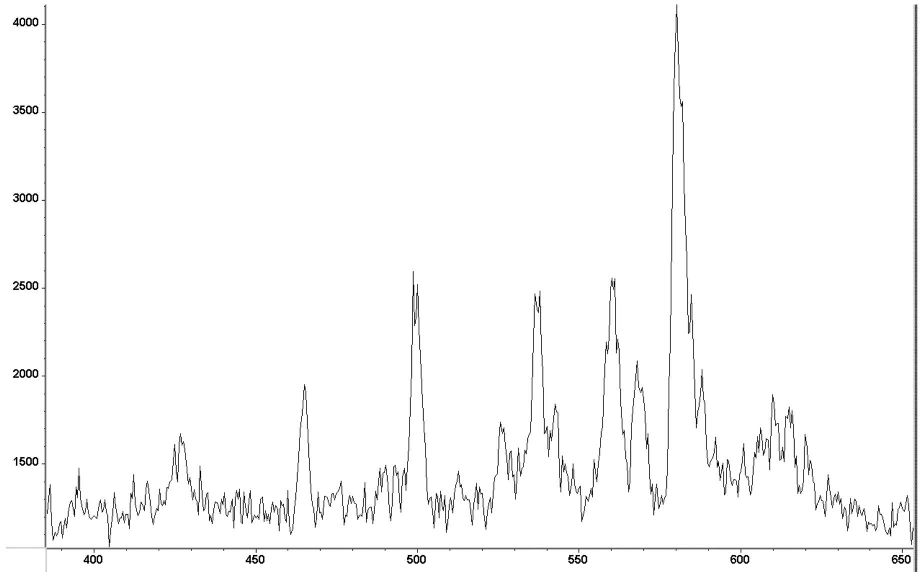

Figure 12. Emission spectra of sulfur deposits, acid gas stream (H_2S), wavelength (390-650 nm).

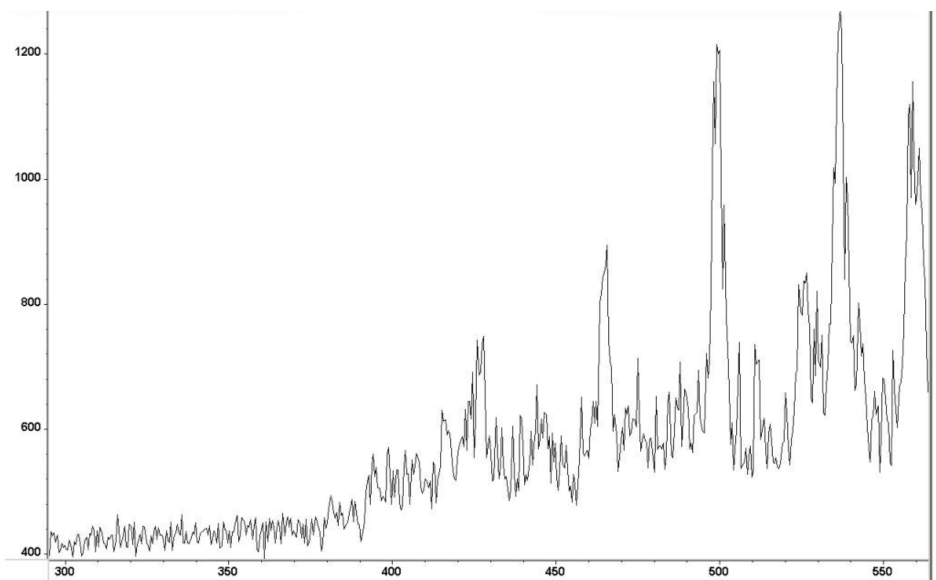

Figure 13. Emission spectra of sulfur deposits, acid gas stream (H_2S+CO_2), wavelength (300-560nm).

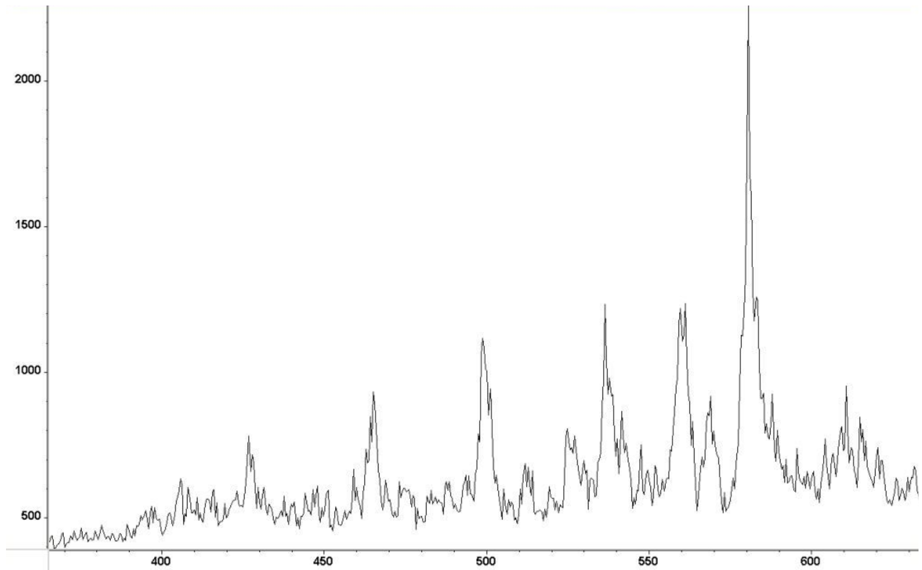

Figure 14. Emission spectra of sulfur deposits, acid gas stream (H_2S+CO_2), wavelength (370-630nm).

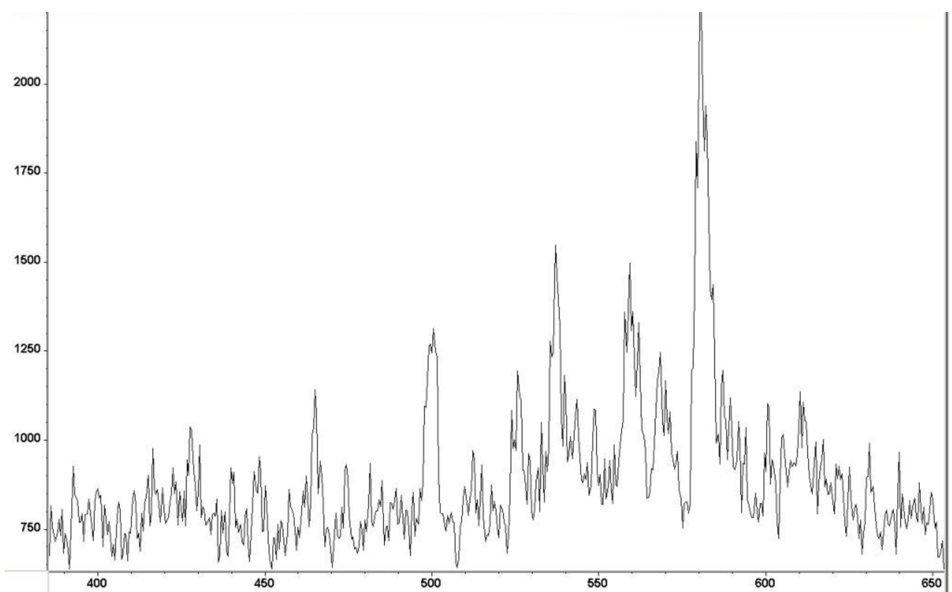

Figure 15. Emission spectra of sulfur deposits, acid gas stream (H_2S+CO_2), wavelength (390-650nm).

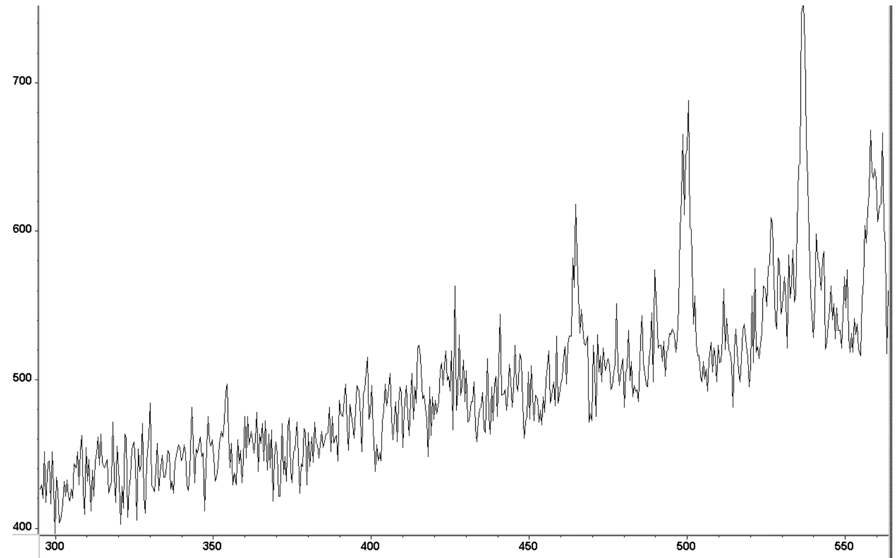

Figure 16. Emission spectra of sulfur deposits, acid gas stream (H_2S+N_2), wavelength (300-560nm).

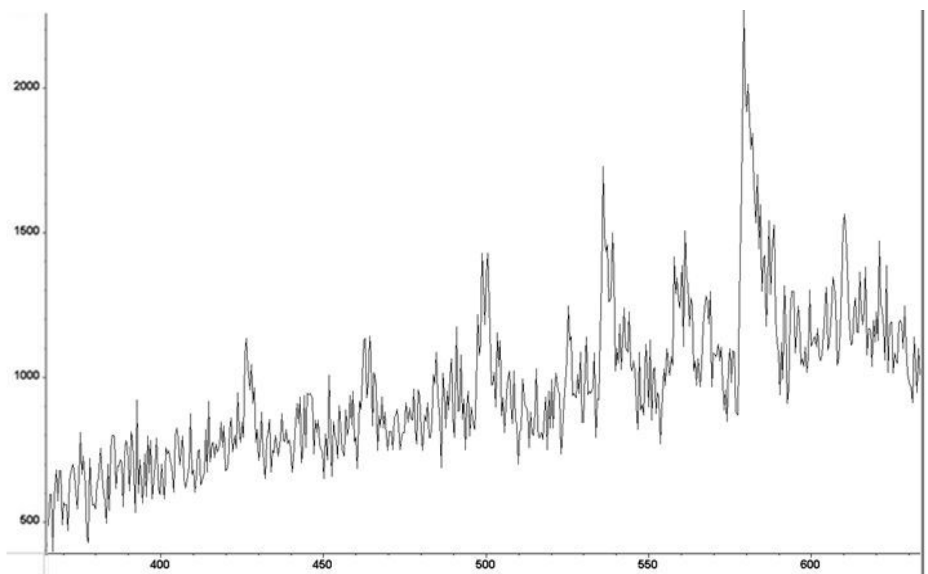

Figure 17. Emission spectra of sulfur deposits, acid gas stream (H_2S+N_2), wavelength (370-630nm).

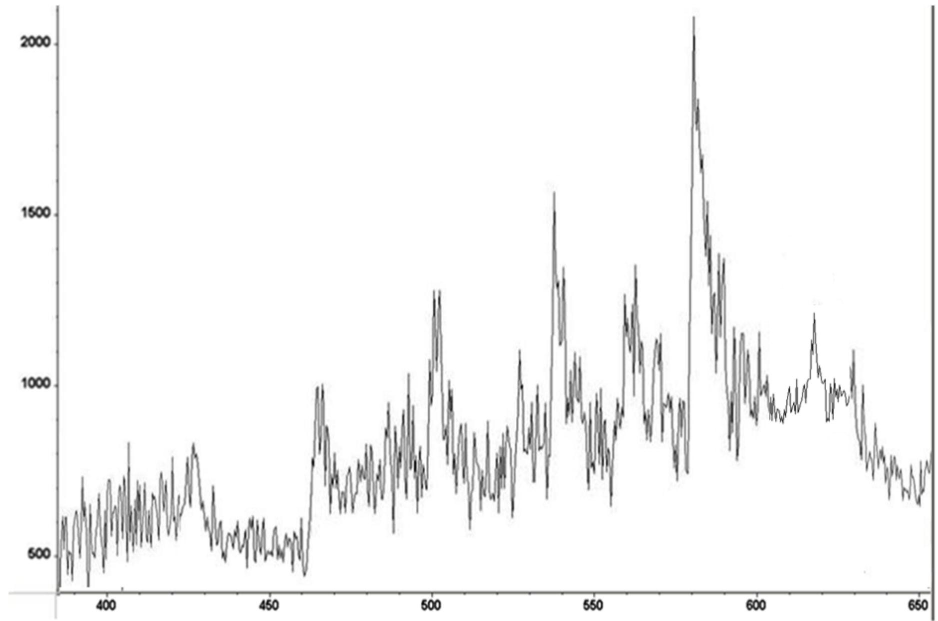

Figure 18. Emission spectra of sulfur deposits, acid gas stream (H_2S+N_2), wavelength (390-650nm).

4.2 Write technical papers

During the past quarter we submitted a rebuttal of the paper named "Fate of Sulfur with H_2S Injection in Methane/Air Flames." The paper was accepted for publication (November 2011) and is now available online at the journal website.

5. Summary

During the reported quarter, progress continued with major focus on the experimental part of the project. Sulfur deposits formed during experiments were collected under different equivalence ratios and from different acid gas compositions (H_2S, CO_2, and N_2). The collected samples were analyzed using selected techniques available. These techniques were x-ray powder diffraction, laser induced breakdown spectroscopy (LIBS) and flame spectroscopy. The experimental setup was further modified to examine the sulfur deposits using flame spectroscopy. Sulfur deposits were combusted using hot combustion products from a hydrogen/air flame. A honeycomb was used to introduce the hot combustion products of H_2/air flame onto the sulfur chunks. The excited emissions species from the test region from the combustion of sulfur were introduced into a spectrometer using a fiber optic cable. A seven-channel spectrometer was used to implement LIBS experiments onto sulfur deposits. The results did not show substantial differences in spectra on the collected samples, although some small differences could be observed. Further investigations are required to determine succinct differences amongst the collected sulfur. A journal paper was submitted to The Journal of Applied Energy titled "Fate of sulfur with H_2S injection in methane/air flames." The paper has been accepted for publication (November 2011) and is now available online at the journal website.

6. References

None

7. Difficulties Encountered/Overcome

None

8. Deliverables for the Next Quarter

- Further examination of sulfur deposits using different techniques
- Preparation of the experimental setup for near-isothermal examination of Claus reactions
- Preliminary results of near-isothermal Claus process reactions

9. Publications

Conference Publications

1. Gupta, A. K. and Sassi, M. "Sulfur Recovery from Acid Gas Using the Claus Process and High Temperature Air Combustion Technology," American J. of Environmental Sciences, Vol. 4, No. 5, 2008, pp. 502-511.
2. Selim, H., Gupta, A. K. and Sassi, M. "Variation of Optimum Claus Reactor temperature with Acid Gas Composition," IECEC Conference, Cleveland, OH, July 28-30, 2008, Paper No. AIAA-2008-5797.
3. Selim, H., Gupta, A. K. and Sassi, M. "Reduced Mechanism for Hydrogen Sulfide Oxidation," 47th AIAA Aerospace Sciences Conference, Orlando, FL, January 5-8, 2009, Paper No. AIAA-2009-1392.
4. Selim, H. and Gupta, A. K. "Nonreactive Study for the Reactants Mixing in Claus Reactions," 7th Intl. Energy Conversion Engineering Conference (7th IECEC), Denver, CO, August 2-5, 2009, Paper No. AIAA-2009-4506.
5. Selim, H, Gupta, A. K. and Sassi, M. "Implementation of Novel Error Propagation Based Reduction Approach in H_2S/O_2 Reaction Mechanism," 48th AIAA Aerospace Sciences Conference, Orlando, FL, January 3-7, 2010, Paper AIAA-2010-1355.
6. Al Amoodi, N., Selim, H., Gupta, A. K., Sassi, M. and Al Shoaibi, A. "Numerical Simulations of the Thermal Stage in Claus Process: Equilibrium and Kinetic Investigation," 48th AIAA Aerospace Sciences Conference, Orlando, FL, January 3-7, 2010, AIAA-2010-1356.
7. Selim, H. Vijayan, V., Al Shoaibi, A., and Gupta, A. K., "Numerical and Experimental Studies on Mixing and Product Species Distribution in a Claus Reactor," 8th Intl. Energy Conversion Engineering Conference (8th IECEC), Nashville, TN, August 2-5, 2010, Paper No. AIAA-2010-7183.
8. Selim, H, Al Shoaibi, A., and Gupta, A. K., "Examination of Emission Spectra from Hydrogen Sulfide Flames," 49th AIAA Aerospace Sciences Conference, Orlando, FL, January 4-7, 2011, AIAA-2011-440.
9. Selim, H, Al Shoaibi, A., and Gupta, A. K., "Spatial Speciation of H_2S Combustion in Methane/Air Flame," To be submitted to 9th International Energy Conversion Engineering Conference (9th IECEC), San Diego, CA, July 31-August 3, 2011.
10. Selim, H, Al Shoaibi, A., and Gupta, A. K., "Effect of CO_2 and N_2 Presence in Acid Gas stream on H_2S Combustion," 50th AIAA Aerospace Sciences Conference, Nashville, TN, January 9-12, 2012.

Journal Publications

1. Selim H et al. Novel error propagation approach for reducing H_2S/O_2 reaction mechanism. Appl Energy (2011), doi:10.1016/j.apenergy. 2011.01.047.
2. Selim, H., Al Shoaibi, A., Gupta, A. K., "Effect of H_2S in methane/air flames on sulfur chemistry and products speciation," The Journal of Applied Energy, Vol. 88, Issue 8, August 2001, pp. 2593-2600.
3. Selim, H., Al Shoaibi, A., Gupta, A. K., "Experimental examination of flame chemistry in hydrogen sulfide-based flames," The Journal of Applied Energy, Vol. 88, Issue 8, August 2001, pp. 2601-2611.

4. Selim, H., Al Shoaibi, A., Gupta, A. K., "Fate of Sulfur with H_2S Injection in Methane/Air Flames," The Journal of Applied Energy, Vol. 92, April 2012, pp. 57-64.

Appendix

Justification and Background

Hydrogen sulfide is present in numerous gaseous waste streams from natural gas plants, oil refineries, and wastewater treatment plants, among other processes. These streams usually also contain carbon dioxide, water vapor, trace quantities of hydrocarbons, sulfur, and ammonia. Waste gases with ammonia are called sour gases, while those without ammonia are called acid gases. Sulfur must be recovered from these waste streams before flaring them. Sulfur recovery from sour or acid gas typically involves application of the well-known Claus process, using the reaction between hydrogen sulfide and sulfur dioxide (produced at the Claus process furnace from the combustion of H_2S with air and/or oxygen), yielding elemental sulfur and water vapor: $2H_2S(g) + SO_2(g) = (3/n)\ S_n(g) + 2H_2O(g)$ with $\Delta H_r = -108$ kJ/mol. Therefore, higher conversions for this exothermic, equilibrium-limited reaction call for low temperatures, which lead to low reaction rates that dictate the use of a catalyst. The catalytic conversion is usually carried out in a multistage, fixed-bed, adsorptive reactor process, which counteracts the severe equilibrium limitations at high conversions. This technology process can convert about 96% to 97% of the influent sulfur in H_2S to S. However, higher removal requires critical examination of the process and use of a near isothermal reactor, since the conversion is critically dependent upon the exothermic and endothermic conditions of the reactions.

Flameless combustion has been shown to provide uniform thermal field in the reactor so that the reactor temperature is near uniform. Reactor size can also be reduced and combustion-generated pollutants emissions can be reduced by up to 50%. Energy efficiency can be increased by up to 30%. The application of this technology appears to offer great advantages for the processes under consideration. The UAE, which pumps about 2.4 million bpd of crude oil, is also home to the world’s fifth biggest gas reserves at about 200 trillion cubic feet. Abu Dhabi Gas Industries (GASCO), an operating company of the Abu Dhabi National Oil Company (ADNOC), is leading a drive to boost gas production in the UAE from five to seven billion cubic feet per day. This calls for sulfur recovery capacity of over 3,000 metric tons per day with the associated SOx and NOx emissions. Therefore, the adoption and further development of flameless combustion technology for sulfur recovery among other commercial and industrial heating processes is expected to be crucial and beneficial, both economically and environmentally.

The conventional sulfur recovery process is based upon the withdrawal of sulfur by in situ condensation within the reactor. The selective removal of water should, however, be a far more effective technique, as its effect on the equilibrium composition in the mass action equation is much greater. The in situ combination of the heterogeneously catalyzed Claus reaction and an adsorptive water separation seems especially promising, as both reaction and adsorption exhibit similar kinetics, and pressure can be adapted to the needs of the adsorptive separation. Such an adsorptive reactor will lead to almost complete conversion as long as the adsorption capacity is not exhausted. There are numerous possibilities for implementing these two functions, ranging from fixed-beds with homogeneous catalyst/adsorbent mixtures to spatially structured distributions or even fluidized beds. Most of the previous studies have concentrated on the Claus catalytic conversion reactors and the TGTU. However, some previous studies have identified the Claus furnace as one of the most important yet least understood parts of the modified Claus process. The furnace is where the combustion reaction and the initial sulfur conversion (through an endothermic gaseous reaction) take place. It is also where the SO_2 required by the downstream catalytic stages is produced and the contaminants (such as ammonia and BTX (benzene, toluene, xylene) are supposedly destroyed. The main two reactions in the Claus furnace are: $H_2S + 3/2\ O_2 = SO_2 + H_2O$, with $\Delta H_r = -518$ kJ/mol, and $2H_2S + SO_2 = 3/2\ S_2 + 2H_2O$, with $\Delta H_r = +47$ kJ/mol. This last endothermic reaction is responsible for up to 67% conversion of the sulfur at about 1200 °C. Moreover, many side reactions take place in the furnace; these side reactions reduce sulfur recovery and/or produce unwanted components that end up as ambient pollutant emissions. Therefore, it would be useful to combine the endothermic and exothermic process using an isothermal reactor offered by flameless oxidation combustion.

Approach

Critical review

We propose to conduct a critical review of the various approaches used for sulfur removal from the sour gas. The emphasis here will be on sulfur chemistry with due consideration to the fate of ammonia. Following the review, an experimental and a CFD numerical study of the flameless oxidation of the fuel will be conducted as follows:

CFD simulation

A numerical simulation study of the flame under normal and flameless oxidation of fuels in the furnace will be conducted using the available codes. Global features of the flow and thermal behavior will be obtained using the Fluent CFD and Chemkin computer codes. These codes provide detailed simulation of the flow, thermal and chemical behaviors (i.e., detailed chemistry) in the reactor flow using gas-phase reactants. The sulfur in the fuel is in gas phase, so we will be able to simulate and monitor the fate of sulfur during various stages of endothermic and exothermic reactions and over a range of temperature regimes, including those covered in the Claus furnace process. The simulation results will also guide the final design of the flameless furnace. The simulations will also help assist in the experimental program for data validation with the eventual goal of implementing the process for sulfur removal.

Experimental study

An experimental study of the flameless vs. normal flame combustion process for the conditions examined in the theoretical study, including that of Claus furnace, will be conducted. We will explore the operating conditions and the exhaust gas analysis under conditions of both flame and flameless modes to determine the extent of sulfur conversion under the two conditions over the temperatures that can simulate endothermic and exothermic conditions in the Claus furnace. The goal is to seek conditions that yield the highest sulfur recovery from a process. To some extent, these conditions will be based on the composition of the acid/sour gas, from sulfur-rich (> 50% H_2S) to lean (< 20% H_2S). It is expected that our fundamental information will contribute to the eventual design guidelines of an advanced sulfur recovery process furnace operating under flameless combustion mode.

Separate Sensible and Latent Cooling with Solar Energy

UMD Investigators: **Reinhard Radermacher, Yunho Hwang**
GRA: **Ali Al-Alili**
PI Investigator: **Isoroku Kubo**
Start Date: **August 2007**

1. Objective/Abstract

The main objective of this project is to design, fabricate and test a solar cooling system with the highest possible cooling COP measured to date. The approach involves combining a very efficient concentrating PV-T collector with separate sensible and latent cooling approach developed at CEEE. This solar cooling system is expected to operate under the UAE's harsh climate conditions.

2. Deliverables for the Completed Quarter

These are the accomplished tasks:

- Finished the desiccant wheel cycle testing
- Finished the complete cycle (VCC+DWC) testing

3. Summary of Project Activities for the Completed Quarter

The focus of this quarter was to complete the desiccant wheel cycle testing and start the whole hybrid A/C testing. The effect of the process air stream's inlet conditions, the regeneration temperature and the rotational speed were investigated in the former test. The later test investigated these variables' effect on the conditioned space when the desiccant wheel cycle was coupled with a vapor compression cycle.

3.1 Desiccant Wheel Cycle Testing

The testing matrix is shown in Table 1.

Table 1. Desiccant wheel cycle testing matrix

T_amb	w_amb	mdot_air	T_gen	R_speed	Run
oC	gw/kga	kga/s	oC	RPH	#
25	16.2	0.085	55	5,10,15,20,25,30,35,40,45,50	10
30	16.2	0.085	55	5,10,15,20,25,30,35,40,45,50	10
35	16.2	0.085	55	5,10,15,20,25,30,35,40,45,50	10
30	20	0.085	55	5,10,15,20,25,30,35,40,45,50	10
30	14	0.085	55	5,10,15,20,25,30,35,40,45,50	10
30	16.2	0.1	55	5,10,15,20,25,30,35,40,45,50	10
30	16.2	0.085	45,65	5,10,15,20,25,30,35,40,45,50	20

The testing was carried out under ARI's humid weather conditions. The following performance indices were used:

- Moisture Removal Capacity (MRC)

$$MRC = \dot{m_1} \Delta x_{1,2}$$

- Moisture Mass Balance (MMB)

$$MMB = \frac{\dot{m_1} \Delta x_{1,2}}{\dot{m_9} \Delta x_{8,9}}$$

- Total Energy Balance (TEB)

$$TEB = \frac{\dot{m_1} \Delta h_{1,2}}{\dot{m_9} \Delta h_{8,9}}$$

- Latent Coefficient of Performance (COP_{Lat})

$$COP_{Lat} = \frac{\dot{m_1} h_{fg} \Delta x_{1,2}}{\dot{m_9} \Delta h_{7,8}}$$

The MRC and the COP_{lat} as a function of the wheel rotational speed are shown in Figure 1. As the ambient temperature increases, both the MRC and the COP_{lat} decreases.

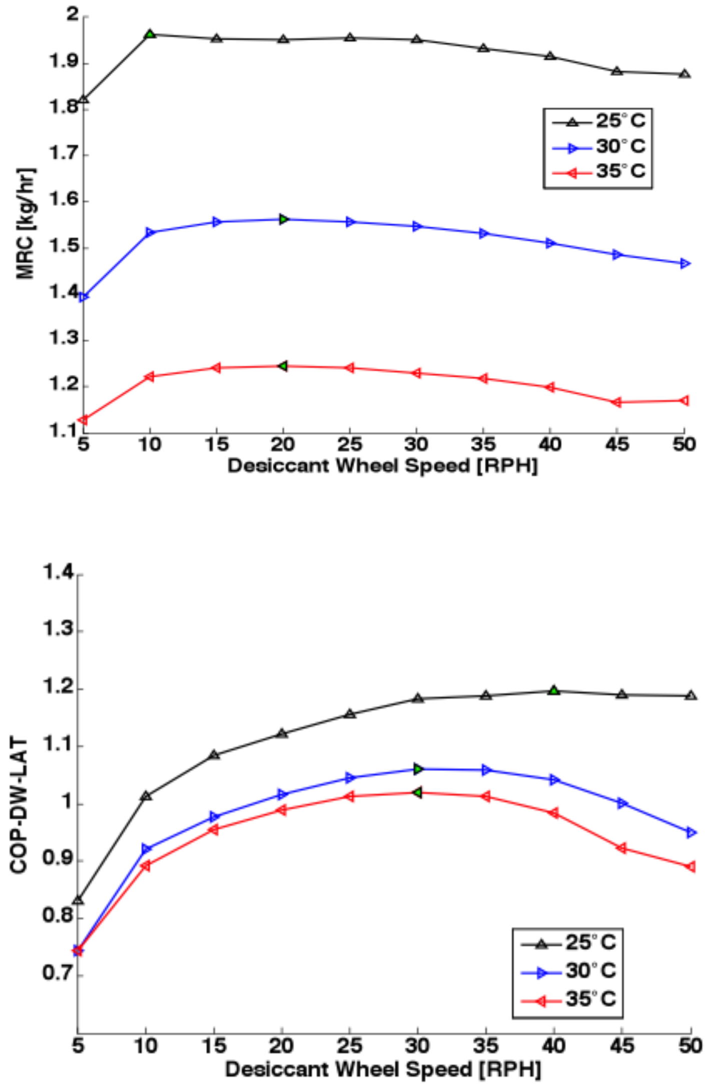

Figure 1. MRC (top) and COP_{lat} (bottom) at different ambient temperatures.

The MRC and the COP_{lat} as a function of the wheel rotational speed for different ambient humidity ratio are shown in Figure 2. As the ambient humidity ratio increases, both the MRC and the COP_{lat} increase.

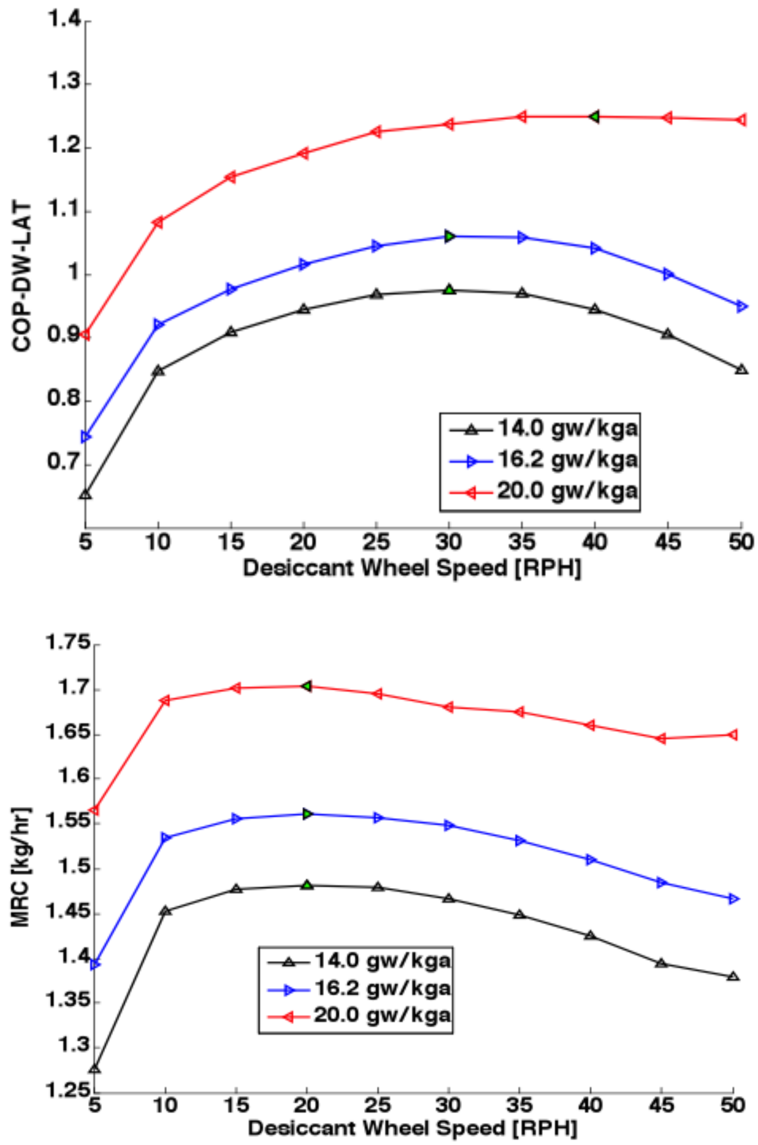

Figure 2. MRC (top) and COP_{lat} (bottom) at different ambient humidity ratios.

The MRC and the COP_{lat} as a function of the wheel rotational speed for different ventilation rate are shown in Figure 3.

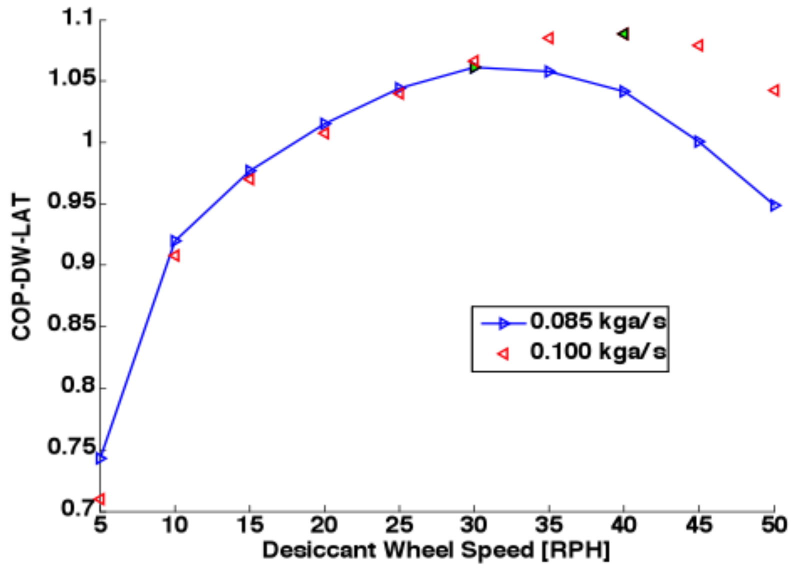

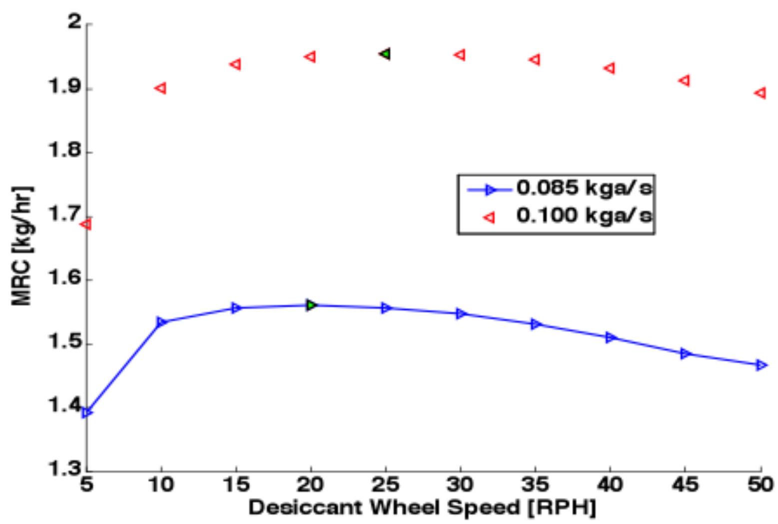

Figure 3. MRC (top) and COP_{lat} (bottom) at different ventilation flow rates

The MRC and the COP_{lat} as a function of the wheel rotational speed for regeneration temperatures are shown in Figure 4.

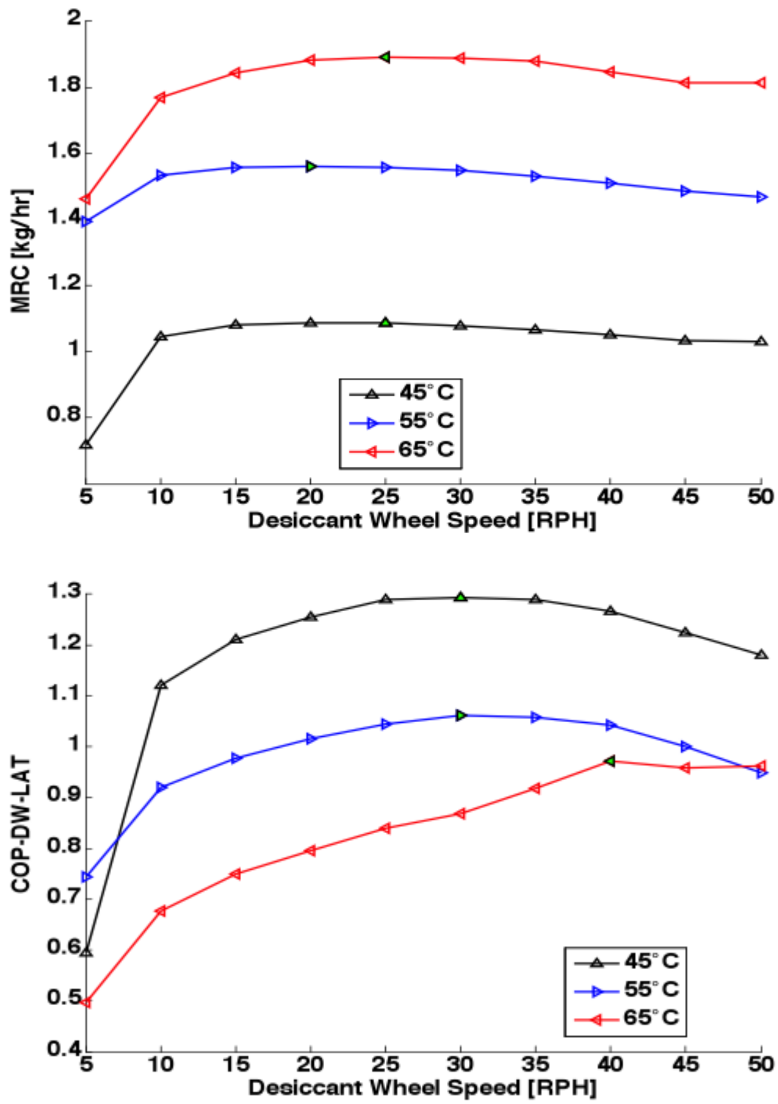

Figure 4. MRC and COP_{lat} at different regeneration temperatures.

Figure 5 shows the moisture mass balance, which should be maintained within 5% based on ASHRAE standards. It also shows the total energy balance of the desiccant wheel. The goal is to maintain the energy balance within 10%. However, the figure shows that this limit is exceeded at lower rotational speeds. The reason is that the lower rotational speeds allow more time for heat to be lost from the circumference of the wheel.

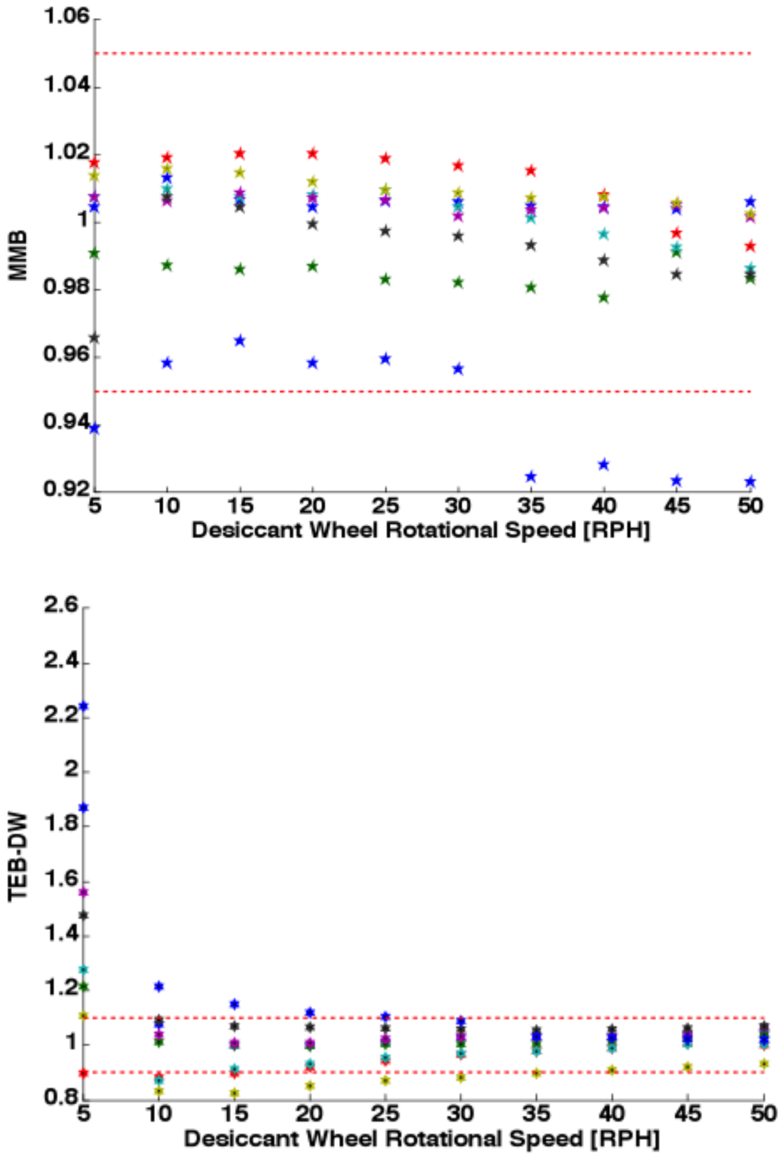

Figure 5. MMB (top) and TEB (bottom) of the desiccant wheel.

3.2 The hybrid system testing

The purpose of this testing is to investigate the performance of the new approach and to experimentally verify the previously simulated system. The experimental studies were conducted to investigate the effect of the ambient temperature and humidity ratio, and the ventilation rate. The testing matrix is shown in Table 2. The first baseline is the VCC alone at ARI-humid conditions with no ventilation load (triangle mark) and the second one is the VCC alone at ARI-humid conditions with ventilation rate of 10% (star mark).

Table 2. The hybrid system testing matrix

T_amb	w_amb	mdot_air	DW_speed,T_gen	Run
ºC	gw/kga	kga/s	RPH, ºC	#
25	16.2	0.085	25,55	1
30	16.2	0.085	25,55	1
35	16.2	0.085	25,55	1
30	14	0.085	25,55	1
30	20	0.085	25,55	1
30	16.2	0.1	25,55	1

Figure 6 shows that the hybrid system (circular mark) is able to maintain the conditioned space in the comfort zone (shown as black solid line) while the two baselines are not.

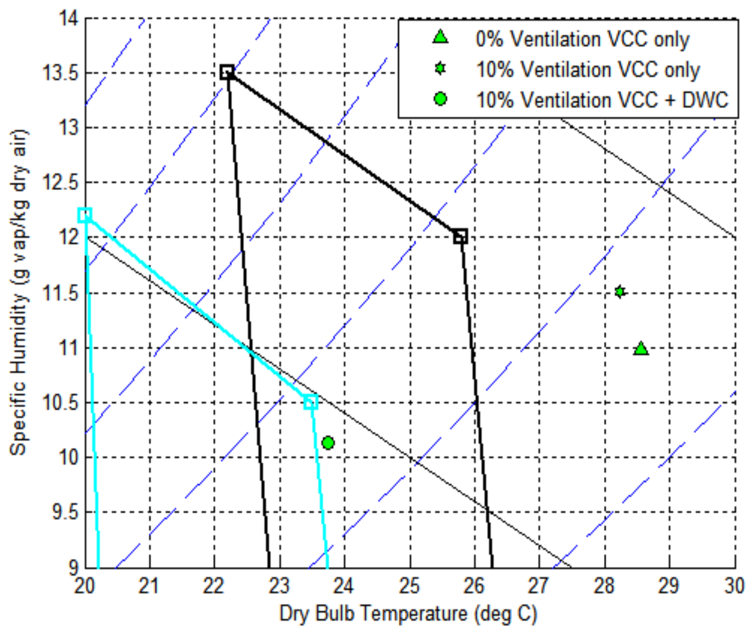

Figure 6. Comparison of the hybrid system to a standalone vapor compression cycle.

Figure 7 shows the indoor conditions of all the hybrid systems tested. It shows that the system is able to maintain very close indoor conditions for various operating conditions.

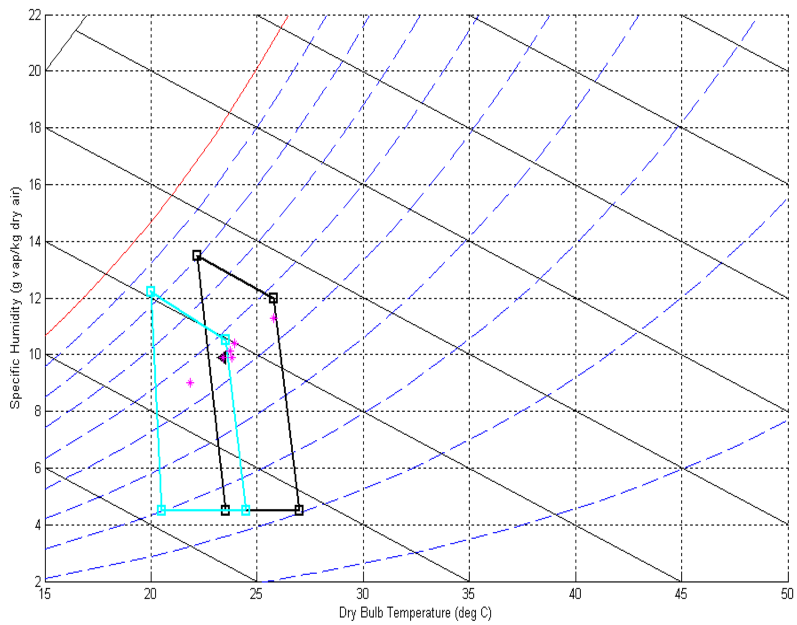

Figure 7. The indoor conditions for all the tests.

4. Difficulties Encountered/Overcome

- Obtaining low ambient temperature and high humidity inside the chamber.

5. Planned Project Activities for the Next Quarter

The following activities are to be conducted in the next quarter:

- Model the VCC using CoilDesigner and VapCyc
- Incorporate the VCC model in the TRNSYS model
- Update the solar collector model in TRNSYS

6. References

[1] Stine, W.B., Geyer, W.B., 2001, Power from the sun, www.powerfromthesun.net.
[2] Threlkeld,.J, Kuehn, T., Ramsy, J.,1998, Thermal Environmental Engineering, Prentice-Hall, Inc, USA
[3] http://www.nrel.gov/rredc/solar_data.html
[4] http://rredc.nrel.gov/solar/old_data/nsrdb/tmy2/State.html
[5] Notton , G. , Poggi, P. , Cristofari, C., 2006, Predicting hourly solar irradiations on inclined surfaces based on the horizontal measurements: Performances of the association of well-known mathematical models, *Energy Conversion and Management*, 47 1816–1829
[6] http://rredc.nrel.gov/solar/old_data/nsrdb/1991-2005/siteonthefly.cgi?id=724060
[7] ASHRAE, 1999, Applications Handbook, CH.32
[8] Kreith, F. and Kreider, J.F., 1978, Principles of solar engineering, *Hemisphere publishing corporation* Washington USA
[9] Kalogirou, S., 2004, Solar thermal collectors and applications, *Progress in Energy and Combustion Science* 30 pp. 231–295

[10] Goswami, Y., Kreith, F. and Kreider, J.F., 2000, Principles of solar engineering, *Taylor and Francis,* PA, USA,

[11] Duffie, J.A., Beckman, W.A., 1991, *Solar engineering of thermal processes*, Second edition, John Wiley & Sons, Inc., New York, ISBN: 0-471-51056-4.

[12] Pasupathy, A., Velraj, R., Seeniraj, R.V., 2008, Phase change material-based building architecture for thermal management in residential and commercial establishments, *Renewable and Sustainable Energy Reviews*, pp.39–64

[13] Dieng, A., Wang, R. , 2001 Literature Review on Solar Adsorption Technologies of Ice-making and Air Conditioning Purposes and Recent Developments in Solar Technology, *Renewable and Sustainable Energy Reviews* 5 pp.313–342

[14] Sumathy, K., Yeug, K, Yong, L., 2003, Technology Development in the Solar Adsorption Refrigeration Systems, *Progress in Energy and Combustion Science* 29 pp 301–327

[15] Roger, A. Messenger, J. V., 2005, Photovoltaic Systems Engineering, 2nd ed. Taylor & Francis

[16] http://www.nfpa.org/

[17] http://ieeexplore.ieee.org/iel5/7946/21930/01019771.pdf?arnumber=1019771

[18] TRANE, "Product Data: 4DCZ6036A through 4DCZ6060A" (2008), 22-1815-03

[19] METEONORM, "Global Meteorological Database for Engineers, Planners and Education,"(2007)

Waste Heat Utilization in the Petroleum Industry

UMD Investigators: Reinhard Radermacher, Yunho Hwang
GRAs: Amir Mortazavi, Abdullah Alabdulkarem
PI Investigators: Saleh Al Hashimi, Peter Rodgers
Start Date: Oct 2006

1. Objective/Abstract

The main objective of this project is to minimize overall energy consumption of gas or oil processing plants and reducing their CO_2 emission by utilizing waste heat and/or improving cycle design with CO_2 capture and sequestration (CCS). Consideration will include the use of absorption chillers and steam cycles, and other options.

2. Deliverables for the Completed Quarter

The following tasks were completed:

- Used pinch analysis to compare the proposed CCS configuration against the conventional CCS configuration.
- Continued to develop robust optimization technique for solving problems with uncertainty

3. Summary of Project Activities for the Completed Quarter

Pinch analysis is a heat and process integration method based on thermodynamic principles. It was used to compare the proposed CCS configuration against the conventional CCS configuration.

Two configurations of gas turbine combined cycle with double pressure steam cycle and gas turbine triple combined cycle with double pressure steam cycle and absorption chillers were optimized as an APCI LNG plant driver cycle. According to our models, the best option consumes 38.2% less fuel than the baseline cycle.

3.1 Pinch analysis and CCS on APCI LNG plant

Pinch analysis can be used to determine the potential in energy consumption reductions by enhancing heat exchanger network. The pinch analysis was developed by Linnhoff and Hindmarsh in 1981. The objective of using pinch analysis here is to investigate the minimum utility cooling or heating that is needed in the proposed CCS configuration as well as the conventional CCS configuration.

In order to find the minimum possible utility cooling or heating or “energy targets,” the problem table algorithm is used which requires each stream supply and target temperatures, heat capacity and mass flow rate. A pinch analysis spreadsheet tool was developed by Kemp (2007) and it was used in this work.

3.1.1 Pinch analysis on the APCI LNG plant

The problem table algorithm for the APCI LNG plant is shown in Table 1. Hot streams are ones requiring cooling whereas cold streams are ones requiring heating.

Table 1. Streams in the APCI LNG plant

Stream Name	Supply Temp. (°C)	Target Temp. (°C)	Mass Flow Rate (kg/s)	Enthalpy Change (kJ/kg)	Heat Flow (MW)	Stream Type
NG from feed to -5°C HX	40.0	-2.0	111.1	-116.0	12.89	Hot
NG from -5°C to -19°C HX	-2.0	-16.0	106.2	46.4	4.93	Hot
NG from -5°C to -33°C HX	-16.0	-30.0	101.9	50.5	5.14	Hot
NG from -33°C HX to LNG	-30.0	-160.0	96.9	674.3	65.32	Hot
NG from Frac1 to LNG	-33.5	-160.0	3.3	672.3	2.18	Hot
Cond_Frac1	-0.5	-33.5	16.3	311.6	5.07	Hot
Boiler_Frac1	130.1	140.6	86.6	124.7	10.79	Cold
Cond_Frac2	79.6	73.6	9.1	181.4	1.65	Hot
Boiler_Frac2	130.0	138.4	14.5	101.7	1.48	Cold
Propane	73.6	-16.0	3.0	494.8	1.46	Hot
Cond_Frac3	64.9	59.6	9.0	213.8	1.93	Hot
Boiler_Frac3	141.1	150.4	14.1	155.0	2.18	Cold
Butane	59.6	-2.0	2.9	458.6	1.34	Hot
Pentane Plus	150.4	40.0	5.1	308.8	1.57	Hot

Using Kemp's pinch analysis tool (2007) at 3°C pinch temperature, the minimum cold and hot utilities are 103.27 MW and 14.21 MW, respectively. The HYSYS model shows that the APCI LNG plant has a cooling capacity of 183.23 MW and requires 14.45 MW of heating. Thus, the APCI LNG plant has an efficiency of 43.63%. The second law efficiency was calculated to be 45.43%. The difference between the two efficiencies is because the pinch analysis does not consider losses associated with pressure drop. The large difference between the APCI LNG plant cooling capacity and the minimum required cooling capacity for natural gas liquefaction is because the APCI also cools the mixed refrigerants of the MCR cycle before using it in natural gas liquefaction.

The hot and cold composite curves for the APCI LNG plant are shown in Figure 1. The overlap between the cold and hot composite curves shows only 0.3 MW of heat can be exchanged between the cold and hot composite curves at a pinch occurred at 131°C. The rest of the heating and cooling comes from the utility. To utilize the 0.3 MW, the Pentane Plus stream could be used to heat the natural gas in the first fractionation column boiler, which would result in 2.78% savings in the first fractionation column boiler heat.

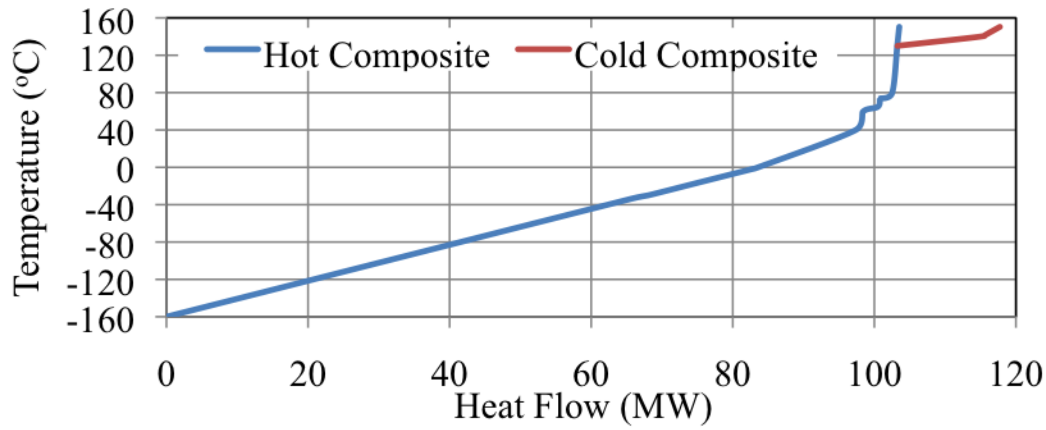

Figure 1. Hot and cold composite curves in the APCI LNG plant.

3.1.2 Plant pinch analysis on the conventional CCS configuration

The conventional CCS configuration includes the LNG plant, the CO_2 removal plant and the multi-stage CO_2 compression cycle. There are three streams to be considered, the natural gas, the flue gas and the CO_2 streams. The problem table algorithm applied for the conventional CCS configuration is shown in Table 2.

Table 2. Streams in the conventional CCS configuration

Stream Name	Supply Temp. (°C)	Target Temp. (°C)	Mass Flow Rate (kg/s)	Enthalpy Change (kJ/kg)	Heat Flow (MW)	Stream Type
NG from feed to -5°C HX	40.0	-2.0	111.11	-116.04	12.89	Hot
NG from -5°C to -19°C HX	-2.0	-16.0	106.23	46.43	4.93	Hot
NG from -5°C to -33°C HX	-16.0	-30.00	101.95	50.47	5.15	Hot
NG from -33°C HX to LNG	-30.0	-160.0	96.87	674.31	65.32	Hot
NG from Frac1 to LNG	-33.53	-160.0	3.25	672.27	2.18	Hot
Cond_Frac1	-0.52	-33.53	16.27	311.57	5.07	Hot
Boiler_Frac1	130.1	140.6	86.57	124.69	10.79	Cold
Cond_Frac2	79.58	73.59	9.14	181.40	1.66	Hot
Boiler_Frac2	129.97	138.39	14.55	101.73	1.48	Cold
Propane	73.59	-16.0	2.95	494.77	1.46	Hot
Cond_Frac3	64.9	59.6	9.05	213.84	1.93	Hot
Boiler_Frac3	141.1	150.4	14.12	154.97	2.19	Cold
Butane	59.6	-2.0	2.93	458.63	1.34	Hot
Pentane Plus	150.4	40.0	5.11	308.79	1.58	Hot
FG Cooler	140.0	40.0	421.0	108.07	45.5	Hot
Rich In	40.9	106.0	424.6	262.42	111.4	Cold
To Reboiler	115.5	117.6	435.1	161.86	70.42	Cold
CO_2 Condenser	104.40	75.92	32.42	825.46	26.76	Hot
Lean Out	117.6	40.0	403.3	-298.2	120.2	Hot
CO_2 to Compressors	75.92	40.0	21.38	237.90	5.09	Hot
Comp. 1 Intercooler	89.75	40.0	19.58	63.38	1.24	Hot
Comp. 2 Intercooler	89.5	40.0	19.44	56.02	1.09	Hot
Comp. 3 Intercooler	89.5	40.0	19.36	52.34	1.01	Hot
Comp. 4 Intercooler	89.5	40.0	19.31	51.26	0.99	Hot

Comp. 5 Intercooler	89.5	40.0	19.29	52.92	1.02	Hot
Comp. 6 Intercooler	89.7	40.0	19.27	60.15	1.16	Hot
Comp. 7 Intercooler	89.5	40.0	19.27	96.76	1.86	Hot
Comp. 8 Intercooler	89.69	54.0	19.27	106.07	2.04	Hot

The minimum cold and hot utilities were calculated at 3°C pinch temperature to be 189.86 MW and 74.64 MW, respectively. The HYSYS model shows that the conventional CCS configuration uses 271 MW of cooling and requires 84.87 MW of heating, as shown in Table 3. The cooling demand is high because a high amount of cooling is needed for the natural gas liquefaction, CO_2 condensing, flue gas cooling and CO_2 compressor intercooling at temperatures that no other stream could exchange heat with.

Table 3. Hot and cold utilities demand from the HYSYS models applied to the conventional CCS configuration

Utility	Demand in APCI (MW)	Demand in FG (MW)	Demand in CO_2 Removal (MW)	Demand in CO_2 Compression (MW)	Total Demand (MW)
Hot	14.45	-	70.42	-	84.87
Cold	183.23	45.5	31.85	10.42	271

The hot and cold composite curves for the conventional CCS configuration are shown in Figure 2. The overlap between the cold and hot composite curves shows 122 MW of heat can be exchanged between the cold and hot composite curves at a pinch occurred at 117°C. To utilize the 122 MW, the "Lean Out" stream in the CO_2 removal plant is used to preheat the "Rich In" stream in addition to using the Pentane Plus stream to heat the natural gas in the first fractionation column boiler.

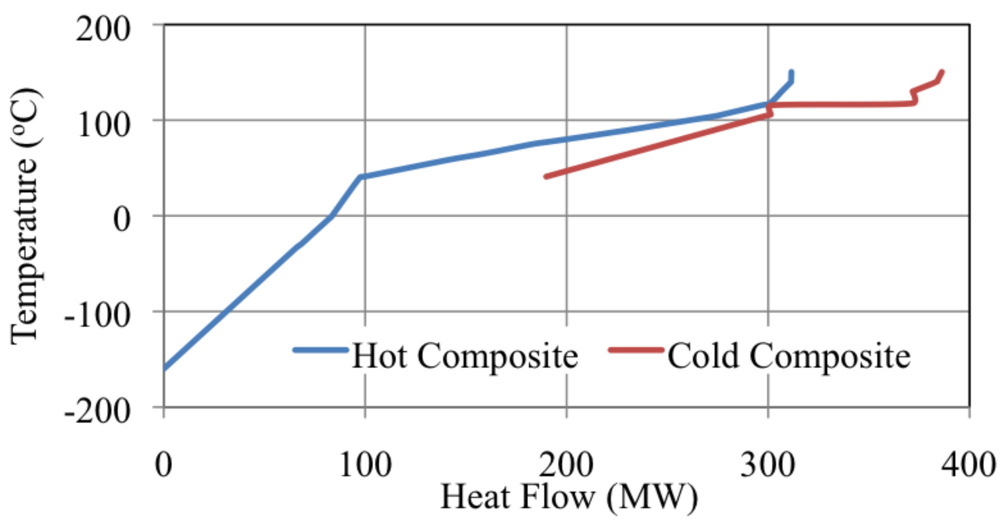

Figure 2. Hot and cold composite curves in the conventional CCS configuration.

3.1.3 Pinch analysis on the proposed CCS

Configuration

The proposed CCS configuration includes the LNG plant, the CO_2 removal plant, the multi-stage CO_2 compression and CO_2 liquefaction plant. There are three streams to be considered, namely the natural gas, the flue gas and the CO_2 streams. The problem table algorithm applied for the proposed CCS configuration is shown in Table 4.

Table 4. Streams in the proposed CCS configuration

Stream Name	Supply Temp. (°C)	Target Temp. (°C)	Mass Flow Rate (kg/s)	Enthalpy Change (kJ/kg)	Heat Flow (MW)	Stream Type
NG from feed to -5°C HX	40	-2	111.11	-116.04	12.89	Hot
NG from -5°C to -19°C HX	-2	-16	106.23	46.43	4.93	Hot
NG from -5°C to -33°C HX	-16	-30	101.95	50.47	5.15	Hot
NG from -33°C HX to LNG	-30	-160	96.87	674.31	65.32	Hot
NG from Frac1 to LNG	-33.5	-160	3.25	672.27	2.18	Hot
Cond_Frac1	-0.5	-33.5	16.27	311.57	5.07	Hot
Boiler_Frac1	130.1	140.6	86.57	124.69	10.79	Cold
Cond_Frac2	79.6	73.6	9.14	181.40	1.66	Hot
Boiler_Frac2	130.0	138.4	14.55	101.73	1.48	Cold
Propane	73.6	-16.0	2.95	494.77	1.46	Hot
Cond_Frac3	64.9	59.6	9.05	213.84	1.93	Hot
Boiler_Frac3	141.1	150.4	14.12	154.97	2.19	Cold
Butane	59.6	-2.0	2.93	458.63	1.34	Hot
Pentane Plus	150.4	40.0	5.11	308.79	1.58	Hot
FG Cooler	80.0	40.0	421.00	44.70	18.82	Hot
Rich In	31.0	105.0	393.12	298.25	117.25	Cold
To Reboiler	115.9	117.9	402.65	174.90	70.42	Cold
CO_2 Condenser	80.0	75.9	33.38	149.80	5.00	Hot
Lean Out	117.9	35.3	370.77	-316.04	117.18	Hot
CO_2 to Compressors	75.9	40.0	22.36	237.71	5.31	Hot
Comp. 1 Intercooler	99.0	40.0	20.48	74.57	1.53	Hot
Comp. 2 Intercooler	99.0	40.0	20.31	65.46	1.33	Hot
Comp. 3 Intercooler	99.0	40.0	20.24	51.88	1.05	Hot
Comp. 4 Intercooler	99.0	40.0	20.22	61.71	1.25	Hot
Comp. 5 Intercooler	99.0	40.0	20.18	62.32	1.26	Hot
Comp. 6 Intercooler	110.4	40.0	20.14	86.34	1.74	Hot
CO_2 Precooler HX	40.0	35.6	20.14	-6.65	0.13	Hot
CO_2 Liquefaction HX	35.6	14.3	20.14	218.71	4.40	Hot
CO_2 Subcooler HX	30.1	32.6	20.14	6.80	0.14	Cold
CO_2 Precooler HX	32.6	35.0	20.17	6.65	0.13	Cold

The minimum cold and hot utilities were calculated at 3°C pinch temperature to be 144.55 MW and 84.43 MW, respectively. The HYSYS models show that the proposed CCS configuration uses 192.71 MW of cooling and requires 85.14 MW of heating as shown in Table 5.

Table 5. Hot and cold utilities demand from the HYSYS models for the proposed CCS configuration

Utility	Demand in APCI (MW)	Demand in FG (MW)	Demand in CO_2 Removal (MW)	Demand in CO_2 Compression and Liquefaction (MW)	Total Demand (MW)
Hot	14.45	-	70.42	0.27	85.14
Cold	150.89	18.82	10.31	12.69	192.71

The hot and cold composite curves for the proposed CCS configuration are shown in Figure 3. The overlap between the cold and hot composite curves shows that 117 MW of heat can be exchanged between the cold and hot composite curves at a pinch occurred at 117°C. To utilize the 117 MW, the "Lean Out" stream in the CO_2 removal plant is used to preheat the "Rich In" stream in addition to using the Pentane Plus stream to heat the natural gas in the first fractionation column boiler and the pressurized CO_2 in precooling the CO_2 stream.

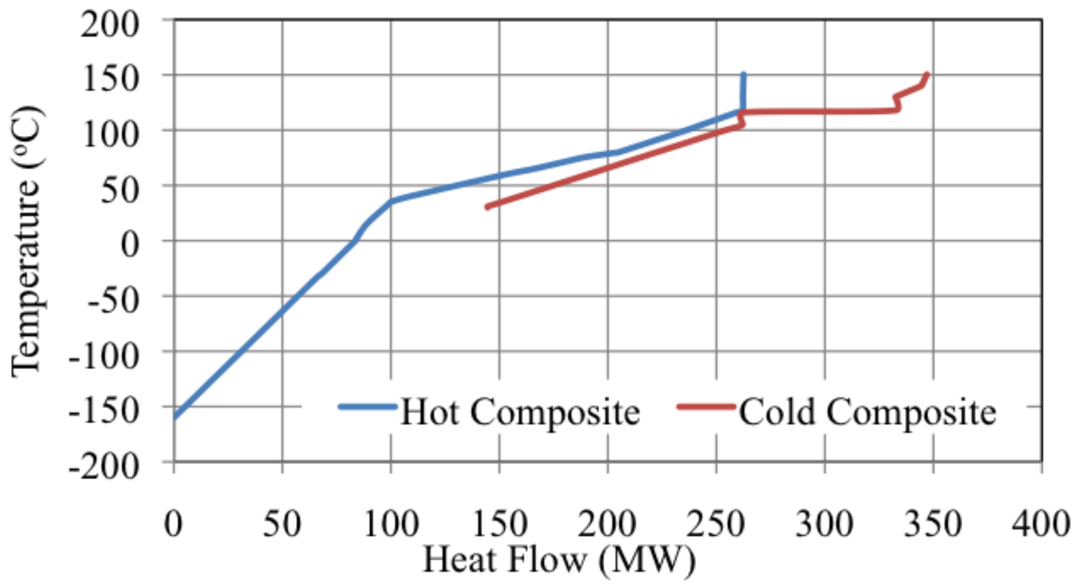

Figure 3. Hot and cold composite curves in the proposed CCS configuration.

Table 6 compares the utility cooling and heating between the proposed CCS configuration and the conventional CCS configuration. The proposed CCS configuration uses 29% less utility cooling than the conventional CCS configuration because of the improved heat integration and waste heat utilization. For example, less utility cooling is needed in flue gas cooling and CO_2 removal plant since part of its cooling is utilized by absorption chillers. Also, smaller APCI capacity is needed because of the replacement of the 22°C and 9°C evaporators by absorption chillers and subcooling the propane cycle to 5°C. However, slightly higher utility heating is required in the proposed configuration due to the required heat to heat up the liquefied and pressurized CO_2. This heat was recovered in CO_2 liquefaction.

Table 6. Utility cooling and heating in conventional CCS configuration vs. proposed CCS configuration

Configuration	Utility	Demand in APCI (MW)	Demand in FG (MW)	Demand in CO_2 Removal (MW)	Demand in CO_2 Comp. and Liq-uefaction (MW)	Total Demand from HYSYS Models (MW)	Minimum Demand from Pinch Analysis (MW)
Conventional CCS	Hot	14.45		70.42		84.87	74.64
	Cold	183.23	45.5	31.85	10.42	271	189.86
Proposed CCS	Hot	14.45		70.42	0.27	85.14	84.43
	Cold	150.89	18.82	10.31	12.69	192.71	144.55

3.3 Developing robust optimization techniques

One of the barriers in development of small remote gas fields is transportation of natural gas from these reservoirs to a specific market, since it is not economical to transport natural gas for long distances by the pipeline. On the other hand, it is not economical to build a stationary LNG plant for a small natural gas reservoir. One solution to this problem might be the development of mobile LNG plants. There are several uncertainties involved in design of mobile LNG plant, including the natural gas composition (feed gas composition). It should be noted for a mobile LNG plant that the design should be insensitive to the natural gas composition of the gas field. Moreover, the mobile LNG plant should be energy efficient. The enhancement options of the research tasks for this project could be implemented in the design of a mobile LNG plant based on APCI liquefaction technology. However, the big challenge is to develop a refrigerant mixture which is both efficient and insensitive to the natural gas composition. Here, the efficient refrigerant mixture refers to a refrigerant mixture composition which leads to minimum amount of energy consumed per unit mass of produced LNG. To develop this refrigerant mixture, the optimization techniques should be employed. However, the conventional optimization techniques cannot handle problems that involve uncertainty. Robust optimization techniques would be the most suitable choice based on the design goal, which is operability of the mobile LNG for different natural gas compositions. However, to the best of our knowledge the current optimization techniques are either incapable of solving optimization problems which involve a simulation model of the LNG plant or are computationally prohibitive. We are currently addressing this issue by developing a novel robust optimization technique. The developed robust optimization technique will be used to develop a refrigerant mixture which is insensitive to the feed gas composition. This refrigerant will be applicable in both stationary and mobile APCI LNG plants dealing with different feed gas composition and mobile APCI LNG plants.

4. Difficulties Encountered/Overcome

None

5. Planned Project Activities for the Next Quarter

The following activities are to be conducted in the next quarter:

- Integrate the proposed uses of the waste heat in the CCS plant.
- Optimizing mobile LNG plants using robust optimization

References

[1] Dopazo J. A., and Fernández-Seara J., 2010, "Experimental evaluation of a cascade refrigeration system prototype with CO_2 and NH_3 for freezing process applications," International Journal of Refrigeration, pp. 1-11.

[2] Venkatarathnam G., 2008, Cryogenic Mixed Refrigerant Processes, Springer-Verlag New York, LLC.

[3] Paradowski H., Bamba M. O., and Bladanet C., 2004, "Propane Precooling Cycles for Increased LNG Train Capacity," 14th International Conference and Exhibition on Liquefied Natural Gas, pp. 1-18.

[4] Alefeld, G., Radermacher, R., 1994, "Heat conversion systems", CRC Press, Boca Raton.

[5] Al-Hamdan, Q.Z., Ebaid, M.S.Y., 2006, "Modeling and simulation of a gas turbine engine for power generation", ASME Journal of Engineering for Gas Turbines and Power, Vol. 128, pp. 302-311.

[6] LNG technology selection, http://www.fwc.com/publications/tech_papers/files/TariqLNG.pdf, Last access, June, 2008

[7] Haring, H., 2008, " Industrial Gas Processing", Wiley-VCH, Weinheim

[8] ASHRAE, 2002, "ASHRAE Refrigeration Handbook", American Society of Heating, Refrigeration and Air-Conditioning Engineers, Atlanta, GA, USA.

[9] ASHRAE, 2005, "ASHRAE Fundamentals Handbook", American Society of Heating, Refrigeration and Air-Conditioning Engineers, Atlanta, GA, USA.

[10] Brant, B., Brueske, S., Erickson, D.C., Papar, R., 1998, "New waste-heat refrigeration unit cuts flaring, reduces pollution", Oil & Gas Journal, May 18, pp.61-64.

[11] Brooks, F.J., 2000 "GE gas turbine performance characteristics", GE Power Systems Schenectady, NY, GER-3567H.

[12] Cohen, H., Rogers, G.F.C., Saravanamuttoo, H.I.H., 1996, "Gas turbine theory", 4th edition, Longman Scientific & Technical, Singapore.

[13] Erickson, D.C., 2000 "LPG recovery from reformer treat gas", US Patent 6,158,241.

[14] Erickson, D.C., Anand, G., Papar, R.A., Tang, J., 1998, "Refinery waste heat powered absorption refrigeration – cycle specification and design", Proceeding of the ASME Advanced Energy System Division, AES-Vol. 38, pp.391-402.

[15] Erickson, D.C., Kelly, F., 1998, "LPG recovery from refinery by waste heat powered absorption refrigeration", IECEC-98-079, 33rd Intersociety Engineering Conference on Energy Conversion, Colorado Springs, CO.

[16] Giampaolo, T., 2003, "The gas turbine handbook: principles and practices", 2nd edition, The Fairmont Press, Lilburn, GA.

[17] Herold, K.E.; Radermacher, R., Klein, S, 1996, "Absorption chillers and heat pumps", CRC Press, Boca Raton.

[18] Kim, T.S., Hwang, S.H., 2006, "Part load performance analysis of recuperated gas turbine considering engine configuration and operation strategy", Energy, Vol. 31, pp., 260-277.

[19] Klein, S.A., 2005, "Engineering Equation Solver" F-Chart Software.

[20] Kurz, R., 2005, "Gas turbine performance", 44th Turbomachinery Symposium, pp.131-146.

[21] Kurzke, J., 2003, "Model based gas turbine parameter corrections", GT2003-38234, Proceedings of 2003 ASME TURBO EXPO: Power for Land, Sea, & Air, Atlanta, GA, USA.

[22] Li, Y.G., Pilidis, P., Newby, M.A., 2006, "An adaptation approach for gas turbine design-point performance simulation", Journal of Engineering for Gas Turbines and Power, Vol. 128, pp. 789-795.

[23] Orlando, J. A., 1996, "Cogeneration design guide", American Society of Heating, Refrigeration and Air-Conditioning Engineers, Atlanta, GA.

[24] Pande, M., 1996, "Tools for fractionator design in ammonia-water absorption machines", Master Thesis, University of Maryland, College Park.

[25] Walsh, P.P., Fletcher, P., 1998, "Gas turbine performance", Blackwell Science, Oxford.

Appendix

Justification and Background

Waste heat utilization opportunities are abundant in the oil and gas industry. Proper use of waste heat could result in improved cycle efficiency, reduced energy usage, reduction in CO_2 emissions, and increased production capacity.

CEEE at the University of Maryland has extensive experience in the design and implementation of integrated combined cooling, heating, and power (CCHP) projects. The faculty at PI has experience in the design and operation of petroleum processing plants. Jointly the team is well equipped to address the challenge posed by this project.

Thrust 2
Energy-Efficient Transport Process Projects

Multidisciplinary Design and Characterization of Polymer Composite Seawater Heat Exchanger Module

PI Investigator: Peter Rodgers
UMD Investigators: Avram Bar-Cohen, Satyandra K. Gupta, David Bigio, H.A. Bruck
GRAs: Juan Cevallos, F. Robinson, T. Hall, W. Pappas, A. Lederer
Start Date: Oct 2006

1. Introduction

Heat exchangers are extensively used in all oil and gas processing operations with seawater as the preferred coolant in near-shore operations. The performance and cost effectiveness of conventional metallic heat exchangers in such environments are severely constrained by corrosion and scale deposits. Polymer heat exchangers, currently under investigation by the EERC team, offer a promising alternative to metallic heat exchangers for the fossil fuel industry. Recent advances in carbon-fiber polymer composites, yielding polymer materials with thermal conductivities equal to or higher than titanium, can be applied to the development of low-cost and low-weight compact heat exchangers for corrosive fluids. These attributes, combined with the low energy investment in the formation and fabrication of these polymer heat exchangers and their ease of manufacturing, appear to make near-term applications of seawater polymer heat exchangers viable. Numerical simulations and laboratory experiments, performed by the UMD/PI EERC team in the first phase of this research, strongly support these conclusions.

2. Milestones/Deliverables

I. Two papers entitled "Polymer Heat Exchangers – An Enabling Technology for Water and Energy Savings" and "Modeling and Validation of Prototype Thermally Enhanced Polymer Heat Exchanger," were presented at the 2011 International Mechanical Engineering Congress & Exposition on November 15th in Denver, Colorado (Task A2, as described in Appendix).

II. A press release entitled "3D-Printed Plastic Heat Exchanger" has been drafted and will be distributed by the Department of Mechanical Engineering at the University of Maryland (Task A1)

III. Completed Task B, developing a manufacturability analysis and mold design, through:
   (a) Explicit construction of moldability-based feasibility boundary
   (b) Feature removal for efficient assessment of mold-filling feasibility of finned-plate geometries
   (c) Methodology for measuring fiber orientation.

IV. Prepared and tested specimens with micro and nanoscale ingredients to study mixing effects in a Twin Screw Extruder to characterize the development of multi-scale structure and associated properties for these novel polymer composites for PHX applications (Task C1).

3. Summary of Project Activities for the Completed Quarter

Two papers entitled "Polymer Heat Exchangers – An Enabling Technology for Water and Energy Savings" and "Modeling and Validation of Prototype Thermally Enhanced Polymer Heat Exchanger" were presented at the 2011 International Mechanical Engineering Congress & Exposition on November 15th in Denver, Colorado

The papers were presented at IMECE 2011, the most important ASME conference of the year, with over 20 technical tracks. The focus of the congress was "Energy and Water Scarcity," and the flagship track was entitled "Energy Water Nexus." The two papers were presented at one of the sessions in this track. The papers were well received and had generally good reviews. Following this positive reception, the papers will be combined into a single article that will be submitted to an ASME journal in the next quarter.

A press release entitled "3D-Printed Plastic Heat Exchanger" has been drafted and will be distributed by the Department of Mechanical Engineering at the University of Maryland

A joint press release by the University of Maryland and Stratasys, Inc. has been drafted to announce the successful design, fabrication, and test of a Webbed Tube Heat Exchanger (WTHX). The press release highlights the following:

- The WTHX is the first plastic heat exchanger made by additive manufacturing
- The 3D-printed WTHX was fabricated at the Stratasys facility in Eagan, MN using Fused Deposition Modeling (FDM) technology
- The WTHX represents the first time that a plastic heat exchanger has been manufactured through additive manufacturing and used to successfully transfer heat through a polymer structure from a hot gas to a cold liquid
- Room air, heated to 120 °C, was cooled by building water at 27 °C, transferring nearly 65W of heat in the 500 cm^3 heat exchanger
- Additive manufacturing technology can build complex geometries in a single step
- Stratasys' FDM technology uses some of the strongest and most heat-resistant thermoplastics found among additive manufacturing technologies
- The WTHX design minimizes the deleterious effect of the low thermal conductivity of polymers
- The WTHX promises to expand the potential applications of polymer heat exchangers to small production volumes and cost constrained systems.
- The work done by Juan Cevallos is part of a research collaboration between the University of Maryland and The Petroleum Institute in Abu Dhabi

Summary of Manufacturability Analysis and Mold Design for PHXs

A feasibility boundary search algorithm was developed to collect points along the feasibility boundary across the entire design space.

A generalized flat-plate mold filling metamodel was developed for predicting mold filling in simplified geometry with flexibility of overall geometry and processing conditions and is shown in Equation 1 where r is the filled radius, T is injection temperature, Q is injection flow rate, P is injection pressure, and H is the base thickness.

$$r(T,Q,P,H) = \begin{cases} 5.3493 \times 10^{-7} TQPH^{1.3358} & H \leq 2 \\ 6.9813 \times 10^{-7} TQPH^{1.0156} & 2 < H \leq 5 \\ 8.8125 \times 10^{-7} TQPH^{0.8723} & H > 5 \end{cases} \tag{1}$$

Using a disc-fin model to isolate the effects of fins on the overall filling behavior, the scaled thickness model shown in Equation 2 was developed to scale the simplified flat-plate representation by the fin influence. A range of test cases was used to find the ideal value for k that minimized the model error, as shown in Equation 2.

$$H_{scaled} = k\left(\frac{V_{filled}}{\pi {r_{filled}}^2} - H_{orig}\right) + H_{orig} \tag{2}$$

We also formulated a sectioning, polishing, and microscope imaging approach for collecting fiber orientation information from a variety of sample geometries. To do this, we developed a fiber orientation image processing algorithm for extracting fiber orientation from microscope images and calculating tensor values for comparison with Moldflow® predictions. We then developed a comparison framework for analyzing the agreement between Moldflow® predictions and measured behavior. This was applied to an L-channel geometry that represented a sharp velocity change. The comparison framework was used to validate predictions and identify situations when predictions may be unsuitable, which can be incorporated into hybrid results for PHX designers

Characterization of mixing of multi-scale ingredients in TSE on structure-property relationships polymer composites for PHXs

Motivation

Polymer composites are being mixed to enhance mechanical and thermal properties. We are determining whether specific throughput and screw speed have any effects on the structure and properties of the composites. The overall goal is to determine how to process polymer composites that will meet the mechanical and thermal demands of the polymer heat exchanger.

Action Plan

Current samples being prepared and characterized are listed by weight percent as follows:

A1= 25% micro fibers only at 2.2 lb/hr and 35 rpm on wide kneading blocks
A2=15% micro fibers only at 2.2lb/hr and 35 rpm on wide kneading blocks
A3=10% micro fibers only at 4.7 lb/hr and 110rpm on wide kneading blocks
A4=5% micro fibers only at 4.7 lb/hr and 110rpm on wide kneading blocks
B1=25% micro and 0.47% nano at 2.6lb/hr and 60 rpm on narrow kneading blocks
B2=15% micro and 0.47% nano at 2.6lb/hr and 60 rpm on narrow kneading blocks
B3=5% micro and 0.47% nano at 2.6lb/hr and 60 rpm on narrow kneading blocks
C1=10% micro and 3% nano at 3lb/hr and 110 rpm on wide kneading blocks
C2=5% micro and 3% nano at 3lb/hr and 110 rpm on wide kneading blocks

PBT is the base polymer that is now being mixed with the micro and nano particles because of its superior thermal and mechanical properties compared to nylon. The first composite strips contained only micro carbon fibers. Fibers were fed through a mirco feeder and entered through the mixing port. The variety of flow rates and screw speeds used helped determine which conditions produced optimal strips. This initial test was also conducted to provide a comparison to the micro and nano composite.

A second batch of samples was prepared using a mix of micro carbon fibers and nano carbon pellets. The micro fibers continued to be fed through the micro feeder and enter through the mixing port. The nano pellets were mixed in with the PBT to create a master-batch that entered in the feed port. All experiments were conducted on the 28 mm twin screw co-rotating extruder we have used previously. For the pure carbon micro composites, the 25% and 15% micro fill ran at 2.2 lb/hr and 35 rpm. The 10% and 5% micro fill ran at 4.7 lb/hr and 110 rpm. The first batch of carbon micro and nano filled composites ran at 2.6 lb/hr and 60 rpm, and the second batch of carbon micro and nano filled composites ran at 3 lb/hr and 110 rpm.

To characterize the relationship between TSE mixing and the composition of the polymer composite, a small-scale tensile tester, shown in Figure 1, was built to characterize mechanical properties using sub-scale ASTM standard dogbone specimens prepared from extruded strips of the micro and micro-nano composites processed in the TSE. The tensile tester was screw-driven, and has a maximum load capacity of 30 lbs with strain rates ranging from 0.01/sec to 0.00001/sec. Strains could be measured using a small-scale mechanical extensometer with a gage length of 6.5 mm or optically with any gage length using Digital Image Correlation (DIC), both of which were previously applied to tensile testing of larger molded polymer composite specimens with just carbon microfibers. Subsequent stress vs. strain curves could then be generated to obtain mechanical properties for comparison.

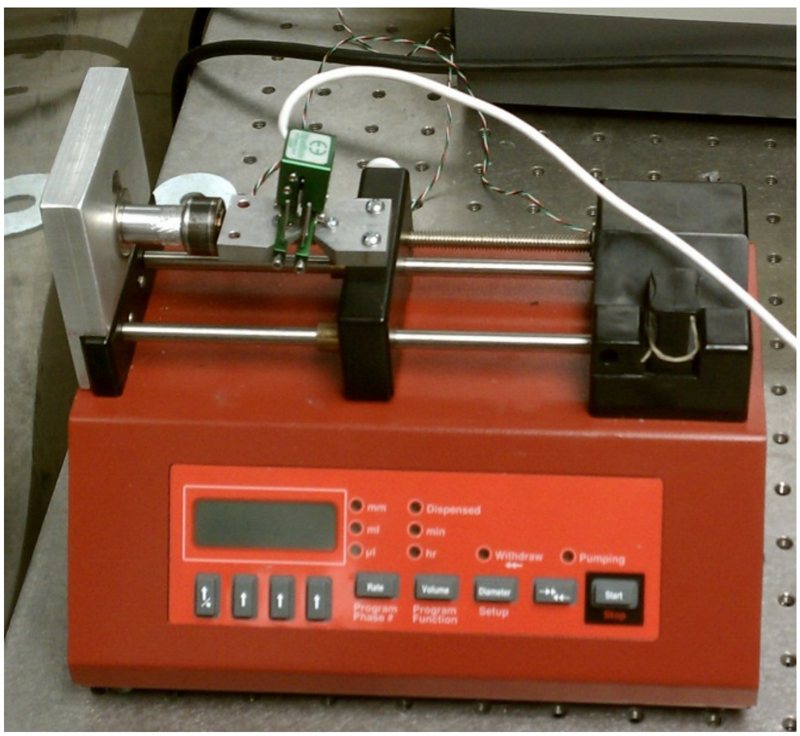

Figure 1. Small-scale tensile tester built to characterize the mechanical properties of TSE processed polymer composites for PHXs.

A modified NE-300 syringe pump machine was used to pull the specimens apart in tension. A load cell and extensometer were used to record the data in LabView. The data were then processed in Matlab to produce stress vs. strain curves.

There were several options for fixing the specimens onto the grips of the small-scale load frame. Since the load capacity was very low (30 lbs), it was possible to use fast-curing cyanoacrylate epoxy adhesive to attach the tabbed ends of the dogbbone specimen. However, to achieve adequate shear strength to resist failure during testing, cure times of up to 12 hours were needed. Therefore, an alternate approach was pursued where the specimen was attached to the grips via screws, as shown in Figure 2, below. It was determined that holes as small as 3 mm could be used on the tabbed ends of the dogbone specimen without causing failure during testing. Thus, it was possible to more quickly fix the specimens and test them than was permitted using the epoxy adhesive.

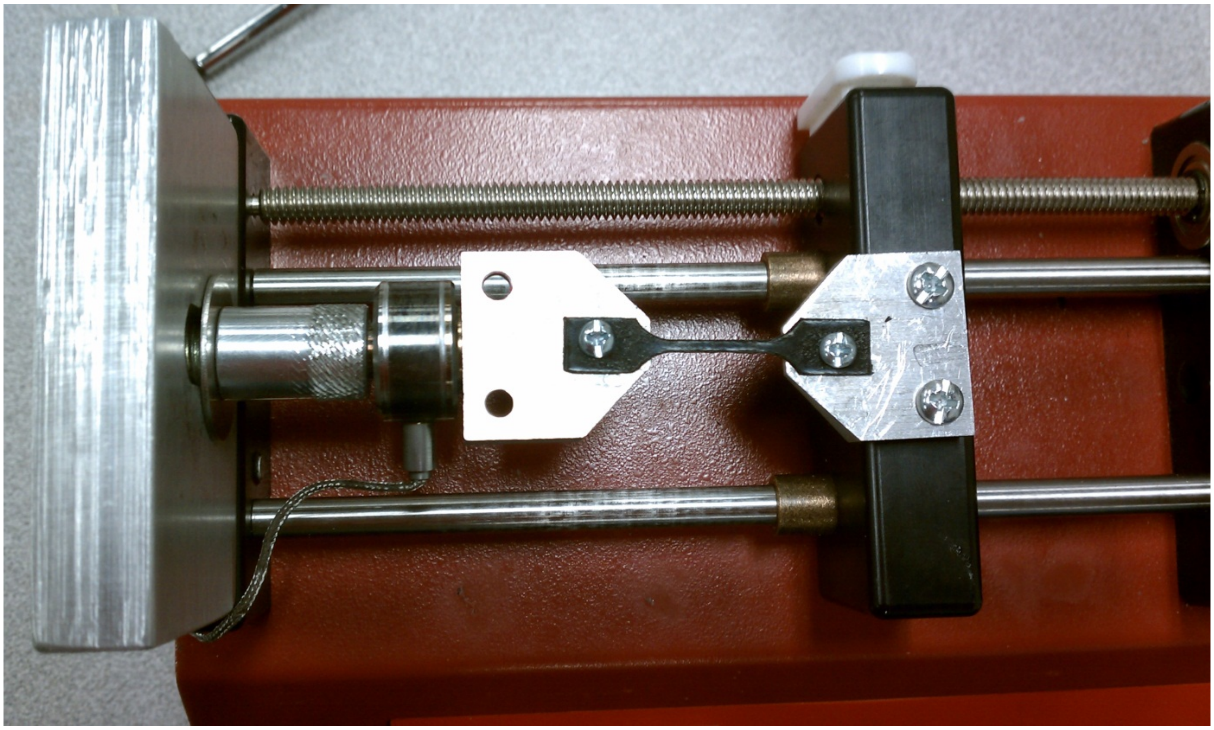

Figure 2. Small-scale dog-bone specimen fixtures to test grips using screws.

The most recent results from tensile testing are presented in Figures 3a-c. For these tests, PBT was used as the polymer due to its enhanced thermal and mechanical properties. Also, PAN-based carbon microfibers that were 6 microns in diameter and approximately 10 mm long were used as the microscale filler, while Pyrograf carbon nanofibers (CNFs) from Applied Sciences, Inc. were used as the nanoscale filler. Both of these fillers have been used previously because of their superior mechanical strength, as well as thermal and electrical conductivity. However, their compatibility with PBT has not been previously investigated, which will substantially affect the strength and ductility after TSE processing. Therefore, for these initial experiments there was no functionalization of the microscale or nanoscale fibers to enhance adhesion with PBT since the focus was primarily on the effects of mixing on structure (e.g., dispersion, fiber attrition, fiber orientation) and the associated physical properties. It is well-known that the functionalization can further enhance the mechanical properties, which is purely a chemistry issue.

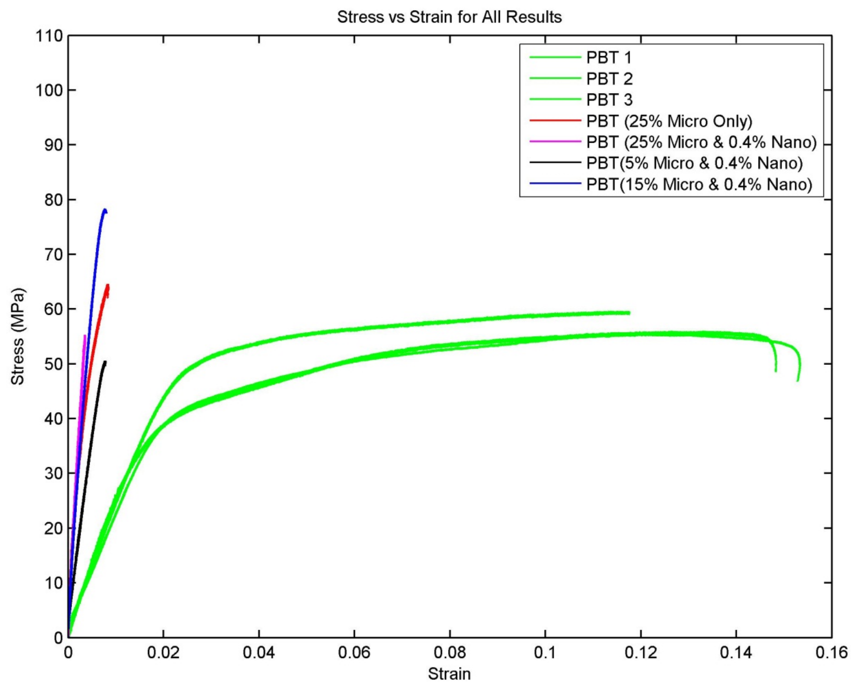
Stress vs Strain for All Results
PBT 1
PBT 2
PBT 3
PBT (25% Micro Only)
PBT (25% Micro & 0.4% Nano)
PBT(5% Micro & 0.4% Nano)
PBT(15% Micro & 0.4% Nano)
Stress (MPa)
Strain
0
10
20
30
40
50
60
70
80
90
100
110
0
0.02
0.04
0.06
0.08
0.1
0.12
0.14
0.16

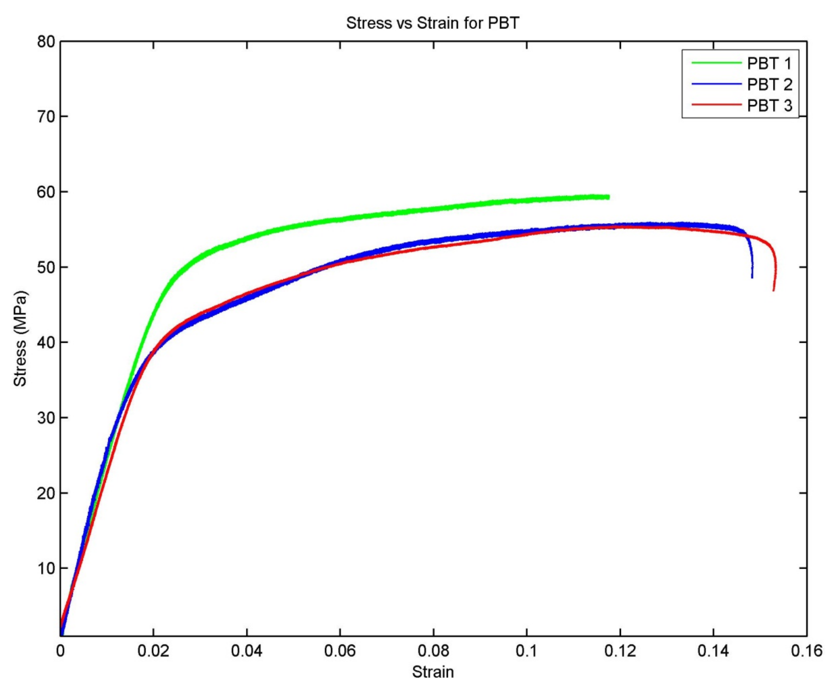
Stress vs Strain for PBT
PBT 1
PBT 2
PBT 3
Stress (MPa)
Strain
10
20
30
40
50
60
70
80
0
0.02
0.04
0.06
0.08
0.1
0.12
0.14
0.16

(a)

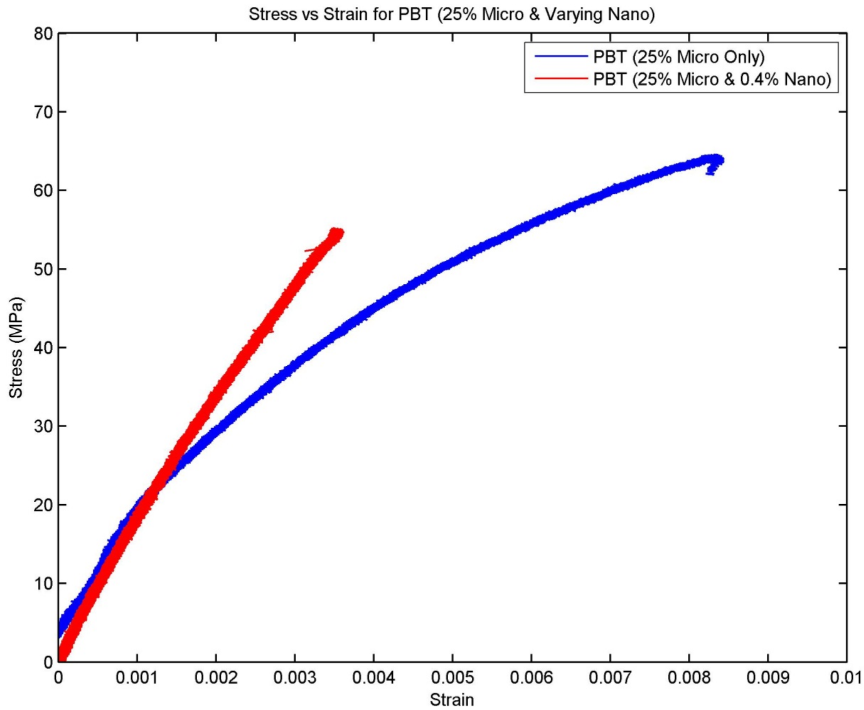

(b)

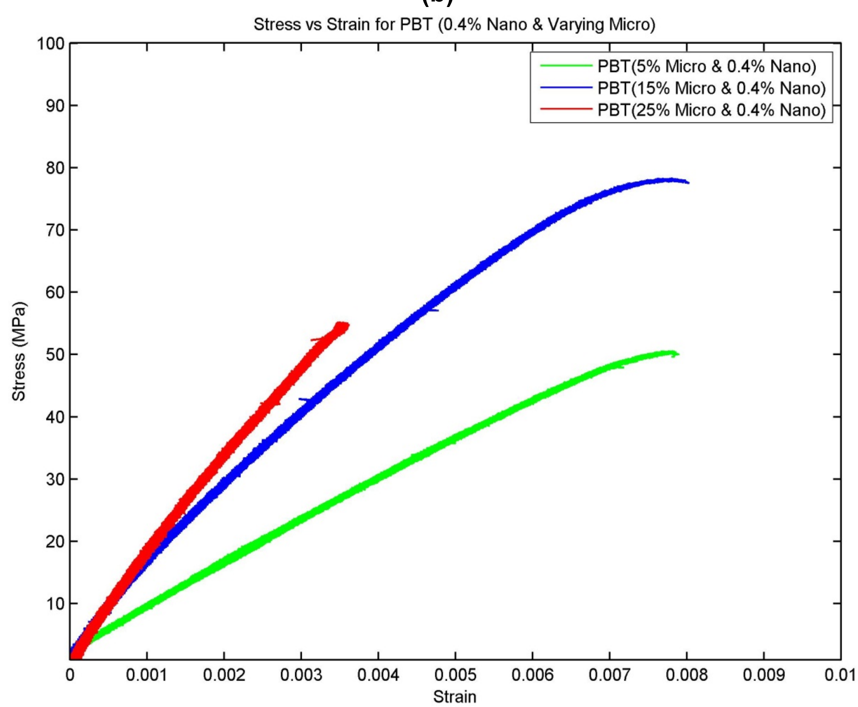

(c)

Figure 3. Comparison of stress-strain curves obtained from TSE processed polymer composites with microscale and nanoscale fillers of varying concentrations. (a) Unfilled (pure) polymer (PBT), (b) highest carbon microfiber concentration (25 wt. %) in PBT with and without 0.4 wt. % carbon nanofibers, and (c) varying carbon microfiber concentrations of 5, 15, and 25 wt. % in PBT with 0.4 wt. % carbon nanofibers.

A summary of results from mechanical testing of PBT with carbon microfibers and nanofibers can be seen in Table 1.

Table 1. Summary of properties obtained by TSE processing of PBT filled with varying concentrations of carbon microfibers and carbon nanofibers

Material	Max Stress (MPa)	Max Strain (%)	Modulus (GPa)	Yield Stress (MPa)
PBT	60	.12	2	45
	55	.15	2.5	35
	50	.15	2	40
5% M & 0.4% N	54	.02	7	40
15% M & 0.4% N	78	.008	15	20
25% M & 0.4% N	55	.0035	20	30
25% M Only	64	.008	15	25

Initial conclusions can be drawn about the addition of micro and nano carbon fibers from these results. The plain PBT exhibited fairly consistent behavior, with a maximum stress of 50-60 MPa, a maximum strain of 12-15%, and a modulus around 2 GPa. When comparing the 25% micro only and the 25% micro and 0.4% nano, it indicated that the nano carbon fibers make the material more brittle and may slightly reduce the strength. When varying the amount of micro carbon fiber filler, initial trends indicate that there may be a threshold for the amount of micro that improves the mechanical properties of the material. When only 5% micro was added, the strength remained about the same, with slightly greater stiffness. Increasing to 15% micro, the highest strength and stiffness were obtained. When 25% micro was used, the stiffness continued to improve; however, the maximum stress started to decrease. This may be because as the filler concentration begins to increase beyond a critical interfiber distance, there is a higher probability that interfiber defects may form when processing the polymer in the TSE.

Overall, PBT with a filler of 15% micro and 0.4% nano exhibited the best mechanical properties, but more characterization is necessary to correlate mixing conditions with the mechanical properties of the composites.

Anisotropic effects of TSE processing on the properties of the filled PBT continued to be investigated using optical microscopy. The images in Figures 4-10 clearly show the preferential orientation of the microfibers. While along the direction of extrusion (axial view) the fibers appear long, as in the automated analysis of fiber orientation during the molding process in the previous 10th quarter PHX report, the cross-sectional view exhibits a more circular appearance. Therefore, we anticipate that using the automated fiber orientation analysis will enable us to quantify the orientation tensor and determine how the extrusion process is affecting the directionality of the fibers when microfibers and nanofibers are combined. This will then enable us to determine the predicted level of anisotropy in mechanical properties from the structural orientation of the microfibers, and compare with actual measurements to determine how the nanofiller can affect the anisotropy of the mechanical properties.

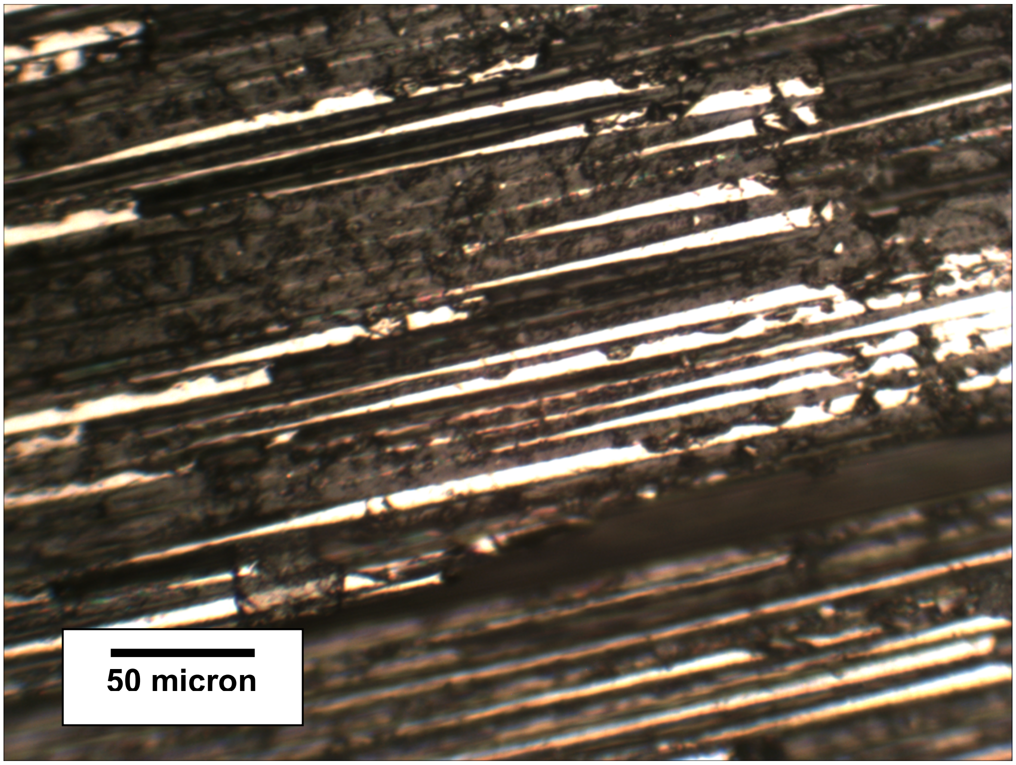

Figure 4. Microfibers (axial view 200x).

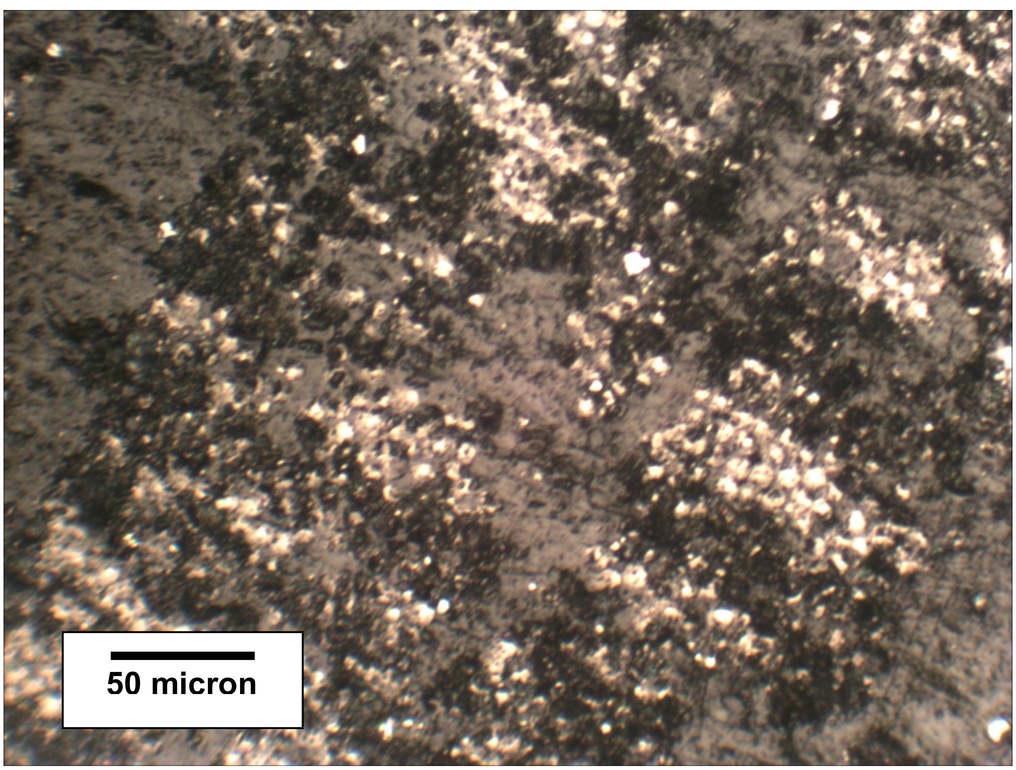

Figure 5. Microfibers (Cross-sectional View 200X).

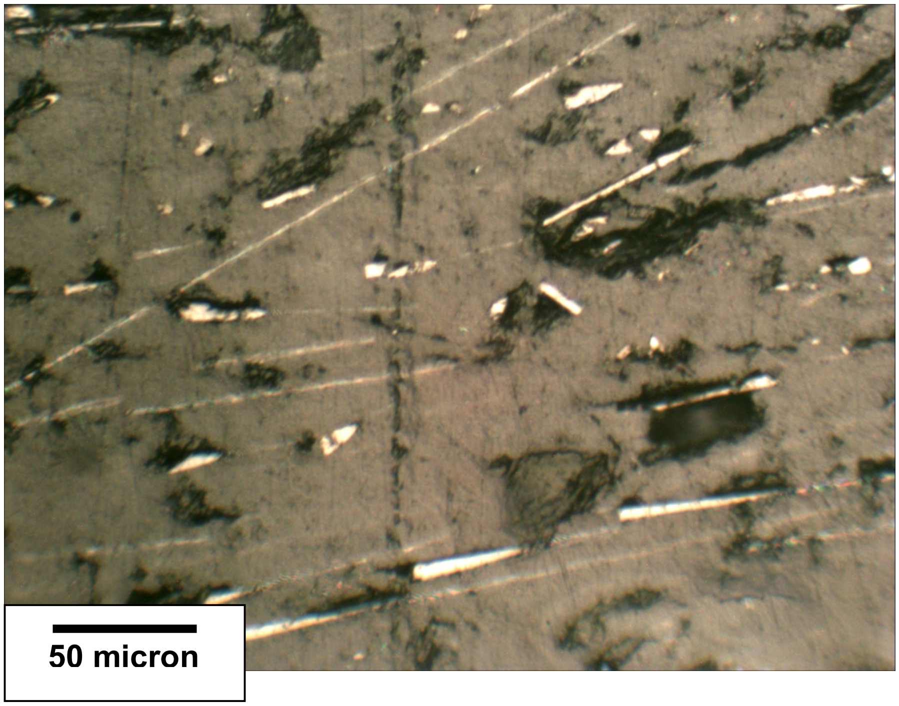

Figure 6. PBT with 25 wt. % microfiber and 0.4 wt. % nanofiber (axial view 200X).

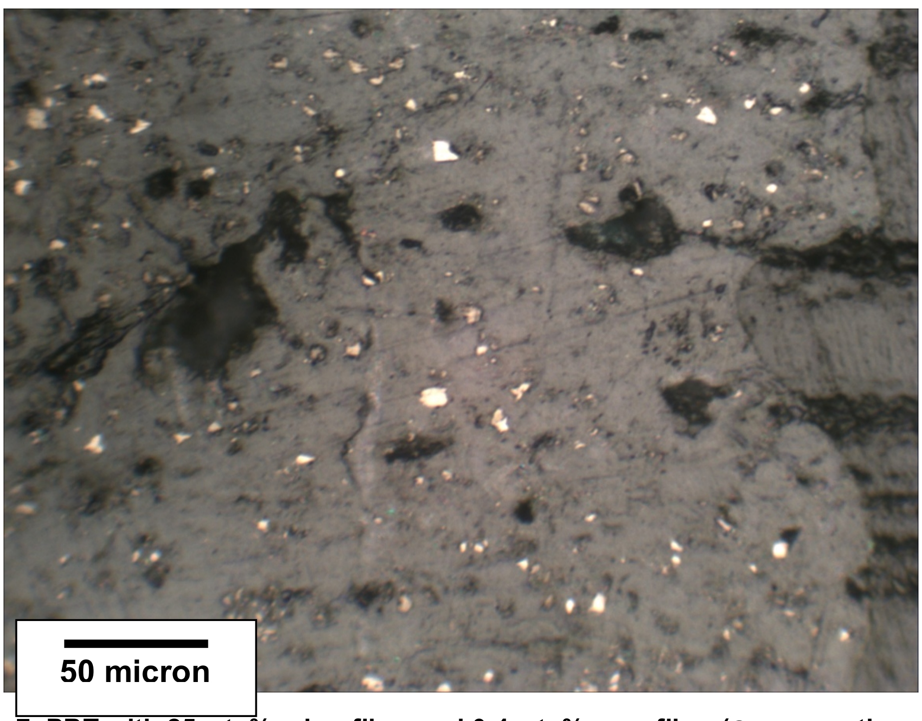

Figure 7. PBT with 25 wt. % microfiber and 0.4 wt. % nanofiber (cross-sectional view 200X).

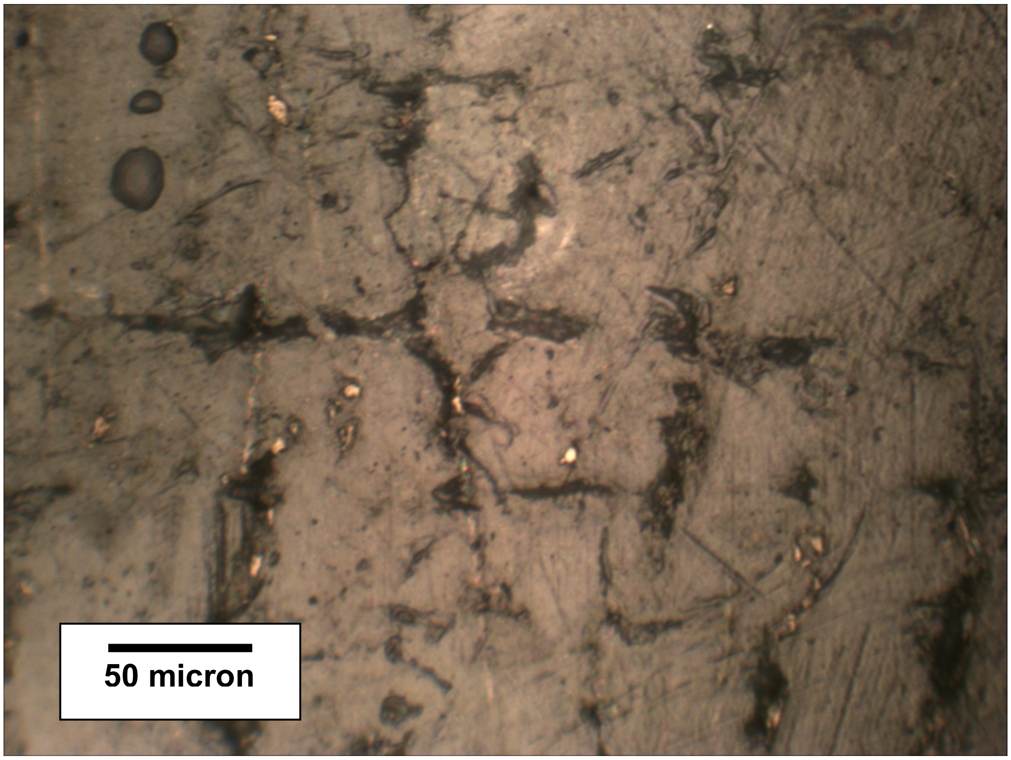

Figure 8. PBT with 5 wt. % microfiber (axial view 200X).

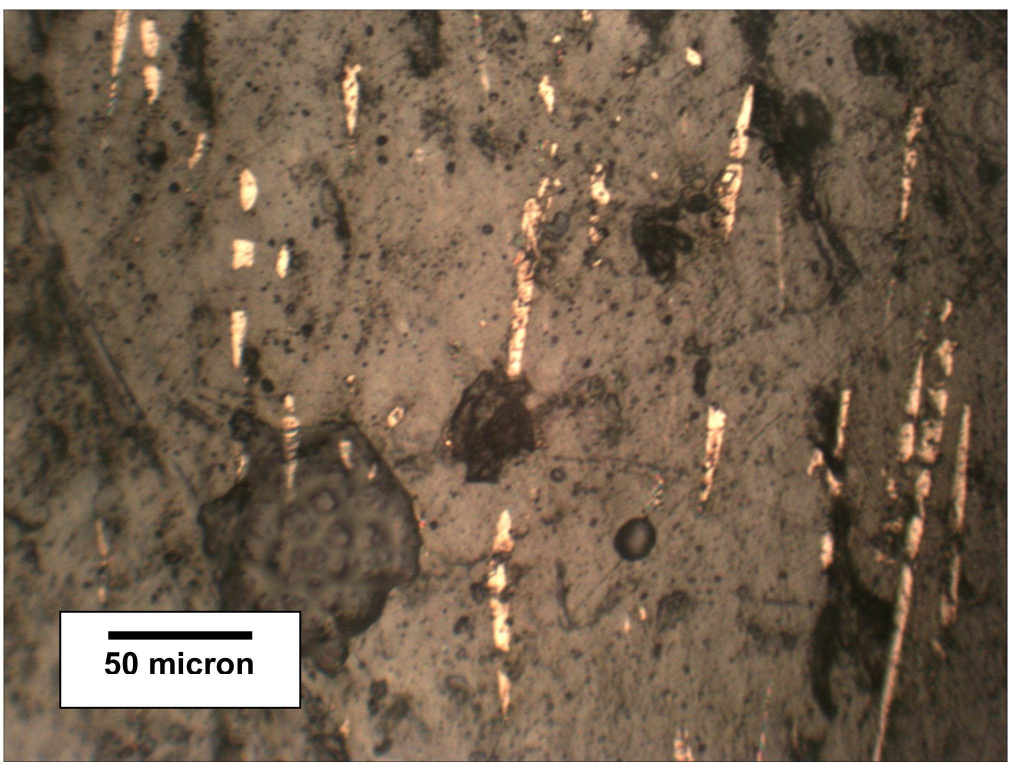

Figure 9. PBT with 25 wt. % microfiber and 0.4 wt. % nanofiber (axial view 200X).

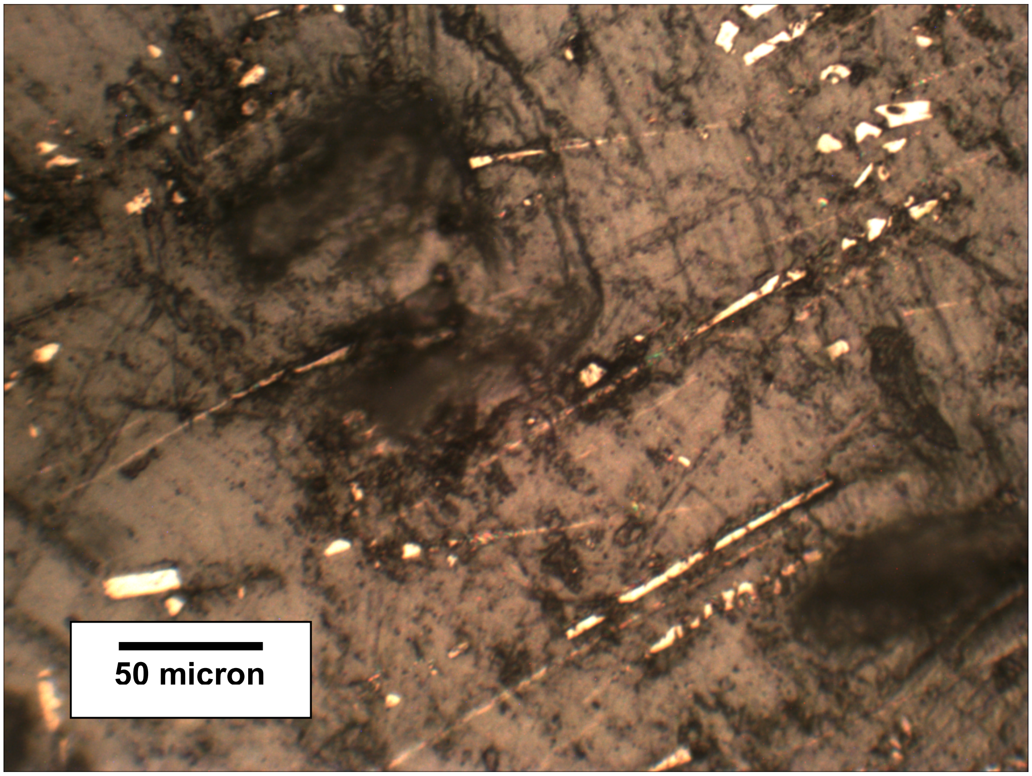

Figure 10. PBT with 25 wt. % microfiber (axial view 200X).

4. Difficulties Encountered/Overcome

- None

5. Planned Project Activities for the Next Quarter

- Continue testing of prototypes of new candidate PHX design in upgraded experimental test rig.
- Test thermal conductivity of candidate composite materials for use in FDM manufacturing (tentative for this quarter).
- Submit article to ASME journal (TBD) based on two articles presented at IMECE2011 in Denver, Colorado.
- Juan Cevallos will present his Ph.D. dissertation proposal to the committee.
- The next step for the mixing work is to continue preparing and testing samples for structural anisotropy due to fiber alignment and subsequent effects on mechanical properties and thermal conductivity. Additional experiments are being focused on identifying the mixing conditions in the TSE for producing the best set of physical properties associated with combining microscale and nanoscale ingredients.

6. References

[1] Bar-Cohen, A., Luckow, P., Cevallos, J.G., Gupta, S.K., 2010, Thermal Anisotropy in Injection Molded Polymer Composite Fins, International Heat Transfer Conference 14 at Washington DC

[2] Cevallos, J.G., Gupta, S.K., Bar-Cohen, A., Incorporating Moldability Considerations during the Design of Thermally Enhanced Polymer Heat Exchangers (under revisions)
[3] Cevallos, J.G., Bar-Cohen, A., Bergles, A.E., Gupta, S.K., Rodgers, P., Polymer Heat Exchangers – History, Opportunities, and Challenges (in progress)
[4] Luckow, P., A. Bar-Cohen, P. Rodgers, 2009, "Minimum Mass Polymer Seawater Heat Exchanger for LNG Applications," accepted for publication, ASME TSEA, January 2010
[5] Robinson, F., Bruck, H.A., Gupta, S.K., and Bar-Cohen, A., 2010, "Saltwater Hygrothermal Aging Studies of Short Carbon Fiber Reinforced Polyamide 12," ASME International Mechanical Engineering Congress & Exposition, Vancouver, British Columbia, Canada, November 12-18, 2010.
[6] Cevallos, J., Robinson, F., Bar-Cohen, A., Bruck, H.A., and Gupta, S.K.,"Polymer Heat Exchangers – An Enabling Technology for Water and Energy Savings" , ASME International Mechanical Engineering Congress & Exposition, Denver, CO, November 12-18, 2011
[7] Robinson, F., Bar-Cohen, A., Bruck, H.A., "Modeling and Validation of Prototype Thermally Enhanced Polymer Heat Exchangers", ASME International Mechanical Engineering Congress & Exposition, Denver, CO, November 12-18, 2011
[8] Cevallos, J., Robinson, F., Hall, T., Bar-Cohen, A., and Gupta, S.K., "An Integrated Approach to Design of Enhanced Polymer Heat Exchangers", accepted fro Journal of Mechanical Design (2011).

Appendix

Goals

The goal of the proposed 3-year EERC II polymer composite heat exchanger (PCHX) project is to develop the science and technology needed to underpin the systematic design of polymer-fiber composite heat exchanger modules that address the needs of the fossil fuel industry. The project team, lead by A. Bar-Cohen, brings together expertise in thermal science and technology (Bar-Cohen, Rodgers) with polymer composite molding and manufacturing (Gupta, Bigio). Design studies and molding simulations, as well as fabrication and testing of laboratory-scale polymer composite heat exchangers, during the first phase of this project, have provided the foundation for aggressive pursuit of such polymer composite heat exchangers.

Successful development of cost-effective, high-performance PCHX's will require a detailed understanding of the limitations imposed on the thermal performance, mechanical integrity, and cost of such heat exchange devices by the candidate polymer material; carbon fiber geometry, orientation, and concentration; thermal and mechanical anisotropy of the polymer-fiber composite; molding processes; thermal and structural failure mechanisms in the molded heat exchanger; and the energy investment in the fabrication and formation of the heat exchangers. The development and experimental as well as numerical validation of a multi-disciplinary computerized design methodology, along with the fabrication and testing of scaled polymer heat exchanger modules, would provide a unique knowledge-base from which low-life-cycle-cost heat exchange systems for the petroleum and gas industries could be developed.

Project Tasks

A. Thermal Design and Characterization of Polymer Composite Heat Exchanger Module
(Prof. Avram Bar-Cohen - UMD, Prof. Hugh Bruck- UMD, Prof. Peter Rodgers – PI)

1. ***Design and thermofluid evaluation of PHX concepts for LNG applications***, including sensitivity of thermal performance to key parameters, quantification of primary thermal and exergy figures-of-merit (metrics), comparison to conventional heat exchangers, and identification of least-mass/least-energy designs;

2. ***Detailed design, fabrication, and thermal characterization of least-energy PCHX module***, including mold fabrication for most promising design, assembly and instrumentation of laboratory prototype, analysis of thermal and structural performance under simulated LNG processing conditions;

3. ***Development of predictive models for anisotropic heat exchanger modules***, including use of molding CFD software for prediction of fiber orientation and effective thermal/ structural properties, numerical and analytical models for molded anisotropic fins, derivation of least-material anisotropic fin equations, determination of heat flow sensitivity to fiber geometry/concentration/orientation;

4. ***Evaluation of convective enhancement features in molded channels***, including identification of "best practices" in conventional heat exchangers, manufacturability analysis of candidate features with attention to mold complexity, part ejection, and warpage, polymer composite molding of 3-5 candidate enhanced channels; thermofluid characterization of candidate enhanced channels under simulated LNG processing conditions; and

5. ***Determination of seawater effects on polymer composite finned plates***, including design and molding of test samples, immersion in saltwater tanks at different temperatures and concentrations for pre-determined periods, surface/bulk imaging and mechanical characterization before and after immersion, analysis and correlation of effects.

B. Manufacturability Analysis and Mold Design for Polymer Composite Heat Exchanger Module (Prof. SK Gupta – UMD, Prof. HA Bruck - UMD) [Completed]

1. *Development of an improved meta-model for mold filling predictions*: We plan to develop an improved meta-model for predicting mold filling for typical heat exchanger geometries. This meta-model will account for multiple gates with adjustable spacing. The data for developing this meta-model will be generated using mold flow simulations. We plan to utilize radial basis function based meta-models to provide the right balance of accuracy and computational speed.

2 *Creation of a computational framework for gate placement to optimize fiber orientation*: We plan to develop a computational framework for placing gates to optimize the fiber orientation, utilizing simulated fiber orientations to select the gates. The sensitivity of the gate locations on fiber orientation will be developed. Gradient-based optimization techniques will be used to optimize the fiber orientation. The optimization problem will incorporate the constraint satisfaction formulation of the weld-line locations to ensure that the fiber orientation formulation produces acceptable weld-lines.

3. *Generation of insert molding process models to incorporate connectors at the weld-lines*: In order to ensure that the weld lines do not compromise the structural integrity, we plan to embed metal connectors at the expected weld-lines locations. In order to accurately place these metal connectors in the structures, we plan to develop process models of the insert molding process and mold design templates for performing insert molding.

4. ***Develop key relationships for the dependence of fiber orientation on the flow geometry of the finned-plate PCHX module,*** in commercially available polymer composites, including the effect of carbon fiber length and diameter, for high and low fiber concentrations, for both base plate and fin passages in the mold, and the effect of fiber orientation/distribution on thermo-mechanical properties, verify relationships with suitable small scale experiments;

C. Polymer-Fiber Interactions in Polymer Composite Heat Exchanger Modules (Prof. David Bigio – UMD, Prof. Hugh A. Bruck - UMD)

1. ***Determine achievable thermo-mechanical property enhancement*** through control of carbon fiber orientation, in the commercially available polymer composites, with attention to flow regimes, mixing processes in the flow of the melt, and heat exchanger module design, and verify experimentally;

2. ***Explore optimization of PCHX polymer composite properties through the creation of novel polymer composite compositions***, including multi-scale filler geometries, develop the molding methods for the desired geometries, create the novel composites and experimentally verify improved thermo-mechanical polymer composite properties.

Study on Microchannel-Based Absorber/Stripper and Electrostatic Precipitators for CO_2 Separation from Flue Gas

UMD Investigators: Serguei Dessiatoun, Amir Shooshtari, Michael Ohadi
GRAs: Christoph A. Dersch
PI Investigators: Mohamed Alshehhi, Ebrahim Al-Hajri, Afshin Goharzadeh
Start Date: July 1, 2009

1. Project Objective/Abstract

This project is focused on research leading to the development of a high-efficiency CO_2 separation mechanism with application to a diverse range of processes in the oil and gas industry, including CO_2 separation separation/injection in petrochemical and refining processes, gas sweetening, and CO_2 capture for enhanced oil recovery applications. The removal of acidic gases such as carbon dioxide from gas streams is an important process in the natural gas industry. In gas sweetening, at least 4% by volume of raw natural gas consists of CO_2, which needs to be lowered to 2% to prevent pipeline corrosion, to avoid excess energy for transport, and to increase heating value. The separation of CO_2 from flue gases and its use for enhanced oil recovery and CO_2 sequestration applications is an increasing area of importance, as evidenced by the large investments in this area by ADNOC and its group companies, as well as affiliated government agencies in Abu Dhabi. A typical CO_2 separation process involves three stages: cooling down the flue gas; separating the solid particles and condensed water droplets; and finally capturing the CO_2 using the absorption process. The microchannel-based CO_2 separator being developed in this project will significantly increase controllability of the thermal state of the reaction and the efficiency of the separation process, while decreasing the reaction time and energy consumption, as well as potentially substantially reducing the equipment footprint and the associated capital investment.

Flue gas also usually contains many contaminants in solid and liquid forms, the bulk of which are separated in gravity and inertia-driven feed gas separators. However, fine particles are carried on with the flow and can damage compressors, contaminate the gas absorption process, and reduce the quality of gas products. Electrostatic separation is one of the most effective techniques for separation of such particles and will be used in this project. The present project will address separation of droplets and particles using an EHD gas-liquid separation technique to remove liquid particles suspended in a moving gaseous medium, followed by the proposed microchannel-based separation of the CO_2 from the stream once the fine particles in the flow have been removed.

The project is being conducted jointly by the team at UMD and at PI. The team at PI is focusing on EHD separation process and absorption modeling, while the team at UMD has focused on the experimental work utilizing micro channel-based CO_2 separation and the absorption solution.

2. Deliverables for the Completed Quarter

- Design improvements for a larger scale technology demonstrator unit (TDU)
- Parametric studies and performance characterization of the TDU

3. Executive Summary of Accomplishments in the Current Reporting Period

During this reporting period additional in-depth study of the processes and analysis of our experimental results contributed to our collective understanding of the physics and reaction kinetics. The team effort continued to advance two fronts, mathematical modeling and experimental study. The main focus of the collaborators in the Petroleum Institute has been on mathematical modeling of the absorption process in microchannels, and during this period the team focused on implementing the chemical absorption into the computational model, which is still ongoing. The focus of the collaborators at UMD has been on the design for a technology demonstration unit, which is able to show the excellent results of the experimental studies of the absorption of CO_2 in microchannels.

During this period, a raw design of a demonstration unit was developed. In addition to the absorption process, the unit should also be able to demonstrate the regeneration process. Therefore a process flow diagram of an acid gas removal unit has served as a basis for calculations. Additional desorption experiments have helped us understand the chemical process of desorption better. Finally, we calculated desorber dimensions based on mass transfer. Some of the major results collected in this period and an outline of the future work are presented in the current report. In this reporting period, the collaborators from the PI and UMD continued to jointly review the project's progress by sharing ideas through weekly audio conferences and emails.

4. Summary of Project Activities for the Completed Quarter

Considerations for the technology demonstrator unit

This section discusses the design requirements for the technology demonstrator unit and which data used for the design. The technology demonstrator unit should demonstrate the whole loop, which consists of both the absorption and the desorption components. Therefore, a regenerator for the absorbent diethanolamine was included in the design.

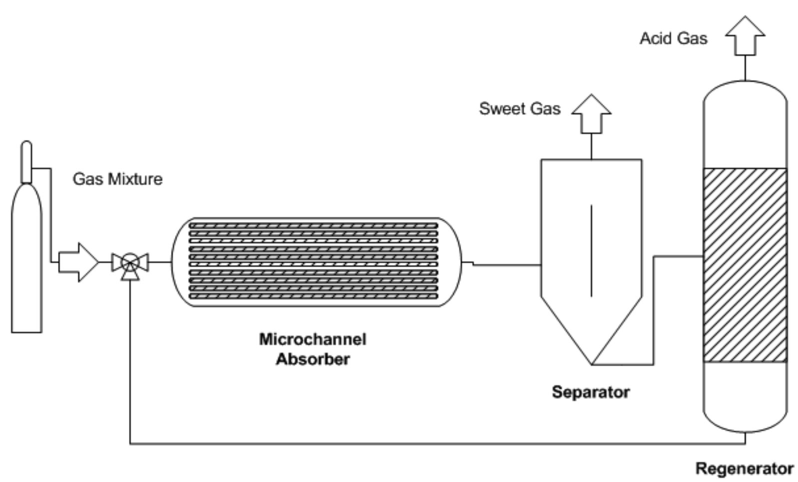

Figure 1. Schematic of the technology demonstrator unit.

Our previous experimental results indicate the most efficient conditions for a gas mixture of 6%, which is similar to the CO_2 content of the natural gas used in the Abu Dhabi acid gas removal plant. Based on these results, the unit will use a 100mL/min diethanolamine-solution flow rate with a 30 PSI, 100 mL/min gas mixture flow rate in a 750 µm Teflon tube.

The technology demonstrator unit should also include a scale up to a larger capacity, and thus ten parallel channels under the experimental conditions will be used. Based on this frame, we calculated the details of the technology demonstrator unit such as

- Temperature increase in the absorber
- Water loss and subsequent rise in concentration of the diethanolamine-solution.
- Lifetime for standard CO_2 and N_2 cylinders.
- CO_2 flow rates and concentrations at the outlets.

- N_2 flow rates.
- Heating and cooling powers.

All of these data were processed in EES, a common computer engineering calculation software, a screenshot of which is shown in Figure 2. To understand the process of a whole loop better, we analyzed the process flow diagram of one of Abu Dhabi National Oil Company's gas removal plants. From this data we calculated streams, process parameters, and efficiencies, especially for the desorption process.

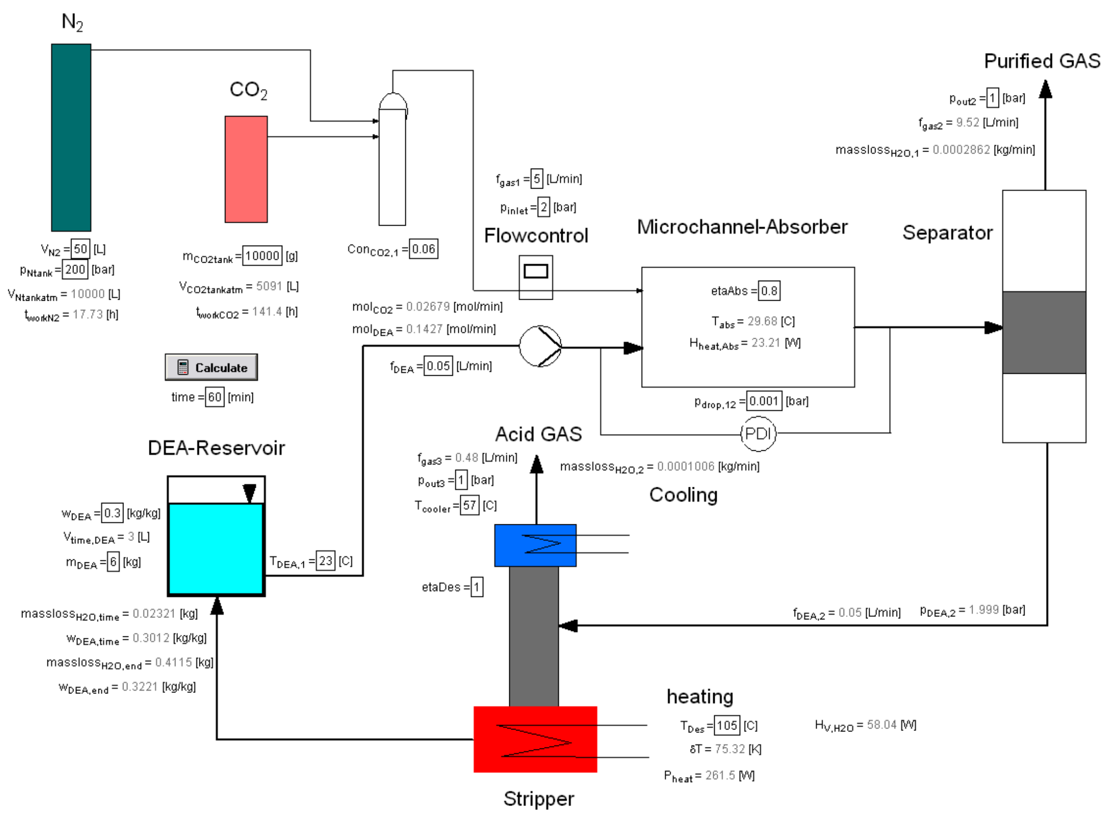

Figure 2. EES program screen shot.

The regenerator should be built using accepted stripper column methods instead of microchannel technology. Based on the work of Theodore and Ricci [1], the first dimensions were calculated for a regenerator column, a schematic of which is shown in Figure 3.

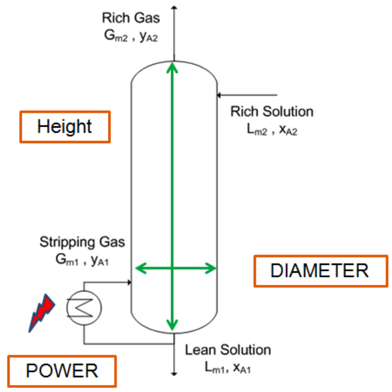

Figure 3. Schematic required dimensions of a regenerator.

The current setup of the technology demonstrator unit is shown in Figure 4, which illustrates the required measurement and control systems for the unit. Note also the microchannel absorbers. We intend to demonstrate, using two different types of microchannels, that channel length can be decreased by decreasing the diameter of the microchannel. The stream passes through a separator. Sweet gas is rejected through the outlet, where the purification of the gas and the efficiency of the absorber can be measured. To drive the experiment without using regenerated diethanolamine solution, the rich diethanolamine solution can be released directly into a storage tank. In the case where the regenerator is used, the whole loop is utilized so that the rich diethanolamine solution enters the regenerator on the left side, gets stripped, and is pumped back into the absorber. For the stripping process, sufficient heating and cooling power is required. The regenerator also requires the use of a number of measurement systems. Besides the need for flow meters, thermocouples, and pressure sensors, we have to measure the CO_2 concentrations, pressure drop, and liquid levels to control the whole plant.

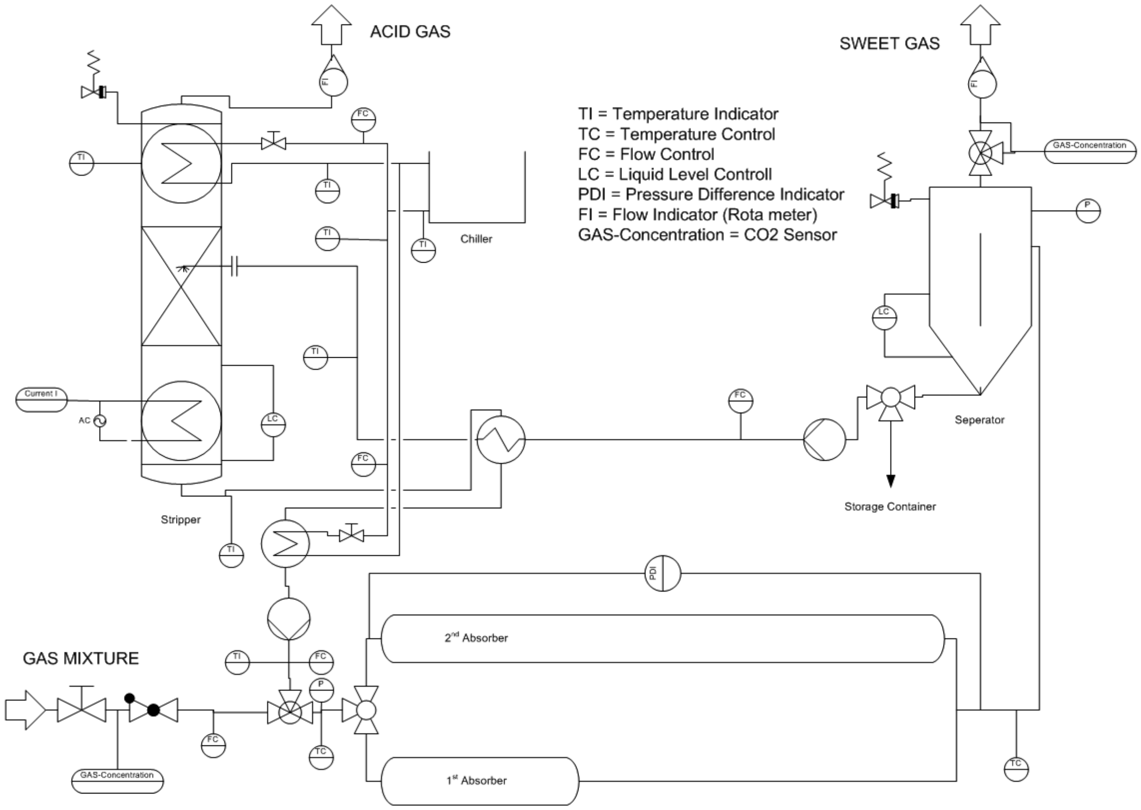

Figure 4. Schematic of measurement systems.

Summary of Results

In the reporting period we investigated the frame conditions for a technology demonstrator unit. We analyzed a detailed process flow diagram. Then, we set all flows and pressures and calculated the accruing reaction heat and required heat and cooling powers. We defined the required measurement and control systems.

Difficulties Encountered/Overcome

Design of a desorption column.

Planned Project Activities for the Next Quarter

- Finish the design of the technology demonstrator unit and assemble it.
- Complete a numerical/analytical model for the system.
- Prepare final project report and recommendations.

7. References

[1] Louis Theodore and Francesco Ricci, *Mass Transfer Operations for the Practicing Engineer* (2010).

Appendix

Justification and Background

The development of environmentally friendly process in industry is one of the major goals that have to be achieved. One way to approach cleaner environment is capturing or minimizing harmful gas components before emission to the atmosphere. One of the main gases which contribute significantly in global warming is CO_2. Due to a necessity to develop more efficient techniques for CO_2 capturing, scientific research in this area has been expanded rapidly. Since in the past very little R&D was devoted to CO_2 capture and separation technologies, opportunities for revolutionary improvements in CO_2 separation technologies is very high To maintain its competiveness and bring environmental friendly industry to the region, ADNOC has adopted various policies and approached it via many plans including “zero-flare” policy, acquiring more energy efficient process and the agreement signed with MASDAR to develop CO_2 capture technology. CO_2 separated from flue gases will be re-injected in oil wells, increasing oil production.

One of the promising concepts which can lead to major technology advancement is microchannel-based absorption units with enhanced kinetics. The objective of this study is to develop a full process of CO_2 separation from flue gas with incorporating micro-channel absorption technology at laboratory scale. The project addresses various stages of separation process: separation of solid particles and condensed water droplets and CO_2 separation using absorption process. Microchannel absorption CO_2 separator developed in this project will, significantly, increase the efficiency of separation process while decreasing energy consumption involved in such operation. Moreover, development of such technology will lead to reduction of equipment’s size and, therefore, minimizing the footprint and cost of equipment. An electrostatic separator will be used prior to CO_2 separation to remove solid and liquid contaminants from flue gas. The ultimate objective is to design all separation stages such that the overall performance will be optimized.

Approach

Detailed analysis and identification of the phenomena and the design challenges involved in effective implementation of the mechanism. Parametric study of existing and improved separators. Design iterations, including numerical flow and field simulations, fabrication, and testing. Creation of database and engineering design correlations.

Three-Year Schedule

The schedule below reflects the revised scope approved by both sides

<u>Year 1:</u>

- Conduct literature review to understand the basic of mass transfer in micrreactor and separation of flue gas;
- Evaluate existing technologies and assess their applicability to CO_2 separation of flue gas;
- Repeat and implement some previous classical examples of microchannel separation to get familiarized with fundamentals and basic challenge;
- Analyze mixing in microchannels and possibility to use it in CO_2 separation;
- Continue improving efficiency of EHD separator for the fine liquid and solid particles;
- Conduct visualization study of liquid and solid particles migration in the electrical field.

<u>Year 2:</u>

- Continue on literature survey;
- Selection of the target alkanolamine;

- Simulate mixing and separation phenomena in microreactor via modeling and analytical means;
- Develop laboratory scale microchannel absorber and desorber for CO_2 separation;
- Conduct Experimental study and design optimization study;
- Continue on visualization study of liquid and solid particles migration in the electrical field.

Year 3:

- Conduct visualization study on absorption and desorption in microchannels;
- Design iterations and implementation;
- Parametric study of CO_2 separation process and experiment on different designs;
- Continue on simulation of mixing and separation phenomena in microreactor via modeling and analytical means;
- Present the best design to ADNOC group of companies;
- Develop design correlation;
- Prepare report.

Microreactors for Oil and Gas Processes Using Microchannel Technologies

UMD Investigators: **Serguei Dessiatoun, Amir Shooshtari**
GRA: **Meera Mahadevan**
PI Investigators: **Afshin Goharzadeh, Ebrahim Al-Hajri**
Start Date: **Oct 2006**

1. Objective/Abstract

Microfabrication techniques are increasingly used in gas and petrochemical engineering to create structures with capabilities exceeding those of conventional macroscopic systems. In addition to already demonstrated chemical analysis applications, microfabricated chemical systems are expected to have a number of advantages for chemical synthesis, chemical kinetics studies, and process development. Chemical processing advantages from increased heat and mass transfer in small dimensions have been demonstrated with model gas, liquid and multiphase reaction systems.

This quarter, we have evaluated different applications of microreactors and their impact on the economy of the UAE industry has been conducted in this quarter. The application of microreactors in the polymerization of ethylene and propylene is feasible and may provide significant economic benefits, and therefore will be considered for further investigation in the current project.

2. Milestones/Deliverables Scheduled for the Completed Quarter

- Obtain useful kinetic data from batch-scale polymerization with the produced catalyst
- Initiate experiments in the microchannel reactor.

3. Summary of Project Activities for the Completed Quarter

Original Reactor Setup

A schematic diagram of the original reactor setup is shown in Figure 1.

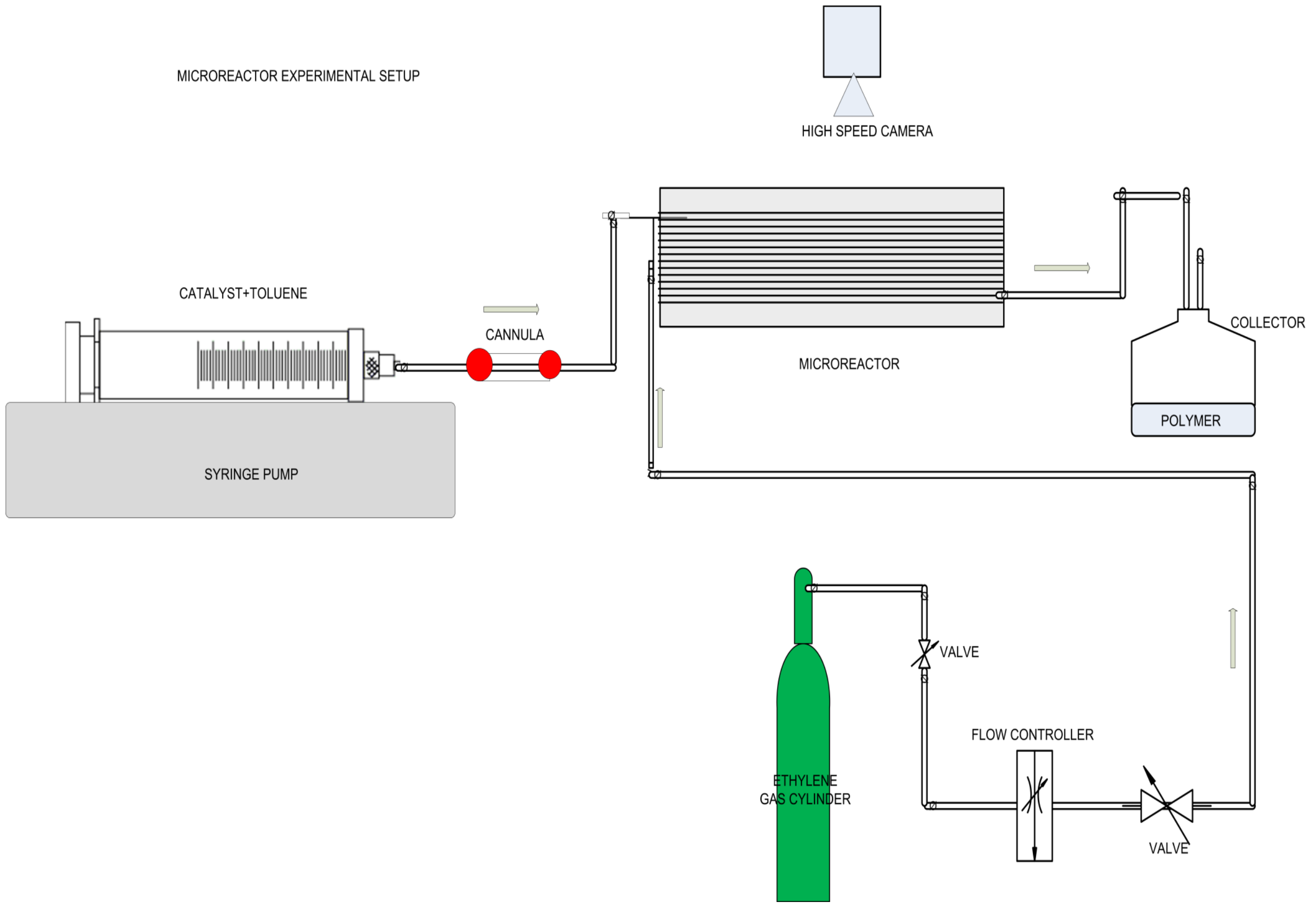

Figure 1. Schematic diagram of the original reactor setup.

To enhance absorption of ethylene in toluene, the reactor setup was modified to include an absorption system consisting of wound circular channels with a separate toluene inlet (from the syringe pump), as shown in Figure 2.

New Reactor Setup

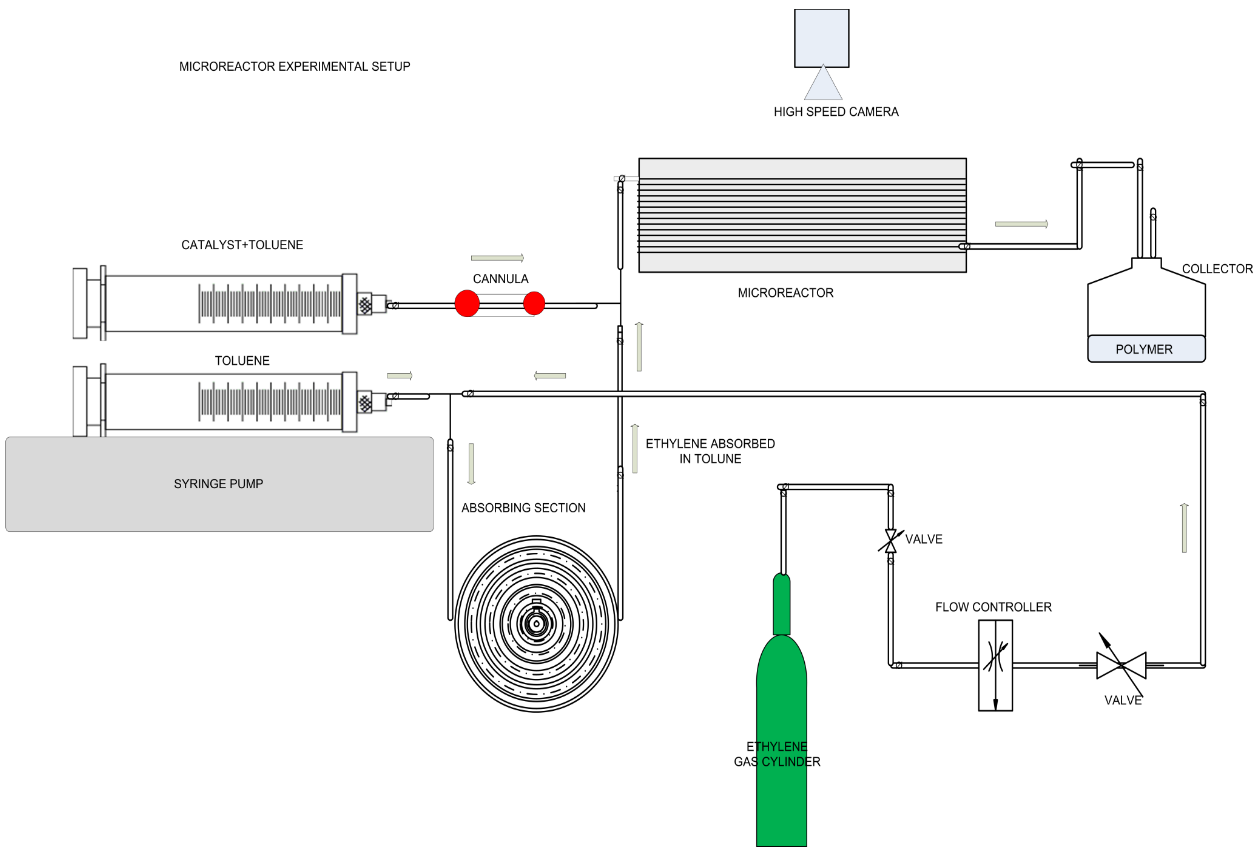

Figure 2. Modified reactor setup.

Photographs of the modified reactor are shown in Figure 3.

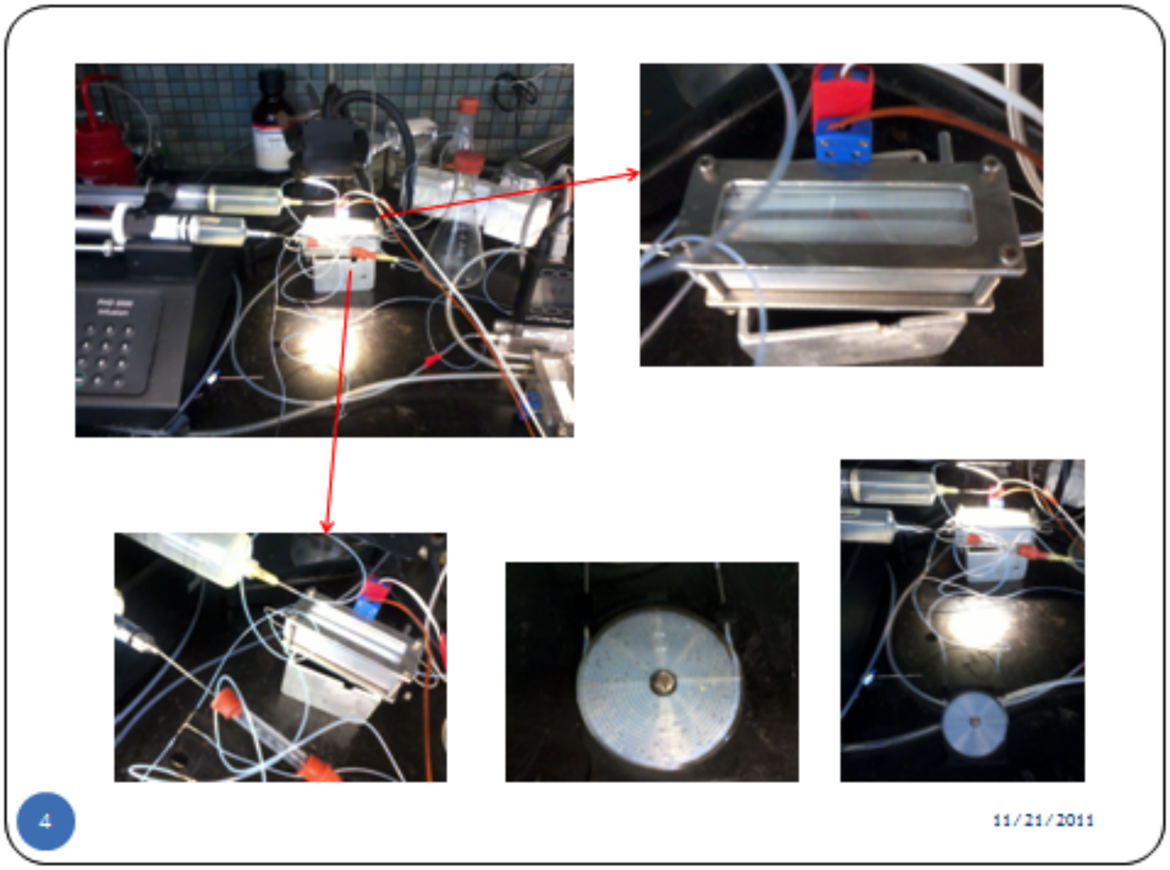

Figure 3. Laboratory setup.

Homogenous EBI Catalyst- Ethylene Polymerization

- **Reaction Conditions**
  - Temperature: 70°C
  - Pressure: 30 psi
  - Catalyst+toluene flowrate: 2 ml/min
  - Ethylene flowrate: 4 ml/min
  - Catalyst concentration: 0.009 g/L

SEM images of the polymer formed

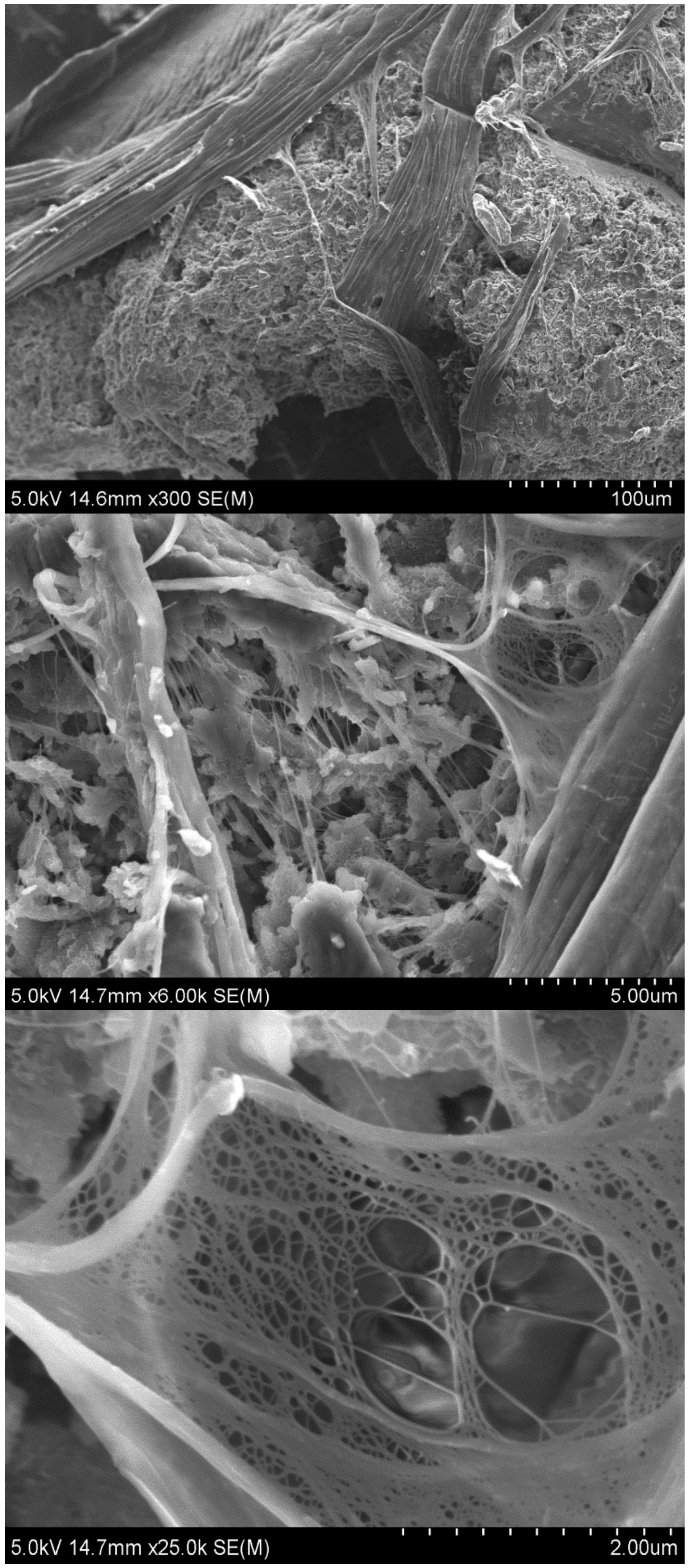

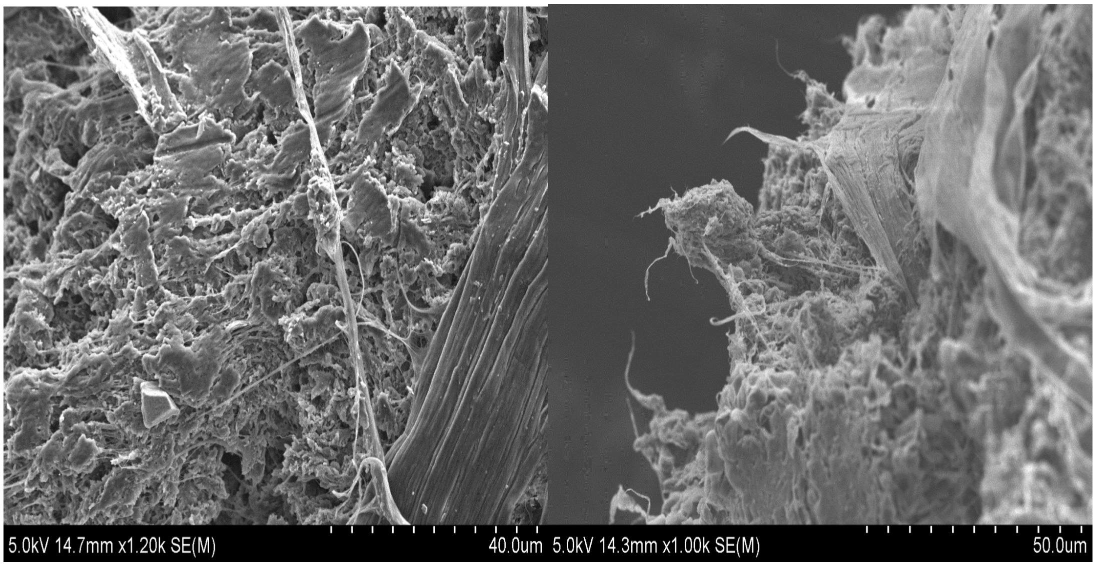

Figure 4. SEM images of the polymer formed with homogenous EBI catalyst-ethylene polymerization.

Using newly prepared nano-silica-EBI/MAO

Reaction Conditions

- Temperature: 70°C
- Pressure: 25 psi
- Catalyst+MAO+Toluene flowrate: 0.1 ml/min
- Toluene flowrate: 0.1 ml/min
- Ethylene flowrate: 2.8 ml/min
- Catalyst concentration: approx.
- Length of reacting portion: 2.2 m
- Diameter of tube: 630μm

SEM images of polymer formed

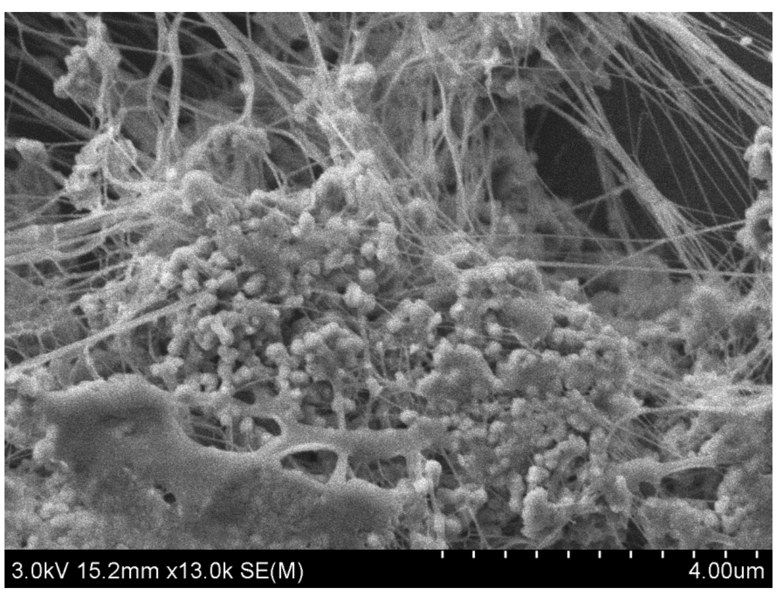

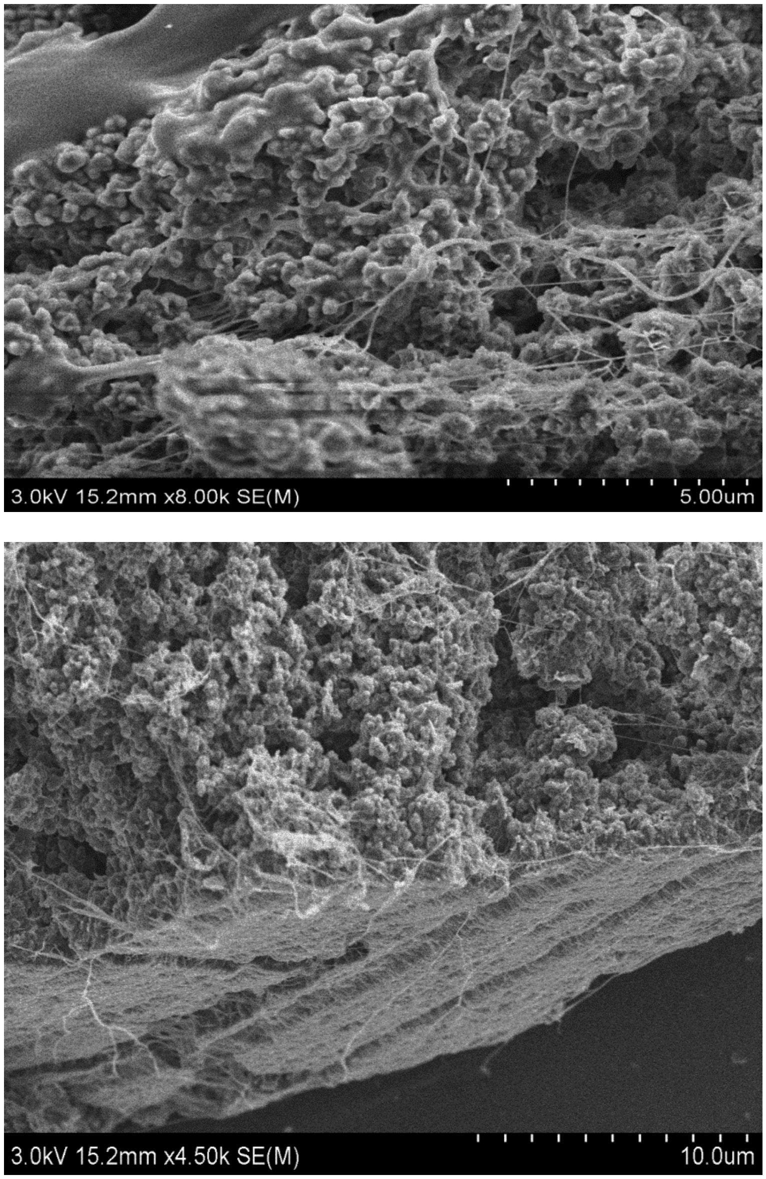

Figure 5. SEM images of the polymer formed using newly prepared nano-silica-EBI/MAO.

Polymer in the Teflon tube

Figure 6. Polymer in the Teflon tube.

Semi batch experiment for newly prepared catalyst

Reaction Conditions

- Temperature: 70°C
- Pressure: 30 psi

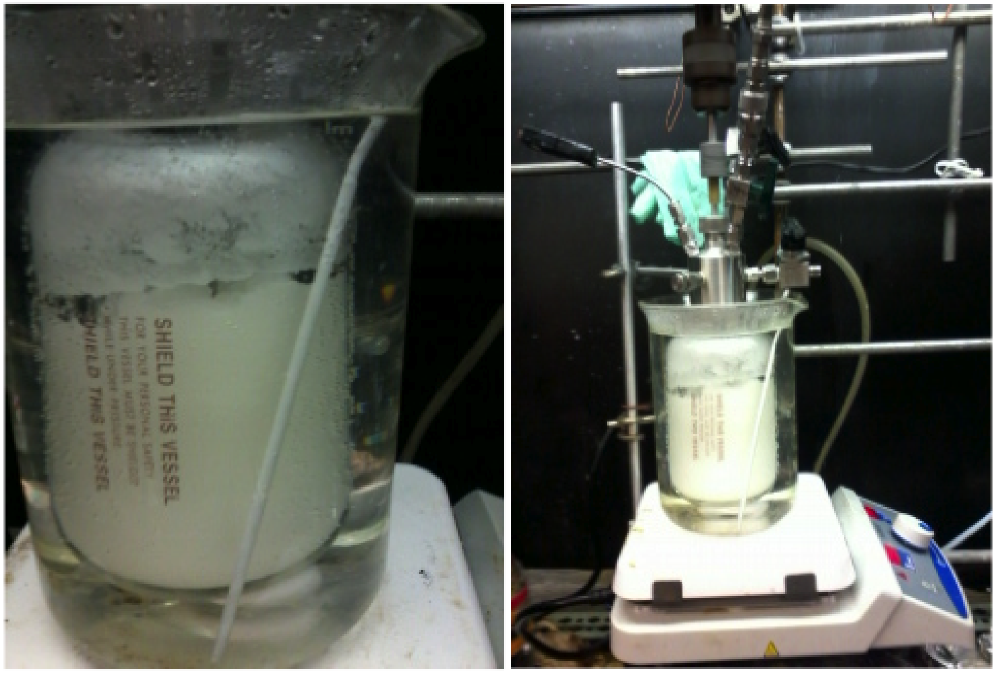

Figure 7. Test setup.

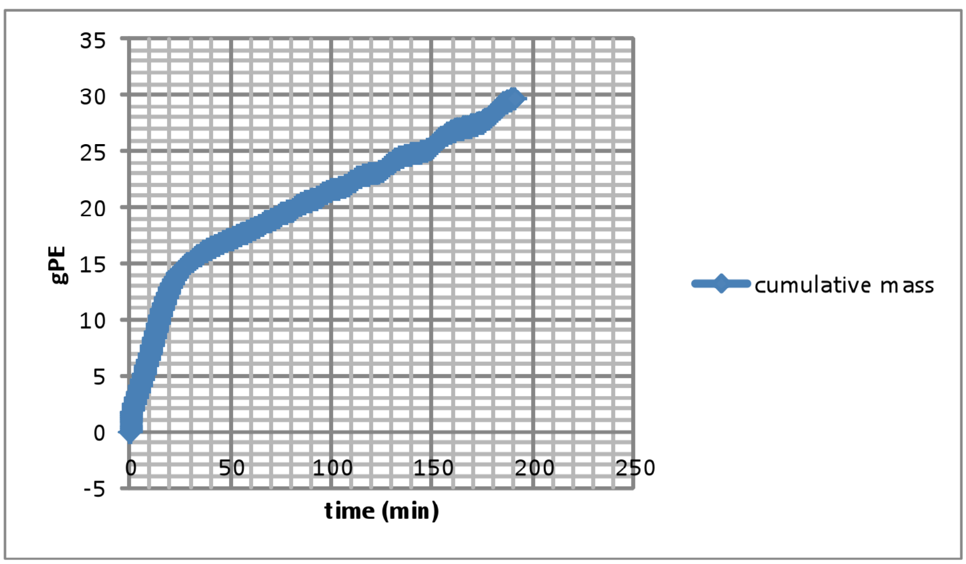

Figure 8.

Comparing kd values for different catalyst support

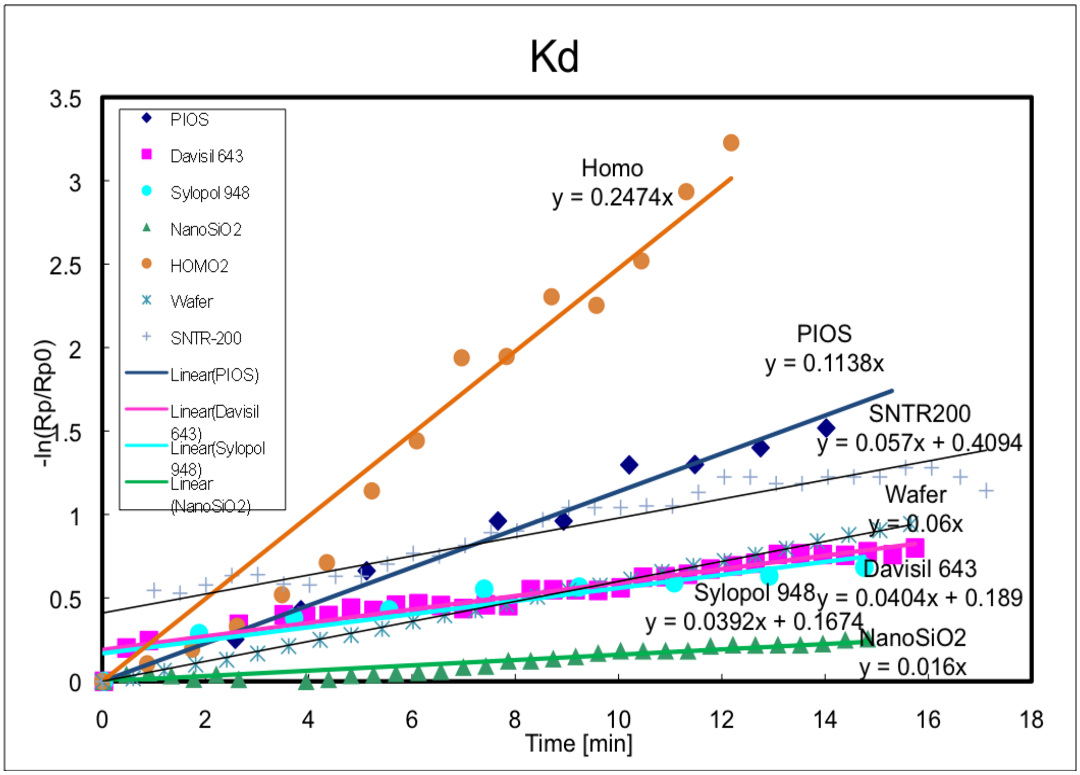

Figure 9. This plot shows that the catalyst prepared with nano silica particles as the support has the lowest kd values and hence a longer half life.

4. Difficulties Encountered/Overcome

- Polymer clogging was difficult to overcome, and sufficient polymer quantity could not be recovered.
- We have ordered some new syringes to minimize exposure of the catalyst and thus reduce reaction losses.
- Catalyst preparation is a tedious and time-consuming process and requires the glove box. This causes a long delay during which we could have conducted regular experiments to obtain more verifiable results.
- Also it would have been helpful to have easy access to polymer characterization equipment, since it gives useful data that covers the vast kinetics of polymerization.
- Despite the experiments being time consuming, we have made fair progress and derived some important results that can be applied directly to production of novel polymers in the microreactors.

5. Planned Project Activities for the Next Quarter

- Execute the reaction in the designed microreactor setup.
- Fine-tune the reaction parameters and conditions to enhance mass and heat transfer.
- Specify desired polymer properties and applications and modify the system parameters accordingly.
- Extend the reactor system to complex polymerizations and smaller channel dimensions.

- Theoretical modeling of particle level mass and heat transfer and fluid dynamics in microchannels.
- Build a test set-up to demonstrate scaled-out output of the reactor system.

Appendix

Justification and Background

Microreactors form a basis for the potential future downscaling of existing chemical processes, allowing tremendous reductions in capital and operating cost. They provide finer control of conditions, allow for faster process times, and improve safety in operation. Also, they should not encounter a significant problem in scaling from laboratory-sized systems to commercial-sized systems, since their operating principle will simply allow them to be stacked together modularly.

Of critical importance to the microreactors' capability to make the jump into industrial applications is the mixing efficiency, which controls the reaction rates and the yield expected from a reactor. Due to the scale of the systems, laminar flow is almost always encountered, which means that the vortices typically associated with turbulent flow are often missing. Instilling vortices into the flows to encourage mixing is accordingly a matter of construction of mixer channels.

Correct design parameters of microreactor influence the process yield. Designing microreactor for appropriate reaction conditions is very important for the reactions to be fast. Microreactors can be energy efficient too by appropriately designing and visualizing heat transfer. The channel dimensions have direct impact on diffusive mixing of reactants.

Approach

- Literature survey of the microreactor technologies as well as microchannel fabrication technologies.
- Selection of the target process for realization in microreactors with maximum benefit.
- Selection of microchannel fabrication technology suitable for microchannel mass production.
- Design and fabrication of a microreactor using microchannel fabricating technology suitable for mass production.
- Microreactor demonstration.
- Prepare experimental set-up and conduct the experiments.

Two-Year Schedule

<u>Year 1:</u>
Conduct literature review to study current technologies for micoreactors, micromixers, and incorporation of catalysts into microreaction technology.
Evaluate existing microchannel formation techniques and their applications to microreactor construction.
Selection of the target process for realization in microreactors with maximum benefit to ADNOC.
Selection of microchannel manufacturing process most suitable for mass production.
Preparation of a microreactor testing facility.
Visualization study of mixing in microchannels.

<u>Year 2:</u>
Literature survey of the olefin polymerization technologies focus on microchannels
Selection of the target polymerization process for realization in microreactors with maximum benefit.
Design and fabrication of a microreactor capable of realization of selected polymerization process
Select type and size of catalyst particles to be used in the process
Investigate propagation of selected catalyst particles in microchannels
Investigate polymerization and polymer particle behavior in microchannels

Parametric study of polymerization process at different temperatures, catalyst and reactant concentration.
Microreactor demonstration.
PI-side participation:
1. Selection in cooperation with Borouge of the catalyst for the target polymerization process for realization in microreactors.
2. Prepare a microreactor testing facility.
3. Visualization study of mixing in microchannels
4. Combine PI/UMD testing of the microreactor
5. Microreactor demonstration to ADNOC representatives
6. Prepare final project report and recommendations.

Thrust 3
Energy System Management

Integration of Engineering and Business Decisions for Robust Optimization of Petrochemical Systems

UMD Investigators: **Shapour Azarm, P.K. Kannan**
PI Investigators: **Ali Almansoori, Ali Elkamel**
UMD GRAs: **Weiwei Hu**
PI GRA: **Adeel Butt**
Start Date: **Oct 2006**

1. Objective/Abstract

The overall objective of this project is to develop a framework for integrating engineering and business decisions. In this quarter, our research efforts focused on two aspects: (1) finalizing a book chapter on optimization, and (2) optimizing operational variables for a refinery model. The manuscript for the invited book chapter on “Multi-Objective Optimization: Techniques and Applications in Chemical Engineering” was completed and submitted. In the book chapter, two Robust Multi-Objective Genetic Algorithms (RMOGAs), i.e., nested and sequential approaches were presented. Furthermore, an efficient online approximation technique which was developed earlier was combined with the two RMOGA approaches to reduce computational effort in a typical chemical process optimization. To extend the dashboard-based Decision Support System (DSS) framework with the crude oil processing units, the RMOGA approaches were connected with the newly developed crude oil refinery model in Matlab. Robust optimization was conducted to obtain optimal operational variables. The results show that the product (light naphtha) output and total cost in the process can be optimized simultaneously with a reasonable amount of computational time using the proposed RMOGA approaches.

2. Deliverables for the Completed Quarter

- Finalized the manuscript for the book chapter in “Multi-Objective Optimization: Techniques and Applications in Chemical Engineering”:
  - Defined and implemented a new objective robustness measure to restrict only downside variation in objective functions
  - Presented two important Robust Multi-Objective Genetic Algorithms (RMOGAs), i.e., a nested approach and a sequential approach
  - Combined an efficient online approximation technique with the two RMOGA approaches and compared them in terms of computational efficiency

- Conducted robust optimization for the newly developed crude oil refinery model and obtained optimal operational variables:
  - Developed a series of crude oil processing modules in Matlab to simulate the crude distillation process.
  - Connected a crude simulation model with a multi-objective optimizer to obtain optimal operational variables
  - Improved the product output and reduced cost in the process in the solutions obtained

- Progress on recent joint publications:

  Journal Papers:

  [1] Hu, W., M. Li, Azarm, S. and Almansoori, A., 2011, "Multi-Objective Robust Optimization Under Interval Uncertainty Using Online Approximation and Constraint Cuts," Journal of Mechanical Design, 133(6), pp. 061002-1 to 061002-9.

[2] Hu, W., A. Almansoori, Kannan, P.K., Azarm, S. and Wang, Z. 2010, "Corporate Dashboards for Integrated Business and Engineering Decisions in Oil Refineries: an Agent-Based Approach" Decision Support Systems, in press.

[3] Hu, W., Azarm, S. and Almansoori, 2011, "Approximation Assisted Multi-objective collaborative Robust Optimization (AA-McRO) under Interval Uncertainty," submitted to Structural of Multidisciplinary Optimization (reviews are back and the paper is under major revisions).

Book Chapter:
[4] Hu, W., Butt, A., Almansoori, A., Azarm, S. and A. Elkamel, 2011, *Robust Multi-Objective Genetic Algorithm under Interval Uncertainty*, in *Multi-Objective Optimization: Techniques and Applications in Chemical Engineering*, submitted.

Working Paper:
[5] Hu, W., Azarm, S. and Almansoori, A., 2011, "Uncertain Interval Reduction Approach with Multi-Objective Robust Optimization with Online Approximation," under preparation.

Working Conference Proceeding:
[6] Butt, A., Almansoori, A., Elkamel, A., Hu, W., Wang, Z., Kannan, P.K. and Azarm, S., "An Agent-Based Approach in an Integrated Corporate Dashboard for Oil Refinery," 2012 Canadian Operational Research Society (CORS) International Joint Conference, June 12-13.

3. Summary of Project Activities for the Completed Quarter

Project meetings held during the eleventh quarter were as follows:

- Four teleconference meetings were held between PI and UMD research collaborators: on Oct. 13, Oct. 30 Nov. 21 and Dec. 19, with Adobe Connection. Highlights of these meetings include:

(1) Progress on joint publications was discussed. Particularly, the timeline and schedule for the book chapter were presented and reviewed.
(2) The oil refinery model, developed by Adeel Butt during his summer internship at UMD, was used as a demonstration engineering example in the book chapter. The optimization result of the oil refinery example was reviewed.
(3) Plans on interacting with TAKREER engineers to extend the applicability of dashboard were discussed.
(4) Future directions of the research between UMD and PI were discussed during the meeting on Nov. 21.
(5) Timeline on finalizing and submitting the book chapter was determined during the meeting on Dec. 19th.
(6) Preliminary schedule on meeting with ADNOC companies (possible in late spring 2012) was briefly discussed.

Research efforts in this quarter included the following:

- Review of Book chapter: Online Approximation Assisted Robust Multi-Objective Genetic Algorithm (RMOGA)

Approximation techniques are commonly used in multi-objective optimization problems to replace a computationally expensive function with a meta-model (surrogate) and to alleviate computational cost (Ray et al., 2009; Voutchkov and Keane, 2010; Hu et al., 2011). Essentially, a meta-model is an inexpensive function which is able to give an estimate of the actual/true function value for a given value of a set of input variables. To construct a meta-model, a few sample points must be selected and then their actual function values observed or calculated. We define the sample space as a multi-dimensional space in which the coordinate axes represent the input variables to a meta-model. It is important to determine how many sample points are required and where these points should be placed in the sample space so that a sufficiently accurate meta-model is obtained.

In RMOGA, approximation can be used to estimate both objective and constraint functions values. Observing different objective and constraint function values using a sample point incurs a function call. The goal in approximation for RMOGA is to locate and observe a limited number of sample points while satisfying the accuracy for all objective and constraint functions. To achieve the goal, samples are placed in two stages. The first-stage (offline) samples are placed in the entire sample space using a space-filling sampling technique (Koehler and Owen, 1996). This is done before RMOGA starts. The second-stage (online) samples are placed based on the intermediate optimum solutions generated by RMOGA. The detail of the two-stage sampling technique is given below. The offline samples are generated initially based on a commonly used space-filling sampling technique called Latin Hypercube Sampling (LHS) (Koehler and Owen, 1996). These sample points are used to construct a meta-model for each objective and constraint function required by RMOGA. Note that each sample point needs to be observed once for all function values. Using the meta-models and the estimated function values, RMOGA obtains a set of estimated optimal solutions. From these estimated optimal solutions, a few are selected and observed, which are designated as the online samples. Both online and offline samples are combined and used to reconstruct/update the meta-models for the objective and constraint functions. Once the meta-models are updated, online sampling is repeated until RMOGA progressively approaches the true optimum solutions. One motivation to use the estimated optimum solution for online sampling is that they are potentially located in the sample space which is close to the true optimum solutions. By observing these sample points, the accuracy for all objective and constraint functions in the nearby region can be significantly improved. This will be beneficial for RMOGA to obtain a good estimate of Pareto optimum solutions.

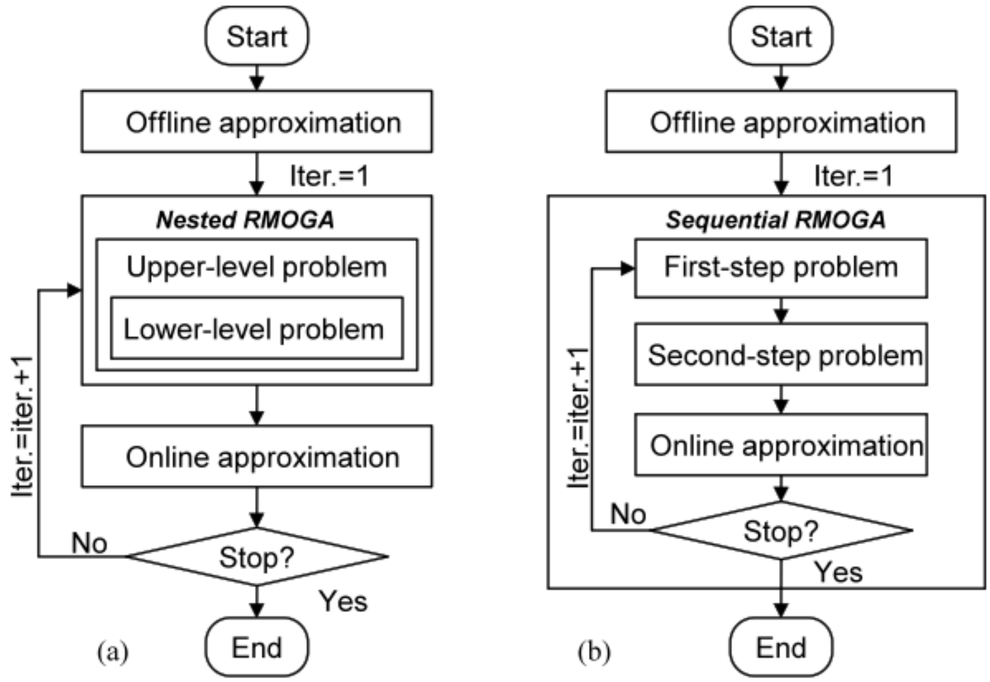

Figure 1. Flow diagram for online approximation assisted RMOGA: (a) Nested approach, (b) Sequential approach.

Generally, the objective and constraint functions in RMOGA can be replaced with meta-models (the approximated functions) when evaluating the objective and constraint functions requires expensive simulations. In Figure 1, the procedure for approximation assisted RMOGA is presented for the nested, Figure 1 (a), and sequential, Figure 1 (b), approaches, respectively. The steps for nested RMOGA approach are shown in Figure 1 (a). Initially, the meta-models for the objective and constraint functions are generated in the 'Offline approximation' block based on the space-filling samples. The meta-models are forwarded to the 'Nested RMOGA' block in which upper- and lower-level problems are solved. Notice that all objective and constraint function evaluations required by the nested RMOGA are approximated using the meta-models. When the nested RMOGA obtains an estimated set of optimum solutions, it sends them to the 'Online approximation' block, in which the online sample points are determined. Next, the online samples are combined with the previous (offline) samples and used to update the meta-models. While the stopping criteria (discussed later) are not satisfied, the updated meta-models are returned to the 'Nested RMOGA' block and the previous steps are repeated. For the sequential RMOGA approach in Figure 1 (b), it also starts with the "Offline approximation" block. However, because the sequential RMOGA needs to iterate between its first-step and second-step problems, the 'Online approximation' step is performed by the end of each iteration of sequential RMOGA as shown in Figure 1 (b). Notice this is different in the nested RMOGA, where online approximation is performed after nested RMOGA obtains the final estimated optimum solutions.

The following stopping criteria are used in both nested and sequential RMOGA approaches. That is, the approach is assumed to reach a solution if: (i) a maximum number of function calls is completed; (ii) no improvement in the Pareto solutions from one iteration to the next is obtained. One last comment in online approximation is that the sample space in RMOGA is a combination of both variables and uncertain parameters. To determine the values of variables for each online sample point, the approximation technique uses the optimum value of variables from each optimal solution. The values of uncertain parameters for the sample points are determined in two ways in the nested and sequential RMOGA. In the nested RMOGA, samples for the parameters are generated in a Latin Hypercube around each nominal point. However in the sequential RMOGA, the first-step problem determines the optimum values of variables and the second-step problem obtains the optimum values for the parameters. Therefore, the optimum value for parameters from the second step are paired with the optimum value of variables and used for online sampling.

- Robust Optimization of crude distillation/separation process

Crude oil distillation is a typical chemical process that is subject to uncertainties presented by the randomness in the input variables. The uncertainties in the input can produce undesirable variations in the process outputs in the objective and/or constraint functions. A traditional Multi-Objective Genetic Algorithm (MOGA) assumes that all inputs are deterministic. However, deterministic optimum solutions obtained from MOGA can be sensitive to uncertainty. In this research, a Robust MOGA (or RMOGA) was applied to obtain solutions that are optimum while also being relatively insensitive to the variations in objective and constraint functions. In our earlier research effort, two RMOGA approaches, one nested and the other sequential, have been developed. In both approaches, a measure of robustness is evaluated using a worst-case analysis. The worst case analysis assumes that the uncertainty in variables is expressed by an interval with pre-specified lower and upper bounds. In the nested RMOGA, in the upper-level, MOGA identifies and improves intermediate points while, in the lower-level, GA evaluates robustness of the intermediate points. In the sequential RMOGA, in the first-step, MOGA solve a multi-objective optimization problem and obtains optimal solutions, while in the second-step, GA evaluates the robustness of each optimal solution. To ease the computational cost, online approximation assisted method can also be applied with the RMOGA approaches. The approximation can be used to replace a computationally intensive simulation for objective and constraint functions with a much less computationally intensive model while adaptively improve accuracy of approximation as the solution is approached.

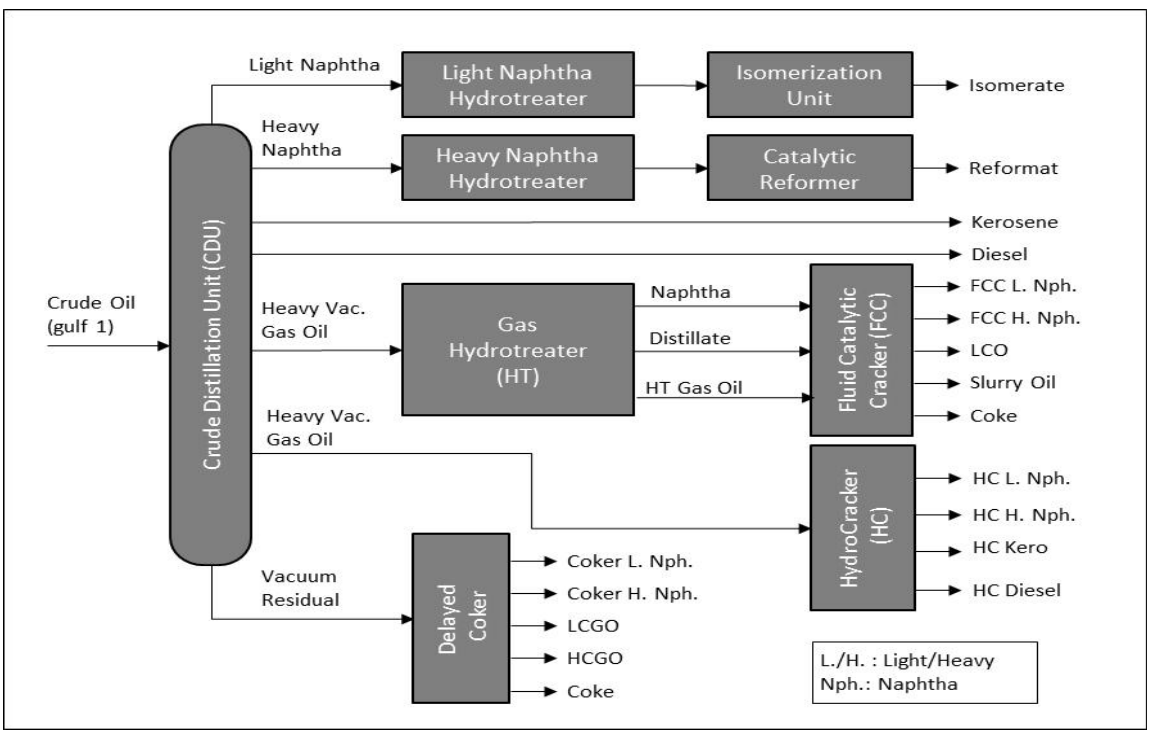

Figure 2. Schematic of crude oil refining model

The goal in robust optimization of the crude oil distillation process is to ensure the operation is efficient and cost-effective in order to maximize the profit for a given amount of crude input.

Figure 2 shows the schematic of a typical crude oil distillation process adopted at many refinery plants. The refinery consists of common unit process/operations, and non-linear correlations are used to predict the yields and properties of the products of each unit. The units in this refinery model are:

1. Crude distillation unit
2. Delayed coker
3. Hydrocracker for heavy vacuum gas oils
4. Hydrotreater for light vacuum gas oils
5. Fluid catalytic cracking unit (FCCU)
6. Hydrotreater for heavy straight run naphtha
7. Catalytic reformer
8. Light naphtha hydrotreater
9. Isomerization unit

The crude processing model as shown in Figure 2 depicts various unit processes and flows of intermediate product streams. The products out of the crude distillation unit are lower straight run (LSR) naphtha, higher straight run (HSR) naphtha, straight run diesel (SRD), kerosene, light vacuum gas oil (LVGO), heavy vacuum gas oil (HVGO) and vacuum residue (VacResid). The vacuum residue is further processed in the delayed coker to get the lighter fractions. The heavy vacuum gas oils are hydrocracked in the hydrocracker to get light naphtha and heavy naphtha fractions. The LVGO, HSR and LSR are hydrotreated to reduce the sulfur contents and further treated in FCCU, Catalytic reformer and isomerization unit respectively to get the products of interest. All naphtha is sent to the blending pool to get the gasoline for the required grade.

The simulation of the described refinery model is done through Matlab with simple non-linear correlations based on the built-in property library and functional relationships defined in PetroPlan. The profit models and physical property calculation models for each block are also included in the library files of software. For example, the assay (composition and material property) data of various type of crude oil can be obtained from a built-in spreadsheet in PetroPlan. It is assumed that 'Gulf' crude is the primary feedstock to the CDU as shown in Figure 2. The flow rate of crude oil to the crude distillation unit is assumed to be fixed with a value of 100,000 BPD (barrels per day). In Figure 1 the properties of outlet product streams from each block can be calculated from the inlet feed stream. For example, the flow rate of intermediate product streams from CDU block such as kerosene, Straight Run (SR) Diesel can be calculated according to the crude oil feed flow rate and the cut point temperatures. The blocks are solved in the order indicated by the user. It is up to the user to decide this sequence so that each block's feeds are calculated by preceding blocks. For simplicity, the schematic in Figure 1 does not include the utility units such as steam, cooling water and electricity. Also, the storage facilities such as crude oil and intermediate product storage tanks are not shown.

The refinery model is formulated as a multi-objective optimization problem as described in Eq. (1). The two objectives are to maximize the product flow rate f_1 and to minimize the cost f_2. Both objectives can be evaluated from the refinery simulation model for a given set of design variables. The variables considered for optimization are the six cut temperatures (t_i, i = 1,…, 6) in the crude distillation unit. The lower and upper bounds for the cut temperatures are given in Eq. (1). It is assumed that t_2 and t_3 are uncertain and the uncertainties are represented by Δt_i, j = 1, 2, and the range of uncertainties are between ±10% of their nominal cut temperature values.

$$
\begin{aligned}
&\max\ f_1(t_i) = \text{flow rate of light naphtha (bbl/day)}\\
&\min f_2(t_i) = \text{total cost(\$/day)}\\
&\text{s.t. } \left\| [f_m(t_i,\Delta t_j) - f_m(t_i)]^+ \right\| \le \eta_f\\
&\quad \forall \Delta t_j^l \le \Delta t_j \le \Delta t_j^u,\ j = 1,2, m = 1,2\\
&\quad 162 \le t_1 \le 198;\\
&\quad 360 \le t_2 \le 440;\\
&\quad 477 \le t_3 \le 583;\\
&\quad 585 \le t_4 \le 715;\\
&\quad 810 \le t_5 \le 950;\\
&\quad 950 \le t_6 \le 1155;
\end{aligned}
\tag{1}
$$

In the refinery example, the absolute values for the two objective functions are not in the same scale, e.g., the flow rate of light naphtha and total cost are in the order of 10^4 and 10^6, respectively. As such, the original value of the flow rate and total cost are first normalized to a value of unity using normalizing factors 10^5 and 10^7, respectively. The advantage of normalization is that using a Euclidean norm to restrict the objective variation as shown by the inequality constraint in Eq. (1), will give equal importance for both objectives. The acceptable variation limit η_f is specified as 0.1 in the refinery example. The optimization problem given in Eq. (1) is solved using both nested and sequential RMOGA approaches. For comparison purposes, the deterministic optimal solutions (assuming no uncertainty in the input) are also obtained. Both RMOGA approaches are run for a total of ten times and a best set of optimal solutions out of the ten runs are selected for each approach. The best sets of optimal solutions for both RMOGA approach are plotted in the objective functions space in Figure 3. It can be seen that the optimal solutions for the refinery example from both RMOGA approaches are consistent as well. It is also observed that the deterministic optimal solutions are better than both RMOGA approaches in achieving maximum flow rate of light naphtha, while the uncertainty in the cut temperature seems to have little effect on the daily total cost.

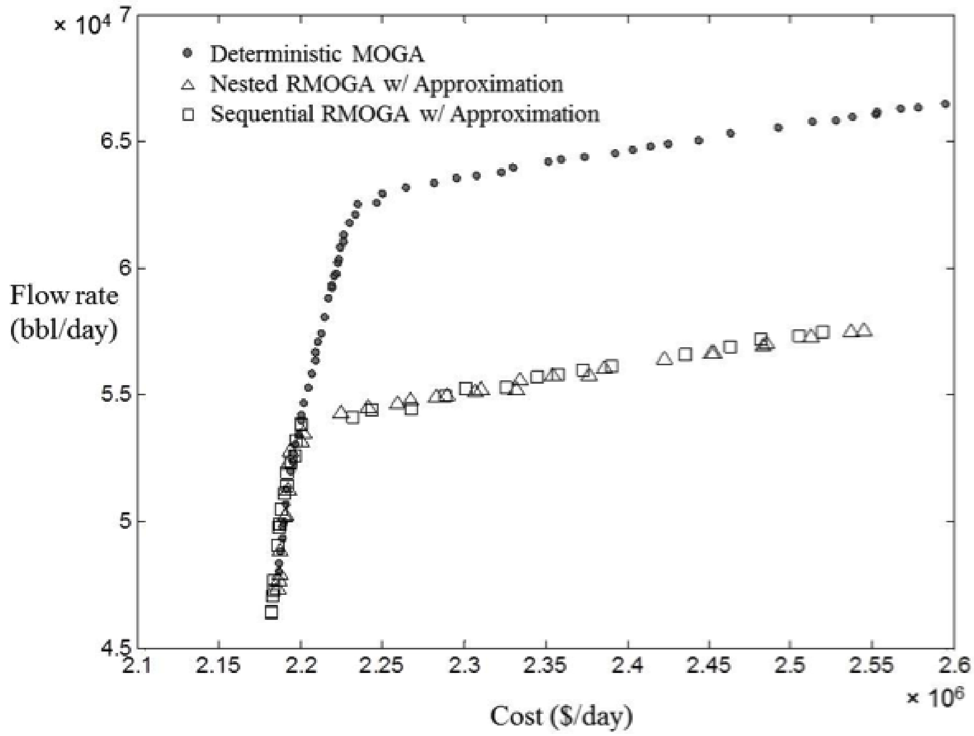

Figure 3. The optimal solutions for the refinery example.

The average value and standard deviation of the optimal solutions based on the ten runs for each of the RMOGA approach are shown in Table 1. The average number of iterations for both RMOGA approaches in the refinery example is 3. In terms of the quality of the obtained Pareto frontier, the sequential RMOGA approach performs slightly better (with a higher spread) than the nested approach. The number of total samples in both approaches is 28. Based on the maximum error in the approximated objective functions (less than 0.001), Kriging provides good accuracy in both RMOGA approaches. This is possibly due to the good characterization of the polynomial relationship between the input and output variables in the refinery model.

Table 1. Comparison between RMOGA approaches

	Nested RMOGA		**Sequential RMOGA**	
	mean	std.	mean	std.
Num. iterations	3	0.3	3	0.5
Hyperarea Difference (HD)	0.676	0.02	0.660	0.01
Overall Pareto Spread (OS)	0.177	0.07	0.219	0.05

4. Difficulties Encountered/Overcome

In last research quarter, a heat-integrated reactor-distillation simulation model was developed in HYSYS. In this simulation model, o-xylene was used to produce phthalic and maleic anhydride from a reactor and two-stage distillation process, where the purity in both phthalic and maleic anhydride columns were fixed and products flow rate are one of the variables. However in reality, the product flow rate is usually fixed or occasionally changes according to the demand of products from the internal and external market. Moreover, the purity for the product is the main variable for which we want to get robust optimal solution under uncertainty. With respect to the practical considerations, the heat-integrated model was modified with two main changes: (1) the purity restriction placed on both phthalic and maleic anhydride column was lifted and (2) the product flow rate was fixed at certain value. Based on the modifications, it was observed that in case of the maleic anhydride column, the product flow rate was in the range between 500 to 600 kg/hr. When the flow rate is slowly increased, i.e. 1kg /hr, the column is converging up-to 600 kg/hr. However, when the flow rate was changed with the step size up-to 10kg/hr, the model was not able to converge. In order to obtain converged solution, some of the operational parameters in both phthalic anhydride and maleic anhydride distillation columns need to be revised so that the maximum mass flow rate of both products can be accommodated. Currently, the o-xylene feed flow rate was set at 7000kg/hr and a maximum amount of phthalic anhydride was recovered from the bottom stream of the distillation column. But in case of maleic anhydride, the product flow rate was about 4300 kg/hr with only 600 kg/hr recovered. This is probably due to the design capacity limitations in maleic anhydride column.

5. Planned Project Activities for the Next Quarter

- Continue revising the HYSYS based heat-integrated simulation model (as presented in the difficulty encountered/overcome section).
- Increase the complexity of the engineering model in dashboard by developing a crude oil refinery simulation model using Matlab based on HPI correlations.
- Refine the business model in dashboard with practical considerations based on the feedback from TAKREER as a case study.
- Remodel the dashboard by integrating the revised engineering and business models.

Extend the scope of the dashboard to include the upstream (crude oil exploration and production) process in the oil company.

6. References

[1] Aspen HYSYS, 2009, http://www.aspentech.com, Aspen Technology.
[2] Deb, K., 2001, “Multi-Objective Optimization using Evolutionary Algorithms,” John Wiley & Sons, Ltd, New York.
[3] Douglas, J.M., 1988, “Conceptual Design of Chemical Processes”, McGraw-Hill, New York, USA.
[4] Forbes, R.J., 1948, “Short History of the Art of Distillation”, Brill, Leiden, Holland.
[5] Gargeya, V., 2005, “Plant Level Performance Measurement: An Exploratory Case Study of a Pharmaceutical Encapsulation Company”, Technovation, 25(12), pp.1457-1467.
[6] Gattu, G., Palavajjhala, S., and Robertson, D., 2003, “Are Oil Refineries Ready for Non-Linear Control and Optimization?” International Symposium on Process Systems Engineering and Control, Mumbai, India.
[7] Grossmann, I. E., 2005, “Enterprise-Wide Optimization: A New Frontier in Process Systems Engineering,” AIChE Journal, 51(7), pp. 1846-1857.
[8] Halemane K. P., Grossmann I. E., 1983, “Optimal Process Design under Uncertainty,” AIChE Journal, 29(3), pp. 425-433.
[9] Hu, W., M. Li, Azarm, S. and Almansoori, A., 2011, "Multi-Objective Robust Optimization Under Interval Uncertainty Using Online Approximation and Constraint Cuts," Journal of Mechanical Design, 133(6), p. 061002.

[10] Jackson, J., Hofmann, J., Wassick, J. and Grossmann, I., 2003, "A nonlinear multi-period process optimization model for production planning in multi-plant facilities", Proceedings FOCAPO2003, pp. 281-284..
[11] Janak, L., Lin, X. and Floudas, C. A., 2007, "A New Robust Optimization Approach for Scheduling Under Uncertainty: II. Uncertainty with Known Probability Distribution," Computers and Chemical Engineering, 31(3), pp. 171-195.
[12] Kaplan, R. and Norton, D., 1996, "Using the Balanced Scorecard As a Strategic Management System", Harvard Business Review, 74(1), pp. 75-85.
[13] Kleijnen, J. and Smits, M., 2003, "Performance metrics in supply chain management". Journal of the Operational Research Society, 54(5), pp. 507–514.
[14] Koehler, J.R., Owen, A.B., 1996, "Computer Experiments," Handbook of Statistics, Elsevier Science, New York. pp. 261-308.
[15] Lin, X., Janak, S. L. and Floudas, C. A., 2004, "A New Robust Optimization Approach for Scheduling Under Uncertainty: I. Bounded Uncertainty," Computers and Chemical Engineering, 28(6-7), pp. 1069-1085.
[16] Linnhoff, B., Townsend, W., Boland, D., Hewitt, F., Thomas, E., Guy, R. and Marsland, H., 1982, "User Guide on Process Integration for the Efficient Use of Energy," IChemE, UK.
[17] Li, M., and Azarm, S., 2008, "Multiobjective Collaborative Robust Optimization with Interval Uncertainty and Interdisciplinary Uncertainty Propagation," Journal of Mechanical Design, 130(8), p. 081402.
[18] Micheletto, S. R., Carvalho, M. C. A. and Pinto, J. M., 2008, "Operational Optimization of the Utility System of an Oil Refinery," Computers and Chemical Engineering, 32(1-2), pp. 170-185.
[19] Netlogo, http://ccl.northwestern.edu/netlogo/, Sep., 2011.
[20] PetroPlan, http://www.ingeniousinc.com/proplan-main.php, Sep., 2011.
[21] Pinto, J., Joly, M. and Moro, L., 2000, "Planning and scheduling models for refinery operations", Computers and Chemical Engineering, 24(9), pp. 2259–2276.
[22] Ray, T., Isaacs, A. & Smith, W., 2009, "Surrogate Assisted Evolutionary Algorithm for Multi-Objective Optimization," Multi-Objective Optimization: Techniques and Applications in Chemical Engineering World Scientific. pp. 131-149.
[23] Sahdev, M., Jain, K., Srivastava, P., "Petroleum Refinery Planning and optimization Using Linear Programming", The Chemical Engineers' Resource Page, http://www.cheresources.com/refinery_planning_optimization.shtml
[24] Simpson, T. W., and Mistree, F., 2001, "Kriging Models for Global Approximation in Simulation-Based Multidisciplinary Design Optimization," AIAA Journal, 39(12), pp. 2233-2241.
[25] Suresh, S. Pitty, Li, W., Adhitya, A., Srinivasan, R., Karimi, A., 2008, "Decision support for integrated refinery supply chains", Computer and Chemical Engineering, 32, pp. 2767–2786.
[26] Voutchkov, I. and Keane, A., 2010, "Multi-objective Optimization Using Surrogates," Computational Intelligence in Optimization. Springer, Berlin. pp. 155-175.
[27] Wang, Z., Azarm, S. and Kannan, P.K., 2011, "Strategic Design Decisions for Uncertain Market Systems Using an Agent Based Approach," Journal of Mechanical Design," 133(4), pp. 041003-1 to 041003-11

Appendix

Justification and Background

Many oil, gas and petrochemical systems involve numerous coupled subsystems. These systems and their subsystems usually have uncertain inputs and thus it can be difficult to make the "best" engineering and business decisions in terms of independent operations of these complex systems. It becomes even more difficult to make those decisions when the system consists of many units or plants producing different products. This difficulty presents an opportunity taken on in this project. A review of mainstream literature has revealed that previous models in management of petrochemical systems have been based on either engineering or business decisions but not both. There is a significant gap in the literature as to how these two types of decisions should be devised and integrated. To address this important gap, the focus of this investigation is to develop an integrated robust decision support framework considering both engineering and business models under uncertain conditions. Our overall objective has several underlying research questions, including: (i) how to develop business models that include management decisions in a multi-unit organization and at the same time account for engineering aspects; (ii) how to determine the relative importance and effects of uncertain system and/or subsystem input parameters on subsystem and/or system outputs (e.g., system performance); (iii) how to define a set of metrics, by way of a dashboard, that will serve as a visualization tool to keep track of a company's financial status in view of competition and market systems and provide for easy communication between various levels in the company, and (iii) how to extend our current single-level robust optimization method to multi-subsystem problems and maintain reasonable computational complexity for the method. These underlying questions and corresponding investigations will be organized into tasks throughout the time frame allocated to the project. The details of these tasks are explained in the next section.

Approach

There are two main tasks in this investigation as detailed in the following.

Task 1 (PI):
Develop and implement engineering analysis models, in a Matlab (or Matlab compatible) environment, for a crude distillation unit case study model.

[28] Task 1.1: Develop a multi-input multi-output analysis model for a representative petrochemical system with corresponding subsystem analysis models.
[29] Task 1.2: Extend the analysis model in Task 1.1 to include: (i) additional complexity, (ii) subsystem details and uncertainty to include reasonable representation of engineering side of a plant. The ultimate goal is to develop an integrated multi-subsystem petrochemical analysis model for a plant or a group of units in a plant.

Task 2 (UMD):
Develop and implement a Robust Decision Support System (RDSS).

Engineering Tasks
[30] Task 2.1: Develop a single level (all-at-once) approximation-assisted robust optimization technique that is able to significantly reduce the computational efforts of making robust decisions.
[31] Task 2.2: Demonstrate an application of the approach from Task 2.1 with a case study in petrochemical systems which will be developed by PI as a part of Task 1.

[32] Task 2.3: Develop an approximation assisted multi-objective multi-disciplinary robust optimization approach, which is an extension to Task 2.1.

[33] Task 2.4: Demonstrate an application of the approach from Task 2.3 with a case study in petrochemical systems which will be developed by PI as part of Task 1.

Business Tasks

- Task 2.5: Develop business models in Netlogo and/or Matlab and solve a simplified refinery supply chain optimization problem with Matlab.
- Task 2.6: Develop a Dashboard and test the robustness and sensitivity of the Dashboard's elements for the model in Task 2.5.

Integration Tasks

- Task 2.7: Inspect engineering and business problems to determine coupling variables between two problems.
- Task 2.8: Integrate Tasks 2.1 to 2.4 with Tasks 2.5 to 2.6 to formulate a refinery optimization problem that considers both engineering and business objectives and constraints.
- Task 2.9: make the supply chain management problem more realistic by considering more decision levels, more finished products and a wider market, and by increasing the size of the refinery's internal network and then repeat Task 2.8.
- Task 2.10: Verify and validate the integrated model.

Dynamics and Control of Drill Strings

UMD Investigator: **Balakumar Balachandran**
PI Investigators: **Hamad Karki and Youssef Abdelmagid**
GRA: **Chien-Min Liao (started in Spring 2007)**
Start Date: **Oct. 2006**

1. Objectives/Abstract

Drill-string dynamics need to be better understood to understand drill-string failures, control drill-string motion and steer them to their appropriate locations in oil wells. Although a considerable amount of work has been carried out on understanding drill-string vibrations (for example, Leine and van Campen, 2002; Elakhessou *et al*., 2003; Spanos *et al*., 2003; Liao *et al*., 2009), the nonlinear dynamics of this system are only partially understood given that the drill string can undergo axial, torsional, and lateral vibrations, and operational difficulties including sticking, buckling, and fatiguing of strings. In addition, the prior models focus on either bending or torsional or axial motions. Hence, it is important to consider coupled axial-bending-torsional vibrations and contact instability in oil and gas well drilling. A better understanding of these vibrations can help keep the drill string close to the center of the borehole and help realize near-circular bores during drilling operations.

The overall goal of the proposed research is to understand the nonlinear dynamics of the drill string and develop a control-theoretic framework for its stabilization enabling energy efficient drilling with longer life span for the equipment. Specific research objectives of this project are the following: i) building on Phase I efforts, develop and study control-oriented models for the drill strings through analytical and numerical means; ii) investigate the control of an under-actuated nonlinear system (drill string) with complex interactions with the environment, and iii) use the drill-string test-beds constructed at the Petroleum Institute (PI) & the University of Maryland (UMD) to validate the analytical findings and suggest possible strategies to mitigate drill-string failures in fixed and floating platform environments.

2. Summary of results

In the previous report, the investigators compared numerical results to experimental data in order to explore the presence of geometric nonlinearities. These geometric nonlinearities are suspected to dominate the dynamics for horizontal and curved drilling configurations. In the current report, the authors examine the torsional vibrations of the experimental drill string apparatus. In order to study large amplitude vibrations in the experiment, a slender drill string was used. The torsional vibration time histories were recorded using strain gages along with a slip ring and data acquisition system.

The rest of this section is organized as follows. In Section 2.1, the experimental apparatus used to study the torsional vibrations is described. In Section 2.2, the obtained experimental data are presented. Advances made in the horizontal drill string experimental apparatus are presented in Section 2.3.

2.1 Experimental arrangement

The experimental arrangement used to study drill string dynamics is presented in Figure 1. The aluminum drill string is 1.82 m long and 3.2 mm in diameter. These dimensions allow for large amplitude torsional vibration amplitudes, which actual drill strings experience while in operation. The torsional strain may then be extracted using a special configuration of strain gages. Under a single mode assumption, the torsional displacement may be estimated from the measured strain.

The “Top Assembly” section of the experimental apparatus was described in a previous report (July 2011); a photograph is shown in Figure 2(a) in order to show the location of the strain gages. An additional photograph of the strain gages is provided in Figure 2(b). For completeness, a photograph of the “Bottom Assembly” is provided in Figure 2(c). The signal from the strain gages is fed through a slip ring assembly, and the signal time history is recorded using a data acquisition system. By using an external trigger, the strain gage data can be synchronized with a video camera, and both strain and video can be recorded as a function of time.

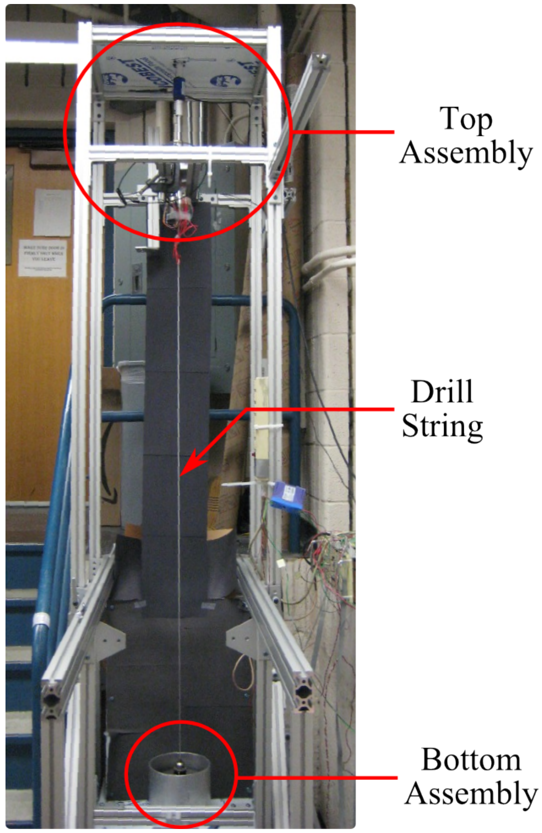

Figure 1. A photograph of the vertical drill string apparatus.

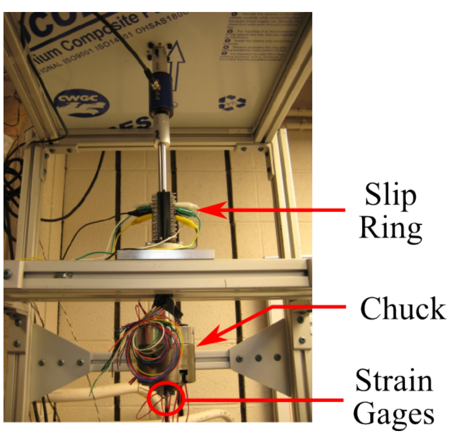

(a)

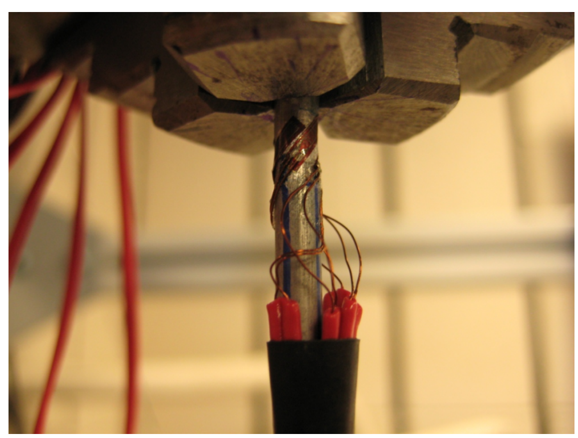

(b)

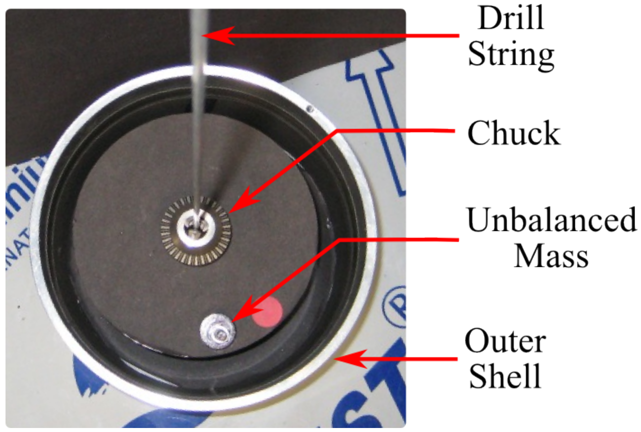

(c)

Figure 2. Photographs of various sections of the vertical drill string apparatus: (a) The top assembly with the location of the strain gages. (b) A close-up photograph of the strain gage configuration. (c) The bottom assembly.

A schematic of the strain gage configuration is seen in Figure 3. Four strain gages are mounted at equal 90 degree spacing around the circumference of the drill string. In order to measure the torsional strain, the gages are oriented at 45 degrees with respect to the longitudinal axis of the string. During the experiments, the sensors measured a combination of the torsional strain and bending strain.

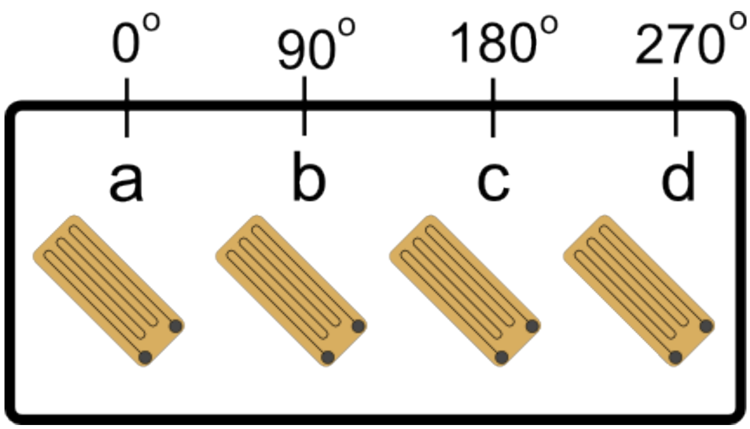

Figure 3. The strain gage configuration seen in Figure 2.1.2(b). The degree denominations indicate the location of the strain gages circumferentially around the string.

For the purposes of these experiments, we wanted to measure only the strain due to torsion, and so the coupling from the bending strain was undesirable. Each of the four strain gage measurements may be decomposed as follows:

$$\begin{aligned}
\varepsilon_a &= \varepsilon_{tor} + \varepsilon_{bc} \\
\varepsilon_b &= \varepsilon_{tor} + \varepsilon_{bc'} \\
\varepsilon_c &= \varepsilon_{tor} - \varepsilon_{bc} \\
\varepsilon_d &= \varepsilon_{tor} - \varepsilon_{bc'}
\end{aligned} \qquad (1)$$

In the above equations, ε_{bc} and $\varepsilon_{bc'}$ are the undesired bending coupling strains. The expression for ε_a and ε_c as well as ε_b and ε_d may be combined, respectively, to eliminate the bending coupling strain and extract the strain from pure torsion. The following section presents experimental results obtained with the experimental apparatus described below.

2.2 Experimental Results

In the current section, data obtained from the experimental arrangement explained above are presented. The strain gage readings may be synchronized with the video camera by using an external triggering system. The data presented in Figure 4 correspond to backward whirling motions. The rotor trajectory is given in Figure 4(a), and the Fourier transforms of the displacements are shown in Figure 4(b). During this specific experimental run, the driving speed of the motor was set to 39RPM, or equivalently 0.62Hz. Due to contact with the outer shell and the ensuing backward whirling motions, the lateral response frequency was approximately 4 times the driving speed, which corresponds to a spike at 2.49Hz in the Fourier spectra as shown in Figure 4(b). Likewise, the torsional strain time histories and Fourier spectra for the motions given in Figure 4(a) are presented in Figure 4(c). The dominating response frequency for the torsional response was approximately 3.3Hz. This response is close to the driving speed plus the whirling speed. The response spectra information is useful for field applications. If the addition of the driving speed and whirling speed coincides with one of the torsional natural frequencies of the system, a resonance may occur and consequently may cause damage to the drill string.

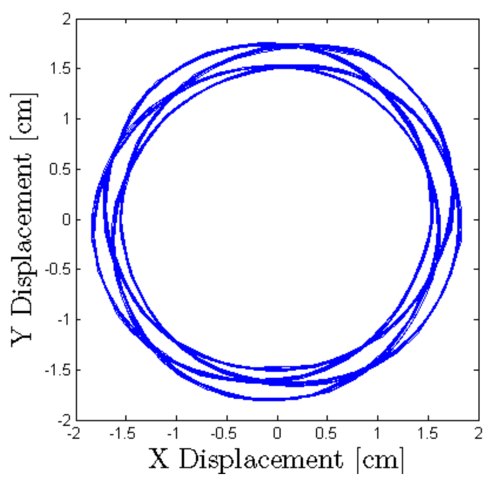

(a)

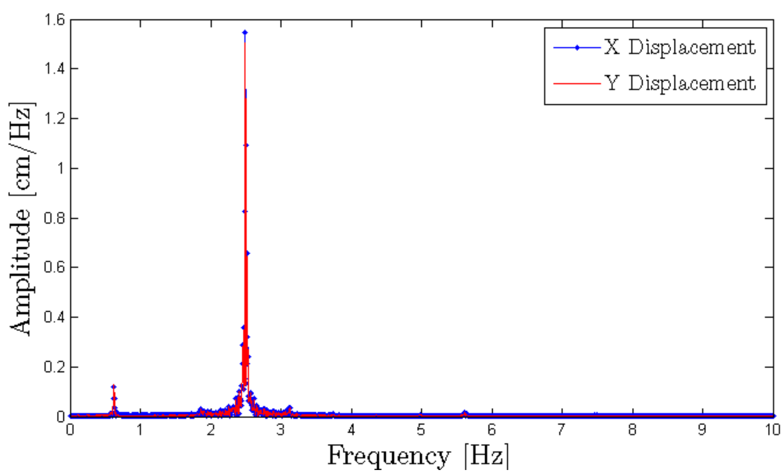

(b)

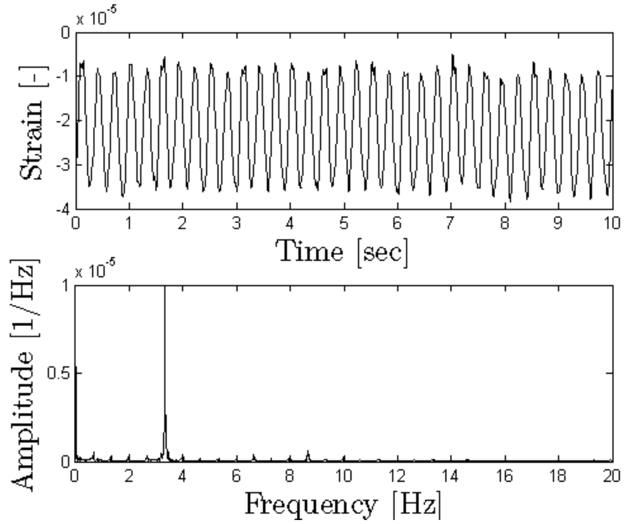

(c)

Figure 4. Experimental results. (a) Trajectory of the rotor geometric center while undergoing backward whirling motions. (b) The Fourier spectra of the lateral displacement histories. (c) The torsional strain history and Fourier spectra for the rotor motions during backward whirling.

2.3 Horizontal drill string experimental apparatus

A previous report (October 2011) contained a conceptual depiction of the bottom assembly mechanism of the horizontal and curved drilling experimental apparatus. The assembly has been completed and a photograph is shown in Figure 5. The actuator and brake pad assembly can be used to excite torsional vibrations, while the rotary encoder can measure rotational displacements of the string. The entire encoder-actuator-brake assembly is mounted onto a platform that sits atop a linear bearing. An electrodynamic shaker excites the entire assembly along the axial direction. The complete bottom assembly is to be used to replicate the forces experienced by a drill bit while in operation. Using the camera and strain gage system described in the previous section, the response of the drill string can be recorded for various excitations.

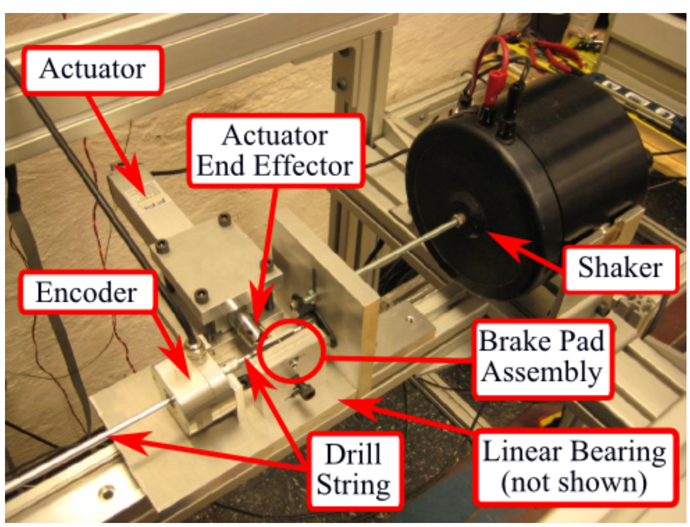

Figure 5. A photograph of the completed bottom assembly mechanism.

3. Discussion and future work

The current report presented experimental results for a vertical drill string that included both lateral and torsional vibrations. From the Fourier spectra of the torsional vibrations, it was found that under whirling conditions the torsional vibrations occur at the drive speed plus the whirling speed. Drill operators should be cautious to avoid these driving speeds, as they may excite torsional vibrations, thus damaging the drill string.

Advances have been made on the horizontal and curved drill string experimental apparatus. The bottom assembly mechanism is complete, and this arrangement can be used to recreate the forces experienced on a drill bit while in operation. Using data from this experiment, recommendations and guidelines can be established to enhance horizontal drilling operations. Future reports will contain data from this experimental arrangement.

4. Interactions

A journal paper is under preparation for the *ASME Journal of Vibration and Acoustics*, and recently, a journal paper was published in the January issue of the International Journal of Mechanical Sciences. The paper information follows:

Liao, C.-M., Vlajic, N., Karki, H., and Balachandran, B., 2012, "Parametric Studies on Drill-String Motions," *International Journal of Mechanical Sciences*, Vol. 54, pp. 260-268.

5. References

[1] Akgun, F. (2004), "A Finite Element Model for Analyzing Horizontal Well BHA Behavior," J. of Petrol. Sci & Eng., Vol. 42, pp. 121-132.

[2] Bednarz, S. (2004), "Design and Exploitation Problems of Drill Strings in Directional Drilling," Acta Montanistica Slovaca, Vol. 9, pp. 152-155.

[3] Downtown, G.,(2009), "*New Directions in Rotary Steerable Drilling"*, Oilfield Review, pp. 18-29.

[4] Feng, Z., and Zhang, X., (2002), "Rubbing phenomena in rotor-stator contact". Chaos, Solitons, & Fractals, 14(2), August, pp. 257–267.

[5] Leine, R. I., van Campen, D. H., and Keultjes, W. J. G. (2002). "Stick-Slip Whirl Interaction in Drill String Dynamics," *ASME Journal of Vibration and Acoustics*, Vol. 124 (2), pp. 209-220.

[6] Liao, C.-M., Balachandran, B., and Karkoub, M., (2009). "Drill-String Dynamics: Reduced Order Models," To appear in Proceedings of ASME IMECE 2009, Nov. 13-19 Lake Buena Vista, FL, USA, 2009; Paper No. IMECE2009-10339.

[7] Melakhessou, H., Berlioz, A., and Ferraris, G. (2003). "A Nonlinear Well-Drillstring Interaction Model," *ASME Journal of Vibration and Acoustics*, Vol. 125, pp. 46-52.

[8] Mihajlović, N., van Veggel, A. A., van de Wouw, N., and Nijmeijer, H. (2004) "Analysis of Friction-Induced Limit Cycling in an Experimental Drill-String System," *ASME Journal of Dynamic Systems, Measurement, and Control*, Vol. 126(4), pp. 709-720.

[9] Mihajlović, N., van de Wouw, N., Rosielle, P.C.J.N., and Nijmeijer, H. (2007) "Interaction between torsionalal and lateral vibrations in flexible rotor systems with discontinuous friction," *Nonlinear Dynamics*, Vol. 50, pp. 679-699.

[10] Nayfeh, A. H. and Balachandran, B. (1995, 2006). Applied Nonlinear Dynamics: Analytical, Computational, and Experimental Methods, Wiley, New York.

[11] Spanos, P. D., Chevallier, A. M., Politis, N. P., and Payne, M. L. (2003). "Oil and Gas Well Drilling: A Vibrations Perspective," *Shock and Vibration Digest* Vol. 35(2), pp. 85-103.

[12] Short, J. A. "Introduction to Directional and Horizontal Drilling " Pennwell Pub, 1993.

[13] Singh, S. P. and Balachandran B. (2009). "Rolling Rub Translations of a Flexibility Connected Disk," pre-print.

[14] Vlajic, N., Liao, C.-M., Karki, H., & Balachandran, B. (2011) "Stick-Slip and Whirl Motions of Drill Strings: Numerical and Experimental Studies," Proceedings of the 2011 ASME IDETC MSNDC Conference, Washington, D.C, Paper No. *DETC2011-47949.*

Appendix

Approach

A combined analytical, numerical, and experimental approach is being pursued at the University of Maryland and the Petroleum Institute. Specifically, the drill string is being modeled as a reduced-order nonlinear dynamical system. Appropriate attention is also to be paid to the interactions with the environment. The experiments at UMD and PI are tailored to address specific aspects of the drill-string dynamics as well as complement each other. Actuator and sensor choices are also to be explored to determine how best to control the system dynamics, in particular, through the rotational speed. The studies will be initiated with drill strings located on fixed platforms, and later extended to systems located on floating platforms.

Three-Year Schedule

Phase II:

January 1, 2009 to December 31, 2009: Carry out quantitative comparisons between experimental results and predictions of reduced-order models for open-loop studies; understand stick-slip interactions and explore continuum mechanics based drill-string models for fixed platform environments; examine different configurations including horizontal drilling

January 1, 2010 to December 31, 2010: Construct control schemes; carry out experimental, analytical, and numerical studies; and identify appropriate schemes; study horizontal drilling configurations through experiments and analysis

January 1, 2011 to December 31, 2011: Continue horizontal drilling studies; carry out experiments, analysis, and numerical efforts and also examine drill-string operations in off-shore environments

January 1, 2012 to May 1, 2012: Compile results obtained for drill-string operations in vertical and horizontal configurations and provide guidelines for enhancing operations.

Studies on Mobile Sensor Platforms

UMD Investigators: **Balakumar Balachandran, Nikil Chopra**
GRA: **Rubyca Jaai**
PI Investigator: **Hamad Karki, S.C. Fok**
GRA: **Hesham Ishmail (ADNOC Fellow)**
Start Date: **April 2009**

1. Objectives/Abstract

Mobile sensor platforms can be employed in a variety of operations including environmental and structural health monitoring operations in harsh and remote environments. In the proposed work, cooperating sensor platforms are to be studied for potential use in oil storage tanks, which are periodically tested for corrosion, cracks, and leaks. These platforms are envisioned for estimating geometrical profile parameters, such as, the tank bottom thickness. To this end, simultaneous localization and mapping (SLAM) algorithms (also known in the literature as concurrent mapping and localization (CML) algorithms) for co-operating sensor platforms operating in harsh environments are being investigated. The SLAM algorithms can enable autonomous inspection for determining the locations of faults in structures such as oil tanks and pipelines.

The overall objective of this project will be to carry out a combined analytical, numerical, and experimental effort to develop mobile sensor platforms and appropriate simultaneous localization and mapping (SLAM) algorithms for cooperative sensor platforms to operate in a harsh environment. Research objectives are the following: i) develop SLAM algorithms based platforms taking into account system constraints such as constrained communication, the type of sensors considered, allowable dynamics, and factors such as sensor failures and reliability of the considered sensors and ii) carry out experimental and supporting simulation studies by using mobile platform test platforms at the University of Maryland and the Petroleum Institute.

In the previous report, simulation results for SLAM algorithms for a mobile platform in an environment of point based landmarks were presented. In this report, the SLAM algorithms presented extend the previous work to include representation of more complex indoor environments using line based maps. An experiment carried out to demonstrate SLAM with a mobile platform by using a laser sensor and encoders for odometry information is presented. The algorithms used for data analysis are also described. The experiment and data analysis results are presented in Section 2, and an outline of the future work is provided in Section 3.

2. Summary of Results

In this report, results obtained from experiments carried out to demonstrate SLAM are presented. Additionally, simulation work completed on the feature extraction and the data association algorithms are demonstrated.

2.1 Experimental setup

The experimental setup has been constructed to collect data in order to demonstrate the working of simultaneous localization and mapping using various filters such as the extended Kalman filter and particle filter along with data association and feature extraction algorithms. The setup includes mobile platforms, a scaled version of a corridor-like environment constructed using Plexiglass structures and cameras to track the mobile platforms movements during experiments. The actual path that the mobile platforms follow within the setup, as well as the environment information such as positions of the walls, can be extracted using an image processing code. This information is used to check the accuracy of the results of the SLAM algorithm. The mobile sensor platform is equipped with encoders and a laser sensor, and this platform is controlled using a C++ code. The encoders collect data on the rotations of the wheels of the mobile platform, thus providing position information for the duration of the SLAM experiment. The encoder data are used as odometry inputs to the SLAM algorithm. The data are used in the motion model of the filter as shown in Figure 1. The laser range sensor provides information on features surrounding the mobile platform. The information is in the form of distance between the mobile platform and the surroundings such as walls. The environmental information is used as input to the feature extraction and feature matching step and is therefore used to build maps. The laser sensor provides readings for every third of a degree for a total of 240° (from -120° to 120° with respect to the mobile platform). It should be noted that there is sensor noise present in the data obtained from both the encoder and the laser sensor. The presence of noise in the position measurements as well the environmental measurements make it necessary to implement probabilistic SLAM algorithms to create a map of the environment.

The mobile platform with the laser sensor in the experimental setup is shown in Figure 1. An experiment with the setup shown in Figure 1 was carried out. The path taken by the mobile platform is also shown in Figure 1. Both encoder and laser sensor data were collected as the experiment was carried out. A sample of the raw laser sensor data is shown in Figure 2. The laser sensor is capable of sensing depths from around 0.05m to 4m and has a field of view of 240°. Feature extraction from the raw depth data and data association are explained in Section 2.3 of this report.

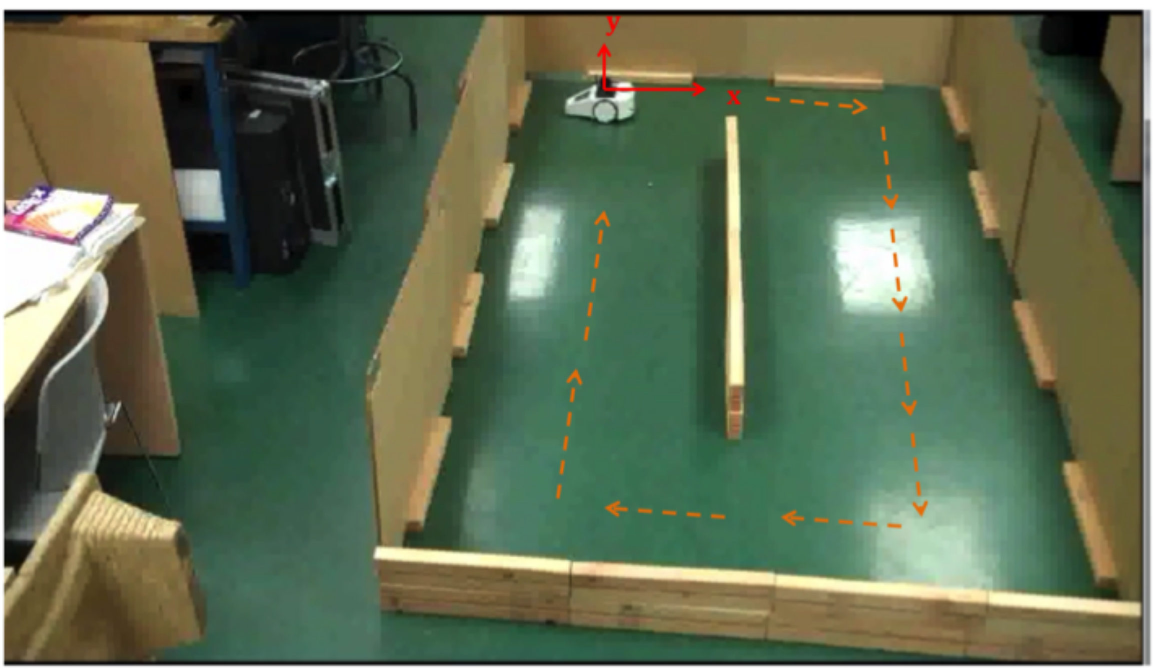

Figure 1. Mobile agent in the experimental setup. The X-Y axes shown in red mark the fixed frame (the origin of the fixed frame is assumed to be the center of the initial position of the mobile platform). The dashes with the arrows indicate the path taken by the mobile platform during the experiment.

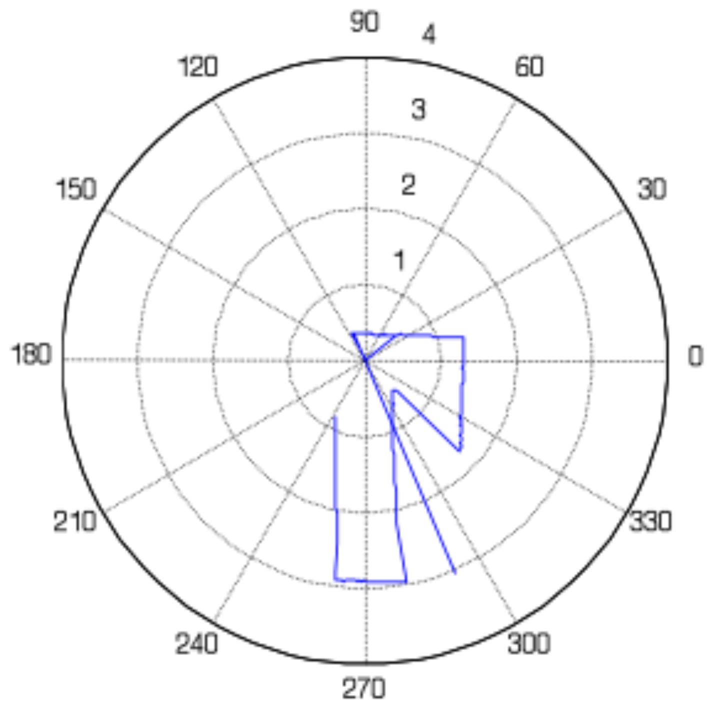

Figure 2. Raw depth data from the laser sensor. At each time step, depth data for a total of 240° around the mobile platform is collected. The measurements are obtained in polar coordinates with respect to the laser sensor that is mounted on the center of the mobile platform.

2.3 Data analysis and results from SLAM experiments

The data analysis of the raw depth information from the laser sensor involves feature extraction and data association (explained in Sections 2.3.1 and 2.3.2). SLAM results obtained by the analysis of the data from the experiment explained in Section 2.1 are shown in Section 2.3.3.

2.3.1 Feature extraction

The raw data from the laser sensor mounted on the mobile platform are first used to detect and extract features of the environment. Since the setup of this experiment is similar to indoor environments, it is described by rectilinear features (such as portions of walls and doors) detectable by the laser sensor. In order to extract the line data from the raw measurements at every time step, the following procedure was applied (Garulli *et al.*, 2005).

The sensor readings are in polar coordinates as shown in Figure 2. The laser sensor provides N range and bearing measurements

$$[d_j,\ \varphi_j],\ j = 1, \ldots, N$$

where d_j is the distance of a point sensed along the angle φ_j . The sensor readings are processed in order to extract the parameters $[\rho_h, \alpha_h]$of the linear features present in the surroundings, by iteratively alternating segmentation and line fitting steps.

In the segmentation step, the sensor readings belonging to the same linear feature are identified while in the line fitting phase, the linear feature parameters of the set of points related to the same line (identified in the segmentation step) are calculated. The pair $[d_j, \varphi_j]$ represent the polar coordinates of the j-th point in the moving reference frame (centered on the mobile platform). Let

$$p_j = [x_j, y_j] = [d_j cos(\varphi_j), d_j sin(\varphi_j)]$$

be the Cartesian coordinates of the j-th point with respect to the moving frame. The segmentation step partitions the sensor readings into subsets S_h (called segments) of collinear points

$$S_h = \{p^{(h)}_1 , \ldots , p^{(h)}_{nh}\}, \quad h = 1, \ldots , q \text{ segments},$$

where n_h denotes the number of points in the h-th segment and there are a total of q such segments. The number of points in each segment need not be the same. Each set is built iteratively. The points p_j are processed sequentially, with the first ten initializing the segment S_h. A new point p_j, is added to this segment if the following conditions are satisfied:

- The normal distance from the current fitting line to the point p_j is less than a threshold value δ_0

- The Euclidean distance from the last point in the current segment to the new point p_j is less than a threshold δ_1.

If a new point, p_j is inserted in the current segment, the parameters of the fitting line are recomputed for the new set of points. A segment is assumed to be completed if N consecutive points do not meet the above conditions and are not added to the segment. A new segment S_{h+1} starting from the ten points after the last one inserted into S_h is then started. Segments made of fewer than N_0 points or shorter than a minimum length are rejected in order to avoid false features.

Once a segment S_h has been identified, the parameters of the corresponding linear feature $[\rho_h, \alpha_h]$ are computed by fitting a line through all the points belonging to S_h. In Figure 3, the parameters of the linear features with respect to the moving frame as well as the fixed frame are illustrated.

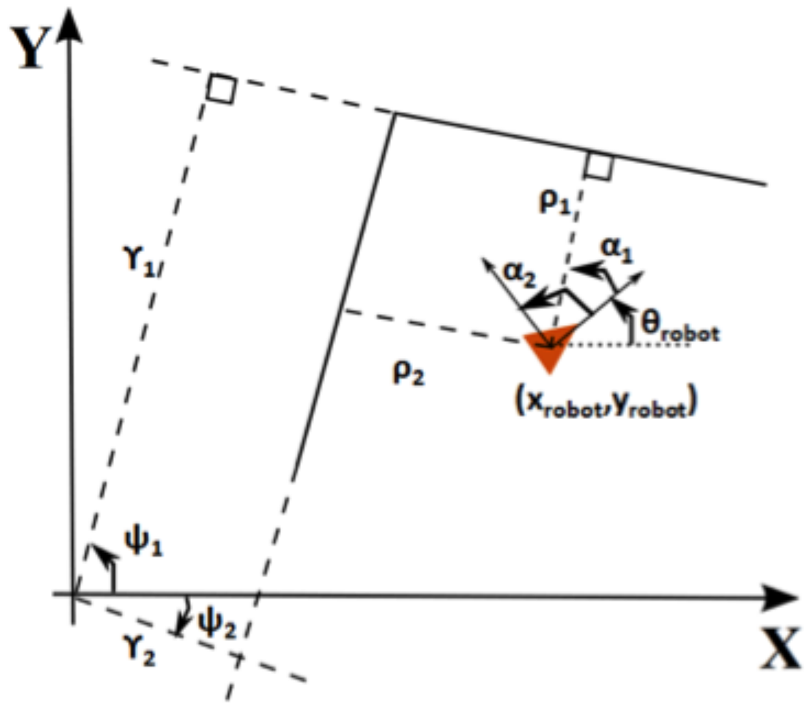

Figure 3 (from Yap *et al*, 2009**). Extraction of line segments (ρ, α) with respect to the robot and (r, ψ) with respect to the origin. The extracted values are then used as a part of the SLAM algorithm.**

The parameters are calculated using the following formula (Garulli *et al*., 2005):

$$\begin{bmatrix} \rho \\ \alpha \end{bmatrix} = \begin{bmatrix} \bar{x}\cos(\alpha) + \bar{y}\sin(\alpha) \\ \frac{1}{2}\arctan\frac{-2S_{xy}}{S_{y2} - S_{x2}} \end{bmatrix}$$

where

$$\bar{x} = \frac{1}{n}\sum_{i=1}^{n} x_i , \qquad \bar{y} = \frac{1}{n}\sum_{i=1}^{n} y_i$$

$$S_{x2} = \sum_{i=1}^{n}(x_i - \bar{x})^2 , \qquad S_{y2} = \sum_{i=1}^{n}(y_i - \bar{y})^2$$

$$S_{xy} = \sum_{i=1}^{n}(x_i - \bar{x})(y_i - \bar{y})$$

The features obtained using the above equations are stored in the state vector in the form of

$$l_i = [r_i, \psi_i]^T$$

where r_i represents the normal distance of the line l_i from the origin of the fixed frame and ψ_i represents the angle of the normal to the line l_i with respect to the X axis of the fixed frame. These are calculated using

$$\begin{bmatrix} r \\ \psi \end{bmatrix} = \begin{bmatrix} -\rho + \hat{x}\cos(\alpha - \hat{\theta}) + \hat{y}\sin(\alpha - \hat{\theta}) \\ \alpha - \hat{\theta} \end{bmatrix}$$

where $[\hat{x}^-, \hat{y}^-, \hat{\theta}^-]^T$ represents the position of the mobile platform after the prediction step and before the update step of the extended Kalman filter. The calculation of the covariance matrices are carried out by determining Jacobian matrices associated with the above equations.

2.3.2 Data association

In order to perform the extended Kalman filter update step, each measurement z(k) extracted from the sensor data must be associated with a corresponding line already present in the map or identify that it is a new line and add a new feature to the state vector. In order to carry out the data association strategy, the feature is expressed with respect to the fixed frame [r ψ]. It is also important to consider that different linear features may lie on the same line (for example, two walls separated by a hallway aligned in the same direction) and to take into account the uncertainty associated with each feature. The data association conditions are as follows (Garulli *et al.*, 2005):

- The squared difference of orientation, weighted by the inverse of its variance, between the extracted line and the feature estimates l_i(k|k−1) should be less than a threshold,
- The squared normal distance, weighted by the inverse of its variance, of the midpoint of the extracted segment to the feature estimate l_i(k|k−1) should be less than a threshold,
- The overlapping rate between the extracted segment and the one associated to the feature estimate l_i(k|k−1) should be less than a threshold.

In the above conditions, l_i(k|k-1) represents the vector of the i-th feature parameters before the update step of the extended Kalman filter.

When a measurement *z*(k) is associated to a feature l_i(k|k−1), the end points of the i-th segment are updated by adding the end points of the extracted segment to the associated feature line l_i(k|k−1) and updating the line parameters. If a measurement *z*(k) does not match any of the lines in the state vector, it is considered as a new feature and the state vector is augmented with the new feature.

2.3.3 Experimental results

In this section, the results of the experimental data analysis conducted using the above feature extraction and data association techniques in the SLAM framework with the extended Kalman filter are presented. In Figure 4, an example of the feature extraction for a particular time step alongside the raw data from the laser sensor is shown. In Figure 5, the SLAM results obtained after feature extraction and data association for the experiment where the mobile platform traversed the path shown in Figure 2 are shown. The map shown in Figure 5 consists of the points that were associated to different lines detected from the laser measurements.

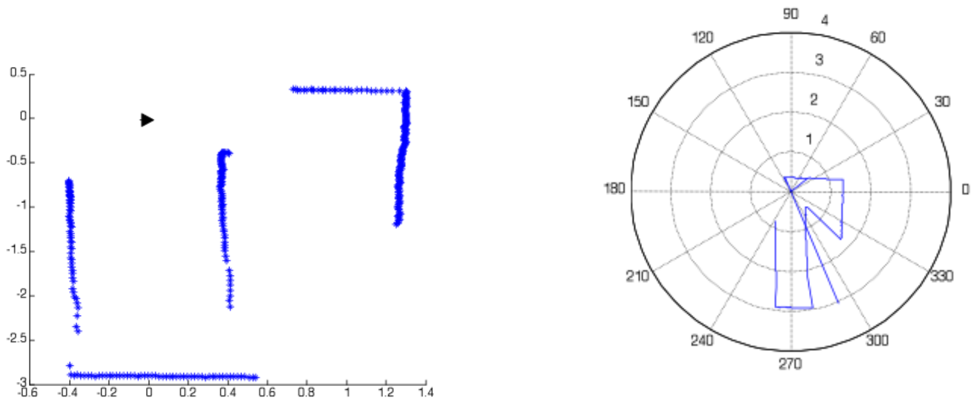

Figure 4. Feature extraction from raw data. The raw data in polar form shown on the right side is converted to linear features with respect to the mobile platform (shown as black triangle).

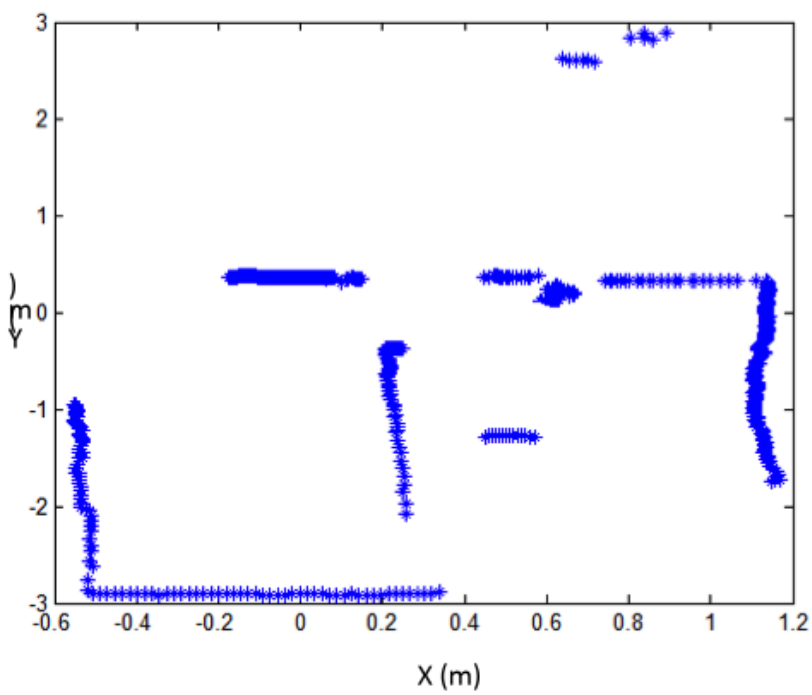

Figure 5. Result after feature extraction and data association. The blue data points indicate points that were associated to the different linear features in the map.

2.4 Interactions

A paper abstract entitled “Simultaneous Localization and Mapping with Consideration of Robot System Dynamics” has been accepted for oral presentation at the 2012 SPIE Smart Structures/NDE conference to take place in San Diego, CA this March.

3. Planned Project Activities for the Next Quarter

Future work includes performing determining a motion model that takes into account the dynamics of the mobile agent and studying its effect on the various SLAM algorithms. Furthermore, motion modeling to include vehicle slip will be studied and adapted to the SLAM framework. An experimental test setup of a scaled pipeline structure to demonstrate the applicability of the SLAM algorithms for inspection purposes will also be constructed.

4. References

[1] Bay, H., Ess, A., Tuytelaars, T., and Gool, L. V., 2008, "SURF: Speeded Up Robust Features," Computer Vision and Image Understanding, Vol. 110, No. 3, pp. 346-359.

[2] Dissanayake, M.W., Newman, P., Clark, S., Durrant-Whyte, H. F., and Csorba, M., 2001, “A Solution to the Simultaneous Localization and Map Building (SLAM) Problem,” Robotics and Automation, IEEE Transactions on, Vol.17, No.3, pp. 229–241, June.

[3] Dudek, G., Jenkin, M., Milios, E. and Wilkes, D., 1996, “A Taxonomy for Multi-Agent Robotics,” Autonomous Robots, Vol. 3,No. 4.

[4] Durrant-Whyte, H. and Bailey, T., 2006, “Simultaneous Localization and Mapping: Part I," IEEE Robotics & Automation Magazine, Vol.13, No.2, pp. 99-110, June.

[5] Durrant-Whyte, H. and Bailey, T., 2006b, “Simultaneous Localization and Mapping: Part II State of the Art," IEEE Robotics & Automation Magazine, Vol.13, No.3, pp. 108-117, 2006.

[6] Garulli, A., Giannitrapani, A., Rossi, A., and Vicino, A., 2005, “Mobile robot SLAM for line-based environment representation,” 44th IEEE Conference on Decision and Control, 2005 and 2005 European Control Conference. CDC-ECC '05., pp. 2041 – 2046, December.

[7] Lemaire, T. and Lacroix, S., 2007, "SLAM with Panoramic Vision," Journal of Field Robotics, Vol. 24, No. 1-2, pp. 91-111, February.

[8] Montemerlo, M., Thrun, S., Koller, D., and Wegbreit, B., 2002, “FastSLAM: A Factored Solution to the Simultaneous Localization and Mapping Problem," in Proceedings of the AAAI National Conference on Artificial Intelligence, AAAI, (Edmonton, Canada).

[9] Neira J., and Tardós, J.D., 2001, “Data Association in Stochastic Mapping Using the Joint Compatibility Test”, IEEE Trans. Robotics and Automation, Vol. 17, No. 6, pp. 890-897.

[10] Smith, R., Self, M., and Cheeseman, P., 1990, “Estimating Uncertain Spatial Relationships in Robotics”, pp. 167-193, Springer-Verlag New York, Inc., New York, NY, USA.

[11] Tardós , J. D., Neira, J., Newman, P. M., and Leonard, J. J., 2002, “Robust mapping and localization in indoor environments using sonar data,” International Journal of Robotics Research, Vol. 21, pp. 311—330.

[12] Thrun, S., 2003, “Robotic Mapping: A Survey,” in Exploring Artificial Intelligence in the New Millennium, G. Lakemeyer and B. Nebel, eds., pp. 1-35, Morgan Kaufmann Publishers Inc., San Francisco, CA, USA.

[13] Thrun, S., Burgard, W., and Fox, D., 2006, “Probabilistic Robotics,” MIT Press.

[14] Yap, T.N., and Shelton C.R., 2009, "SLAM in Large Indoor Environments with Low-Cost, Noisy, and Sparse Sonars," Proceedings of the IEEE International Conference on Robotics and Automation, pp. 1395-1401.

[15] Zhang, S., Xie, L., and Adams, M., 2005, “An Efficient Data Association Approach to Simultaneous Localization and Map Building,” International Journal of Robotics Research, Vol. 24, pp. 49-60.

Appendix

SLAM and its Components

The basic aim of the simultaneous localization and mapping (SLAM) algorithm is to make a mobile platform autonomous by providing the capability to navigate through an unknown environment from an initially unknown location. This is achieved by iteratively building a consistent map of the environment and by simultaneously determining its location within the map (Durrant-Whyte and Bailey, 2006). Therefore, SLAM is the process by which a mobile platform can build a map of the environment and at the same time use this map to compute the platform's location within the map (Thrun, 2003). This ability is useful particularly in applications such as search and rescue, inspection and surveillance, and exploration, which require accurate localization within unknown environments. For example, in the inspection problem, with SLAM techniques, the mobile sensor platform can be used to determine locations of faults thereby providing an autonomous solution and reducing the need for external sensors to perform the same task.

In the SLAM problem, an agent or a mobile sensor platform traverses an unknown area and uses relative sensing information between the agent and the surrounding environment. The data collected from the experiment includes the following:

1) Encoder or inertial measurement unit (IMU) data providing information on the mobile agent's movements
2) Sensor data measuring the relative distance and angle between the mobile agent and the environment (using sensors such as laser, ultrasonic, camera and so on).

The solution to the SLAM problem involves the implementation of a probabilistic framework to analyze experimental data and build a map that constitutes the locations of landmarks or features in the surrounding environment as well the platform's position within the map. This is due to the presence of noise in the sensor data. The steps in a typical SLAM implementation are as follows. The encoder or IMU data is processed to get the relative motion (distance and angle) moved by the mobile agent with respect to its last position. A motion model describing the evolution of the position (x, y, and heading angle) of the mobile agent with time and the relative motion data is constructed. The relative motion data is used in an estimation algorithm such as the extended Kalman filter along with the motion model to predict the position of the mobile agent at every time step. The sensor measurements of the environment are processed by using feature extraction algorithms to identify distinct landmarks. At every time step, a data association algorithm is used to determine if the identified features are new or already present in the map. The relative positions of previously identified landmarks are used to update the map and the position of the mobile agent. New landmarks are added to the map for future processing. A block diagram of the important steps in SLAM implementation is shown in Figure 2.1.

Well known solutions to the SLAM problem include the use of extended Kalman filter (EKF) algorithm to estimate the positions of landmarks and the pose (i.e., position and heading) of the robot as Gaussian distributions or particle filters that allow for non-Gaussian representations or their combinations (known as FastSLAM) (Smith *et al*., 1990, Montemerlo *et al*., 2002).

Before fusing new sensor data into the SLAM map, new measurements are associated with existing map landmarks by using data association algorithms such as joint compatibility and nearest neighbor (Neira and Tardos, 2001, Zhang *et al.*, 2005). The problem is that incorrect data association can cause the map estimates to diverge. Additionally, the incorrect data association can lead to failure in the localization of the mobile platform within the map. Practical SLAM solutions are therefore fragile to incorrect association of observations to landmarks. Additionally, it is necessary to solve the loop-closure problem that occurs when a robot returns to observe landmarks that were previously observed after a long route and the algorithm needs to recognize this has occurred by correctly associating new measurements to landmarks that were observed in the beginning of the robot path. The association problem is compounded in environments that are not simple points (Durrant-Whyte and Bailey, 2006b).

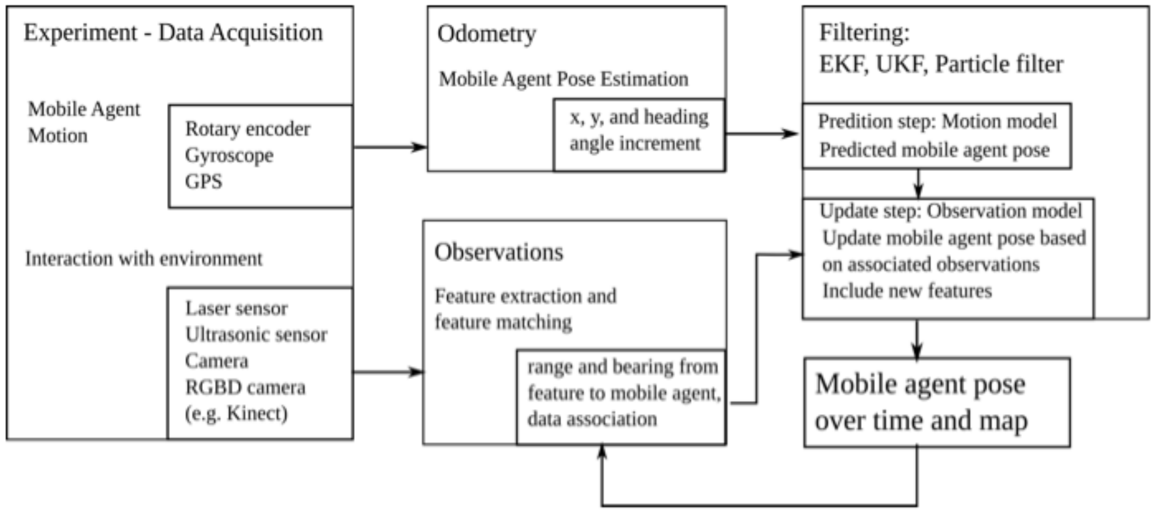

Block diagram describing the steps in SLAM.

Feature extraction is another component of the SLAM problem that is critical. In environments that are not simple, correct data association also involves representing the environment by features extracted from the sensors provided on the mobile platform. Some examples include extracting line features in indoor environments typically from sonar and laser sensors (Tardos *et al*., 2002; Garulli *et al*., 2005), and extracting corners and scale invariant features from stereo camera data by using techniques from computer vision (Bay *et al*., 2008; Lemaire *et al*., 2007).

Three-Year Schedule

Phase II:

April 1, 2009 to December 31, 2009: Carry out analytical and numerical investigations into SLAM algorithm based mobile platforms for representative geometrical profile measurements, and construction of experimental test platforms.

January 1, 2010 to December 31, 2010: Continuation of analytical, experimental, and numerical efforts, with one of the focus areas to be development of appropriate communication and motion planning protocols for co-operative multi-agent platforms. Construction of experimental setup for ground based mobile agents with attention to the environment.

January 1, 2011 to December 31, 2011: Continuation of experimental and numerical studies and formulation of recommendations for appropriate sensor and mobile platform configurations for use in oil tanks and pipes.

January 1, 2012 to March 31, 2012: Continuation of experimental and numerical studies for proof of concept for appropriate sensor and mobile platform configurations for use in oil tanks and pipes.

Development of a Probabilistic Model for Degradation Effects of Corrosion-Fatigue Cracking in Oil and Gas Pipelines

UMD Investigator: **Mohammad Modarres**
PI Investigators: **Abdennour Seibi**
GRA: **Mohammad Nuhi**
Start Date: **Oct 2006**

1. Objectives/Abstract

This research continues Phase-I mechanistic modeling of the corrosion-fatigue phenomenon for applications to pipeline health, risk and reliability management. The objective of this study is to perform additional mechanistic-based probabilistic models derived from physics of failure studies and validate them using the state-of-the-art experimental laboratory being developed at the PI as part of the Phase I of this study. Where possible, observed field data from ADNOC operating facilities will be used to supplement observations from the laboratory experiments based on the well-established Bayesian approach to mechanistic model updating and validation developed in Phase I. Uncertainties about the structure of the mechanistic models as well as their parameters will also be characterized and accounted for when such models are applied. The proposed models will allow the end users (e.g., maintenance analysts and Inspection crew) to integrate observed performance data from a wide range of pipelines and selected refinery equipment, such as pumps, compressors and motor-operated valves. Admitting the fact that modeling all degradation mechanisms would be a challenging undertaking, the proposed research will additionally address the following degradation phenomena related to the petroleum industry: creep, pitting corrosion, and stress cracking corrosion (SCC).

2. Background

A number of deterministic models have been proposed to assess reliability and life-remaining assessment of pipelines. Among these models is the ASME B31G [1] code, which is most widely used for the assessment of corroded pipelines. However, these models are highly conservative and lack the ability to estimate the true life of the pipelines and other equipment used in the oil industry. To address this shortcoming it is necessary to develop a best-estimate assessment of the life (to assess reliability and risk imposed) by these structures and equipment and assess the uncertainties surrounding such estimates. The proposed probabilistic mechanistic models, when fully developed, would integrate the physics of failure of some of the leading failure degradation mechanisms in the oil industry into the formal risk and reliability assessments. Such physical models will be validated using a state of the art reliability assessment laboratory (being developed at PI). Uncertainties about the model structures and parameters will also be quantified. Such models will incorporate inspection data (characterizing limited and uncertain evidences). The rate of degradation is influenced by many factors such as pipeline materials, process conditions, geometry and location. Based on these factors, a best estimate of the structure (pipeline) or equipment (primarily valves, pumps and compressors) service life (reliability and remaining life) is to be calculated and uncertainties associated with the service life quantified. This estimate would serve as a basis that guides decisions regarding maintenance and replacement practices.

Phase I of this research focused on developing a corrosion-fatigue model. It successfully proposed such a model and developed an advanced laboratory for testing this phenomenon at PI. The current research continues in the same line of research by investigating and developing additional degradation phenomena (SCC, pitting corrosion, and creep-fatigue) and integrates these phenomena with reliability and risk assessment through four different tasks. The long-term objective of this research is to develop a comprehensive library of probabilistic mechanistic models for all degradation phenomena pertinent to structures (piping, and pressure vessels) used in the oil industry.

3. Test Facilities

The test rig for this research exists at the University of Maryland. The rig is used to conduct experimental studies reflecting field conditions for model validation developed in EERC Phase I & II. The equipment include an MTS fatigue machine, heating furnace, corrosion test cells, autoclaves, multiphase flow loops, and testing machines for slow strain rate and crack growth testing. This activity also requires a complete line of monitoring equipment for evaluation of corrosion, scaling, and chemical treatment for field and laboratory. This test rig will be a useful tool for performing fatigue, corrosion, corrosion-fatigue, creep, and creep-fatigue, as well as teaching and possibly training field engineers from operating companies.

4. Summary of Results

The following tasks have been completed in the last three months (Final PI Report):

4.1. Introduction
4.2. Classification of the creep models
4.3. The proposed probabilistic model
4.4. Development of parameters of the proposed probabilistic model
4.5. Case study (field application): Estimation of probability of exceedance (PE) on 0.04% strain level

4.1. Introduction

Creep and creep-corrosion, which are the most important degradation mechanisms in structures such as piping used in the nuclear, chemical and petroleum industries, have been studied. Sixty-two creep equations have been identified, and further classified into two simple groups of power law and exponential models. Then, a probabilistic model was developed and compared with the mostly commonly used and acceptable models from phenomenological and statistical points of view. This model is based on a power law approach for the primary creep part and a combination of power law and exponential approach for the secondary and tertiary part of the creep curve. This model captures the whole creep curve appropriately, with only two major parameters, represented by probability density functions. Moreover, the stress and temperature dependencies of the model have been calculated. Based on the Bayesian inference, the uncertainties of its parameters have been estimated by WinBUGS program. Linear temperature and stress dependency of exponent parameters are presented for the first time.

The probabilistic model has been validated by experimental data taken from Al-7075-T6 and X-70 carbon steel samples. Experimental chambers for corrosion, creep-corrosion, corrosion-fatigue, stress-corrosion cracking (SCC) together with a high temperature (1200 ^{0}C) furnace for creep and creep-corrosion furnace have been designed, and fabricated. Practical applications of the empirical model used to estimate the probability of exceedance of failures at 0.04% strain level for X-70 carbon steel.

4.2. Classification of the Creep Models

More than sixty-two creep relations from the Kelvin-Voigt creep model (1898) [1] to the Holmström-Auerkari- Holdsworth (Logistic Creep Strain Prediction model (2007) [2] were identified. Thirty-three of these models describe the creep process with power law, and twenty-eight of them are based on the exponential approach. In this classification, the logarithmic approach was considered as power law and sine hyperbolic and cosine hyperbolic relations as exponential.

It should be mentioned that nearly all of the exponential approaches are based on the idea of the Kelvin-Voigt model of visco-plastic deformation of creep in materials. Recent investigation shows that this approach is unable to describe the primary part of the creep curve; in addition, Evan's [4] recent attempt to extend his 4-theta to 6-theta model (by addition of more parameters) shows that the exponential approach is not an adequate approximation for describing the creep process.

The Kelvin-Voigt model is described as a first-order differential equation for stress to explain the creep behavior:

$$\sigma(t) = E \cdot \varepsilon(t) + \eta \frac{d\varepsilon}{dt} \tag{1}$$

where σ is the applied stress, E is the elastic modulus, $\varepsilon,t.$ is the time dependent strain, and η is the viscosity.
Solving this differential equation leads to the following relation:

$$\varepsilon(t) = \frac{\sigma_0}{E} \cdot \left[\mathbf{1} - \mathbf{exp}\left(\frac{-E}{\eta} \cdot t\right)\right] \tag{2}$$

This model is more applicable to materials such as polymers and wood for applying a small amount of stress.

Garofalo's empirical equation [5] can be represented by:

$$\varepsilon = \varepsilon_0 + \boldsymbol{\varepsilon_t}\left[\mathbf{1} - \mathbf{exp}\left(-\frac{t}{t_r}\right)\right] + \dot{\varepsilon}_s \cdot t \tag{3}$$

where ε_0 corresponds to initial time independent strain that contains elastic and plastic parts, ε_t is the transient creep strain, t_r by Garofalo represent the transient time between the primary and secondary parts and ,,ε-s.. is the strain rate of the secondary part.
Evans complicated the 4-Theta model [6] could be written as:

$$\varepsilon_f = \theta_1[1 - \exp(-\theta_2 \cdot t)] + \theta_3[\exp(\theta_4 \cdot t) - 1] \tag{4}$$

$$\log(\theta_i) = a_i + b_i \cdot T + c_i \cdot \sigma + d_i \cdot \sigma \cdot T \tag{5}$$

$$\varepsilon_f = A + B \cdot T + C \cdot \sigma + D \cdot \sigma \cdot T \tag{6}$$

where θ_i, a_i, b_i, c_i, d_i, and A, B, C, D are constants estimated by curve fitting and regression analysis.

Garofalo's empirical equation (3) and Evan's model (Equation (4)) contain the following common term for describing the primary creep:

$$[1 - \exp(-\alpha \cdot t)] \tag{7}$$

which is exactly the same term in the Voigt's (Equation (2)) for describing the creep process. Sawada et al. [7] criticized the exponential relations describing the primary part of creep curve, and showed that the power law is a better representation of that part of curve (this is the reason that our empirical model uses a power law to account for the primary part of the creep process).

4.3. Proposed probabilistic model

The investigation of creep models shows that almost all of the creep relations can be reduced to two general approaches: power law and logarithmic.

Regarding the limitations of the creep models (reported in the previous PI report), a new probabilistic model is developed as follows:

$$\varepsilon_c = \varepsilon_P + \varepsilon_{S/T} = At^n + Bt^m \exp\,(pt) \tag{8}$$

where ε_P is the primary strain, $\varepsilon_{S/T}$ is the secondary and tertiary strain. Parameters n, m, and p are material constants.

4.4. Development of parameters of the proposed probabilistic model

The proposed probabilistic model is able to estimate the uncertainties in material parameters A, n, B, m, and p. Parameters A, and B are lognormally distributed (also not deterministic), and can be refined by updating experimental field data. Parameters n, m, and p are temperature and stress dependent.

Table 1 and Table 2 represent the numerical values for the corresponding parameters of the proposed empirical model for Al-7075-T6 and X-70 carbon steel estimated by the WinBUGs program.

Table 1. Numerical values for corresponding parameters of the proposed empirical model for Al-7075-T6

T [°C]	T [°K]	σ [MPa]	A	n	B	m	p
405	678	460	0.00016	0.602	1.787E-12	1.2309	0.00073
415	688	480	0.0002	0.6348	1.674E-10	1.3564	0.00147
418	691	493	0.0002	0.6497	3.202E-09	1.4138	0.002327
430	703	520	0.0025	0.6913	1.4696E-06	1.5728	0.00601

Table 2. Numerical values for corresponding parameters of the proposed model for X-70 carbon steel

T [C]	T[K]	σ [MPa]	A	n	B	m	p
418	691	133	8.1E-5	0.6041	2.87E-9	1.0488	0.000182
425	698	185	8.8E-5	0.6087	1.46E-9	1.0397	0.000239
450	723	346	1.2E-4	0.6255	1.8E-10	1.01	0.000639
470	743	445	1.5E-5	0.6374	4.969E-11	0.989	0.0014
500	773	620	2.12E-4	0.6567	5.1085E-12	0.955	0.00455

Considering the temperature, and stress dependencies of parameters, and plugging them in the proposed model, the creep equation has the following form:

$$\varepsilon = A' \cdot [\exp\,(\alpha \cdot \boldsymbol{\sigma}) \cdot \exp\,(Q_A/RT)] \cdot \boldsymbol{t}^{\beta T + \gamma\sigma + \delta} + B' \cdot \boldsymbol{exp}(\beta \cdot \boldsymbol{\sigma_i}) \cdot \boldsymbol{t}^{\beta' T + \gamma' \sigma + \delta'} \cdot \exp\,(p \cdot \boldsymbol{t}) \tag{9}$$

Parameters A and B are lognormals distributed. The probability density functions (PDFs) of these parameters are calculated for X-70 carbon steel, and are shown in Figure 1.

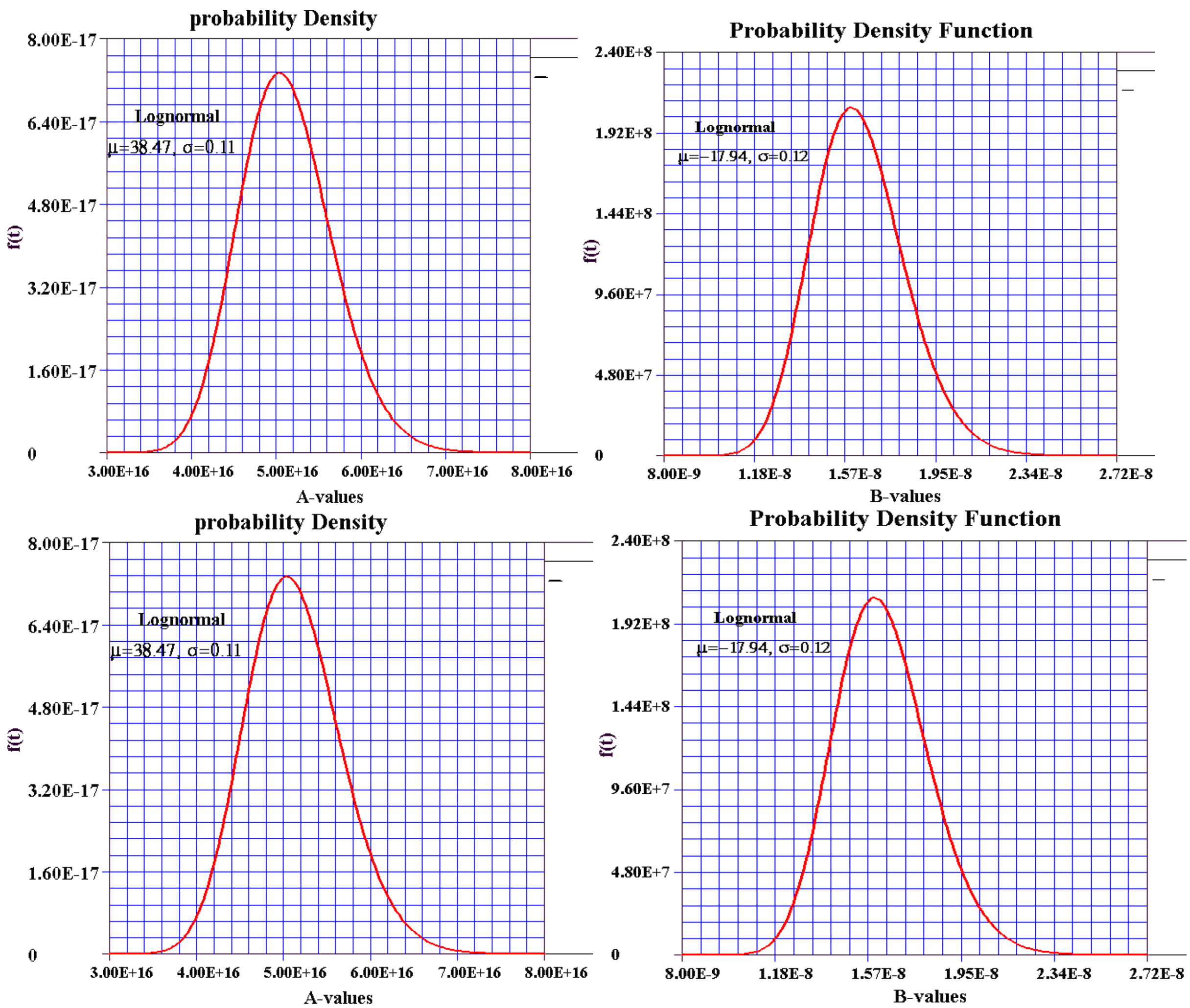

Figure 1. PDF of parameters: A = LN (μ=38.47, σ=0.11), and B= LN (μ= -17.94, σ=0.12).

Creep curves evaluated for X-70 carbon steel by MATLAB are given in Figure 2. The color curves (blue, red and thick black curves) are evaluated with experimental data and the proposed creep model. The thin black and green curves are the predictions of the proposed creep model.

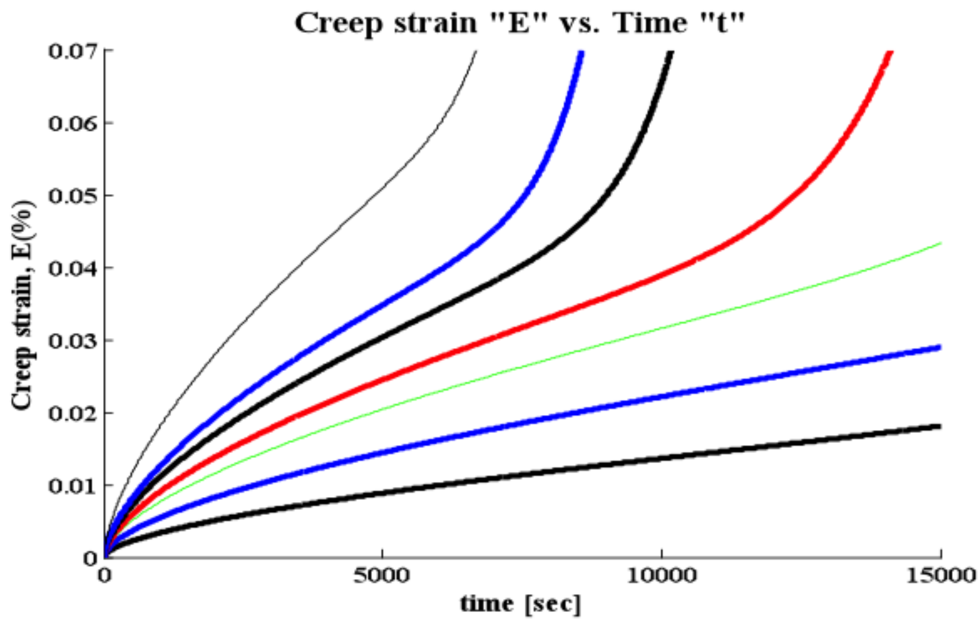

Figure 2. Creep curves of X-70 carbon steel at different T and σ from data given in the above table (bulk) and predicted creep curves for proposed temperature and stresses (thin lines).

The WinBUGS program [8] is a windows-based environment for Markov Chain Monte Carlo Simulation (MCMC). This program has been previously used in uncertainty management [9] as well as accelerated life testing data analysis [10] and has proved to be a reliable tool for such calculations. In this research the WinBUGs platform was used for solving posteriors of parameters. The general steps of the WinBUGS program are given in left-hand-side of Figure 3. The distributions of all proposed model parameters are given in the right-hand-side of Figure 3.

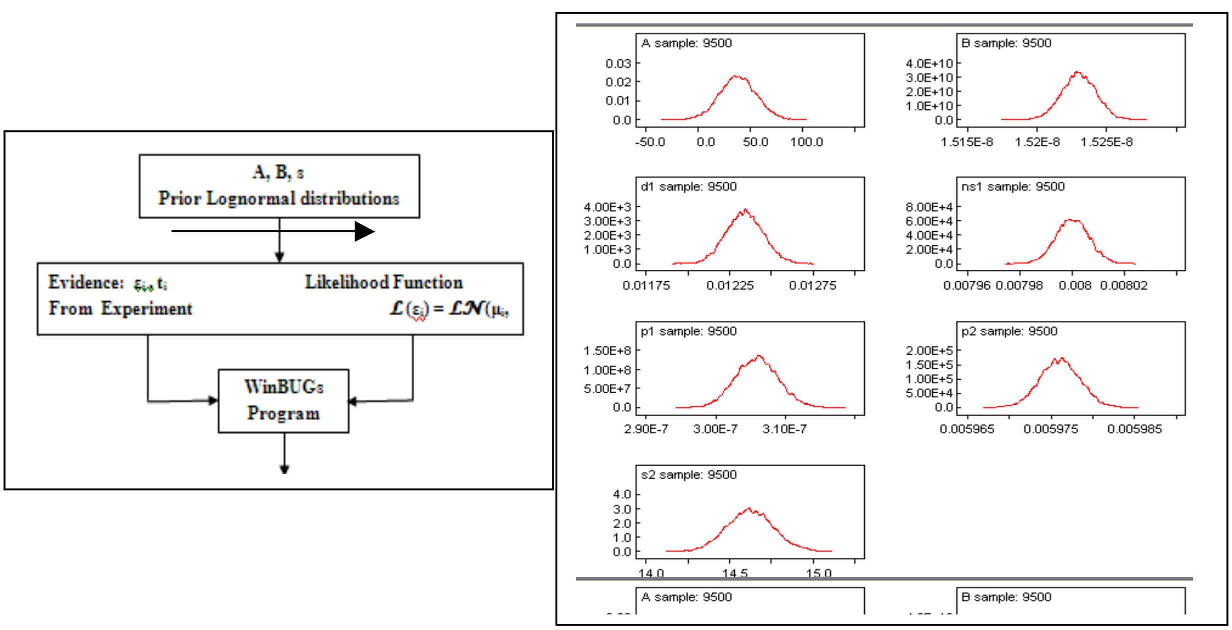

Figure 3. Algorithm for the Bayesian approach in WinBUGS program (left), and the corresponding posterior distributions of A, B, s, and other parameters (right) for X-70 carbon steel.

The posterior distributions for parameters A, and B for X-70 carbon steel samples are given by the following probability density functions:

$$A = Ln(\mu = 38.05, \sigma = 0.012)$$

$$B = Ln(\mu = -17.999, \sigma = 0.11)$$

$$s = Ln(\mu = 2.68, \sigma = 0.1381)$$

The general node statistics of the parameters from WinBUGS program are given in Figure 4.

Node statistics

node	mean	sd	MC error	2.5%	median	97.5%	start	sample
A	38.05	17.6	0.194	3.133	37.96	72.74	501	9500
B	1.523E-8	1.008E-10	1.033E-12	1.521E-8	1.523E-8	1.525E-8	501	9500
d1	0.01234	1.093E-4	1.031E-6	0.01213	0.01234	0.01255	501	9500
ns1	0.008	6.293E-6	5.58E-8	0.007988	0.008	0.008013	501	9500
p1	3.059E-7	3.041E-9	2.905E-11	3.0E-7	3.059E-7	3.12E-7	501	9500
p2	0.005976	2.392E-6	2.45E-8	0.005971	0.005976	0.005981	501	9500
s2	14.63	0.1381	0.001353	14.36	14.62	14.91	501	9500

Figure 4. Values of node statistics for X-70 carbon steel model parameters taken from WinBUGS program.

Similar approaches have been done to estimate the creep properties of Al-7075-T6 samples.

4.5. Case study (field application): Estimation of probability of exceedance (PE) on 0.04% strain level

The end point of the secondary region or the beginning point of the tertiary part of the creep curve is used to estimate the service and residual life of material. Severe structural deformation of material begins at this point, where most of the cavities begin to agglomerate, and leads to a big crack. Figure 5 shows the creep curves of X-70 carbon steel samples at different temperatures and stresses. If 0.04 % strain line on the creep curve (for 723 °K and 346 MPa) is taken as the critical level of inspection, then it is possible to estimate the probability of exceedance above 0.04% strain level at different times. The brown areas above 0.04 % strain (at t= 6000, 8000, 10000, and t=12500 sec) in Figure 5 below show the amounts of failure accumulated (exceedance) on the creep curve at 450°C.

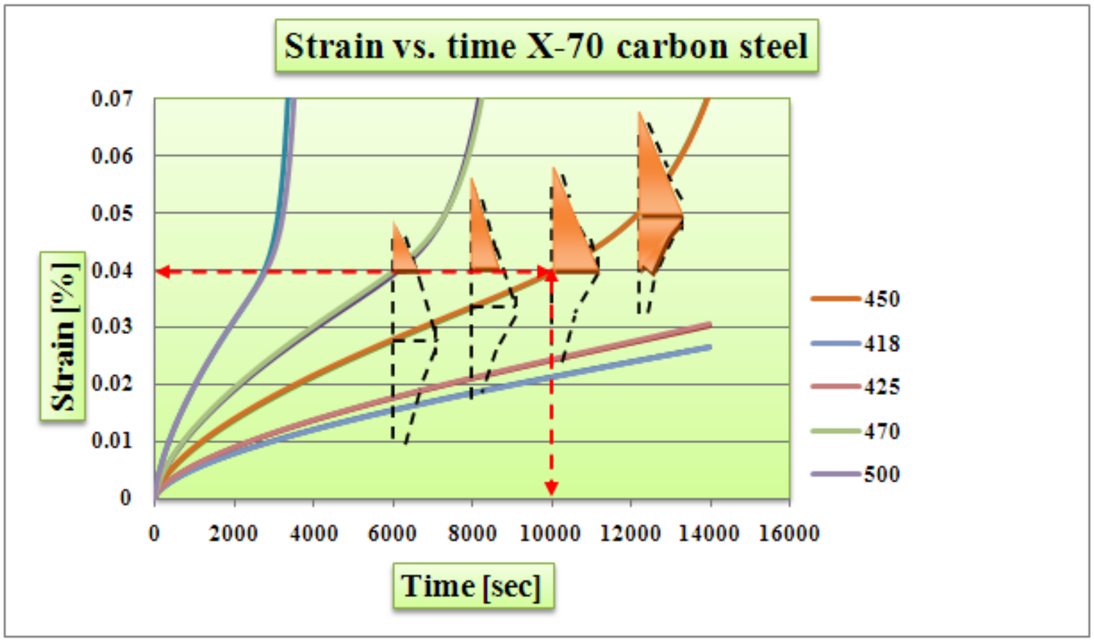

Figure 5. Lognormal distributions estimated on 0.04 % strain with their corresponding probability of exceedance (filled brown areas).

A MATLAB code was written to calculate the probability of exceedance (P_E) at different times based on the proposed empirical equation applied to the experimental data. The distributions in Figure 6 are the probability of exceedance above 0.04% strain level at different times for X-70 carbon steel, calculated by the MATLAB code.

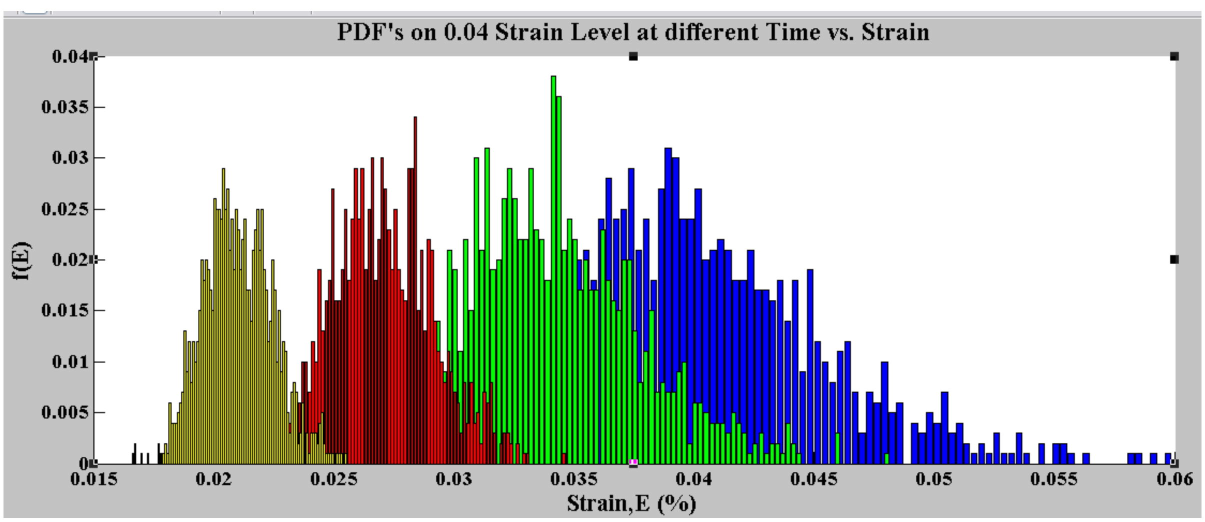

Figure 6. Lognormal pdfs calculated with MATLAB code for 0.04 % strain level (practical strain limit in service) for X-70 carbon steel.

Figure 7 shows the cumulative distribution of the exceedance at different times above 0.04% strain level for X-70 carbon steel, calculated by the MATLAB code.

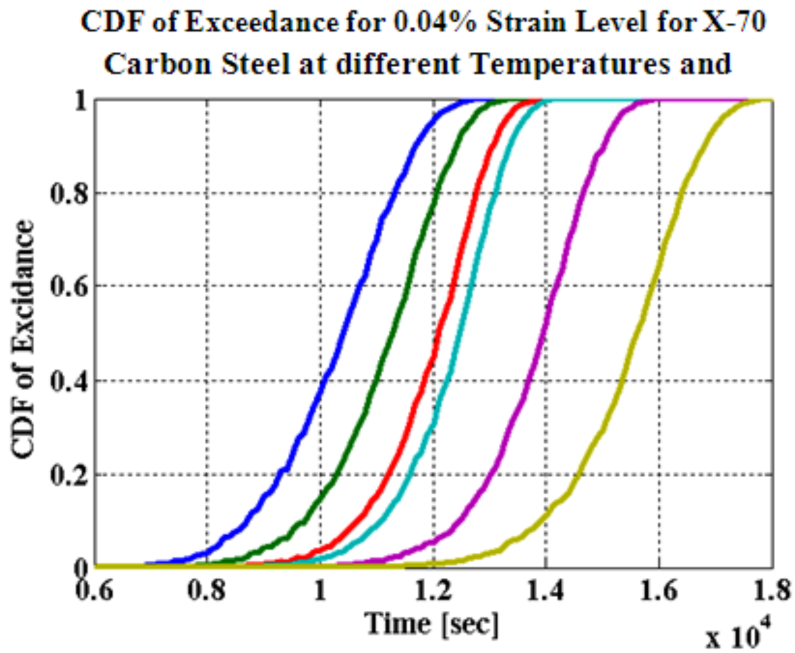

Figure 7. Lognormal cumulative distributions calculated by Weibull++ for 0.04 % strain level (practical strain limit in service) for X-70 carbon steel between 450°C and 500°C.

EXCEL and Weibull++ program were used to calculate the probability of exceedance (P_E) at different times. Again, the proposed empirical model was used to evaluate the corresponding experimental data. Figure 8 shows the related graph.

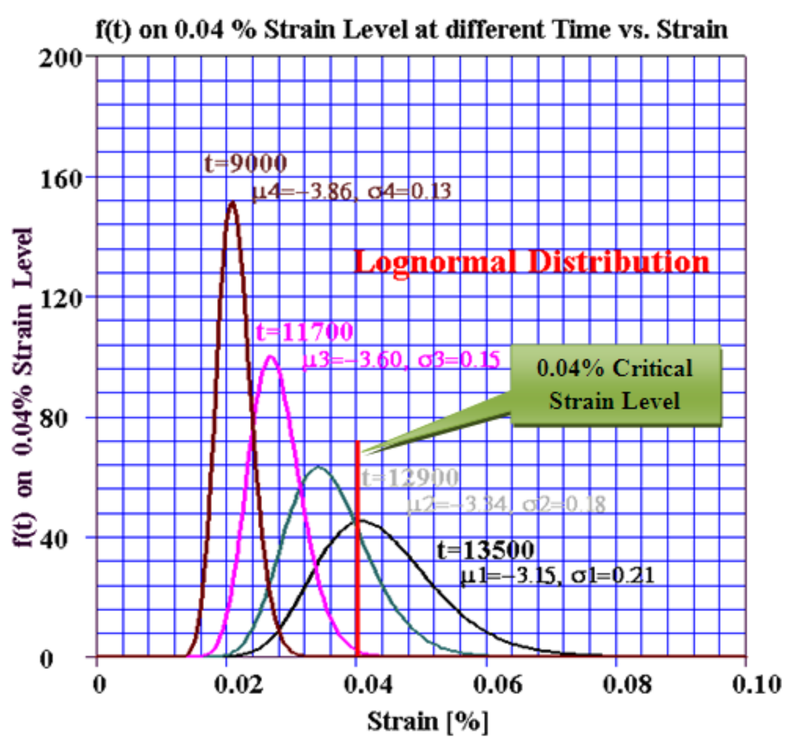

Figure 8. Lognormal pdfs calculated by EXCEL, and drawn by Weibull++ for 0.04 % strain level for X-70 carbon steel.

Table 3 shows the probability of exceedance (P_E) calculated according to

$$P_E = 1 - P(\varepsilon > 0.04) = 1 - \int_0^{\varepsilon=0.04} f(\varepsilon) d\varepsilon \quad (10)$$

at 0.04 strain level for different times.

Table 3. Probability and probability of exceedance on the 0.04 strain level at different times

Time [hrs]	P	P_E
13500	0.5434	0.4566
12900	0.9571	0.0429
11700	~1	4.5×10^{-8}
9000	1	0

According to the values given in Table 3, more than 40% degradation of X-70 carbon steel occurs before 13500 hrs. Therefore, the inspection time should be chosen between operation times t=11700 and t=12900 hrs.

Summary

A probabilistic creep model is proposed, and is completely verified and justified (100%) by the data extracted from experiments performed on Al 7075 and X70 dog bone shaped specimens. The statistical evaluation of the experimental data and nonlinear regression analysis by the MATLAB program is 100% done, (i.e., the MATLAB program is formulated and prepared). It should be mentioned that the proposed model was compared with other empirical models in previous PI reports.

5. Near Future Plans

1. It is planned to publish a review paper about the classification of creep models; the proposed creep model will be introduced in this paper.
2. It is planned to publish a paper about the experimental results for Al-7075-T6 and X-70 carbon steel based on the proposed probabilistic creep model.

6. Papers Published in Phase II or prepared for publishing by the team

1- M. Chookah, M. Nuhi, and M. Modarres, "Assessment of Integrity of Oil Pipelines Subject to Corrosion-Fatigue and Pitting Corrosion", presented by Prof. Modarres at the International Conference of Integrity- Reliability-Failure (IRF) in Porto, Portugal, July 20-24 2009**.** (The cost of the conference and associated travels was not covered by EERC)

2- Development of a Probabilistic Mechanistic Model for Reliability Assessment of Gas Cylinders in Compressed Natural Gas Vehicles, S. Chamberlain, M. Chookah, M. Modarres, Journal of Risk & Reliability, Vol. 233, pp 289-231(2009).

3- Reliability Analysis for Degradation Effects of Pitting Corrosion in Carbon Steel Pipes, M. Nuhi, T. Abu Seer, A. M. Al Tamimi, M. Modarres, A. Seibi, 11th International Conference on the Mechanical Behavior of Materials, Lake Como, Italy, June 5-9, 2011

4- A paper on "Reliability Analysis for Degradation Effects of Pitting Corrosion in Carbon Steel Pipes" is prepared and sent it to a conference in Italy. This paper was presented by PI members on ICM conference. This paper is published in Procedia Engineering 10, 1930–1935, 2011.

5- A Probabilistic Physics-of-Failure Model For Prognostic Health Monitoring of Piping Subject to Pitting and Corrosion-Fatigue, M. Chookah, M. Nuhi, and M. Modarres, Reliability Engineering & System Safety, Volume 96, Issue 12, December 2011, pp. 1601-1610.
6- A Probabilistic-Mechanistic Approach to Modeling Stress Corrosion Cracking Propagation in Alloy 600 Components With Applications, Gary Wu, Mohammad Modarres, Proceedings of the 11th International Probabilistic Safety Assessment and Management (PSAM) Conference & The Annual European Safety and Reliability Conference (ESREL), June 25-29, 2012, Helsinki, Finland.
7- A Critical Review of Creep Models, M. Nuhi, M. Modarres (In Manuscript under development)
8- A Creep Fatigue Model for Applications in the Petroleum Industry, M. Nuhi, M. Modarres (In Manuscript under development)

7. References

[1] ASME-B31G, Manual for Determining the Remaining Strength of Corroded Pipelines. A Supplement of ASME B31G Code for Pressure Piping, ASME, New York, 1995
[2] Kelvin- Voigt creep model, *cube.case.edu/EMAC403/EAMC403_Mechanical%20**Model**s.**pdf***
[3] Holmström, S., Auerkari, P., Holdsworth S. "Predicting creep strain response from rupture data and robust creep curve model", International Conference on Life Management and Maintenance for Power Plants. Helsinki-Stockholm-Helsinki, 12-14 June 2007. Vol. 1., 2007
[4] M. Evans, "Predicting times to low strain for a 1CrMoV rotor steel using a 6-theta projection technique", Journal of Materials Science, **35,** 2937 – 2948, 2000
[5] Garofalo, F. "Fundamental of creep and creep-rupture in metals", 16 (Macmillan), 1965
[6] Evans, R.W., and Wilshire, B.; "Creep of metals and alloys", Institute of Metals 1985
[7] Sawada, K. et.al."Analysis of long-term creep curves by constitutive equations". Material science and engineering A 510-511, 190-194, 2009
[8] Spiegelhalter, D., Thomas, A., Best, N., and Lunn, D., WinBUGS 1.4 Manual, 2003
[9] Azarkhail, M., and Modarres, M. "A Novel Bayesian Framework for Uncertainty Management in Physics-Based Reliability Models," *Proceedings of IMEC2007*, 2007 ASME International Mechanical Engineering Congress and Exposition, Seattle, Washington, USA, 2007
[10] Azarkhail, M., and Modarres, M. "Markov Chain Monte Carlo Simulation for Estimating Accelerated Life Model Parameters," *Annual Reliability and Maintainability Symposium (RAMS) Proceedings*, Orlando, FL, USA, 2007

Appendix

Two-Year Schedule

This project involves three distinct tasks. The first task is the development of the mechanistic models, development of a corresponding simulation tool to help both model development and field applications. The second task focuses on experimental activities to generate relevant data to validate the proposed models of Task 1. Finally, the third task involves the actual validation of the models proposed in Task 1 with the experimental results obtained in Task 2, including Bayesian estimation of the model parameters.

Task 1: Develop the best estimate mechanistic (physics of failure) empirical models for pitting corrosion, SCC, and fatigue-creep. The model development involves the following activities.

Task1.1: Gather, review and select most promising physics of failure based methods and algorithms proposed in the literature.

- Literature surveys for creep and stress corrosion cracking (SCC) degradation mechanisms are almost completed and will be classified for finding the relevant models (100% done).

Task1.2: Select, develop or adopt a detailed mechanistic model (one deterministic model for each phenomenon) that properly describes the degradation process.

- Development of the mechanistic models and of a corresponding simulation tool to help both model development and field applications after classifying the models and choosing the appropriate one should be done in the next future (100% complete).

Task 1.3: Develop a Monte-Carlo based mathematical simulation routine on MATLAB depicting the detailed mechanistic model of each degradation phenomenon (far faster than real-time).

- This part was completed for the empirical model developed based on the works of the PI interns for pitting corrosion. After proposing the similar models for SCC and creep-fatigue, it will be repeated (100% completed).

Task 1.4: Based on the results of the simulation a simplified empirical model that best describes the results of simulation will be proposed. Such a model relates the degradation (e.g., depth of the pit or the crack growth rate) to applied loads such as pipeline internal pressure and chemical composition of the product inside the pipeline, as a function of time or cycle of load application.

- This part is completed for the pitting corrosion and corrosion-fatigue (100% complete).

Task 2: A PoF reliability analysis laboratory has been designed and being developed at PI. The advanced corrosion-fatigue purchased by the PI that was installed at the University of Maryland (the Cortest Rig) has been sent to Cortest to ship to PI. (100% done).

Task 2.1: Completing the remaining corrosion-fatigue tests being conducted by Mr. Nuhi and Chookah. (100% Completed)

Task 2.2: Pitting Corrosion Experiments (develop test plan, prepare samples and the facility, perform the test, and evaluate the test results) (100% Completed).

Task 2.3 SCC Experiments (develop test plan, prepare samples and the facility, perform the test, and evaluate the test results). (Used results of experiments done by others, 100% Completed)
Task 2.4 Creep-Fatigue Experiments: The equipments and samples are completely ready (100% completed); the tests will be performed in future and the results will be evaluated.

- A small-scaled corrosion-fatigue (or creep) chamber has been designed (not as part of this project), made and tested for dog-bone and CT specimens and checked its workability on the UMD MTS machines using Aluminum alloy samples. Moreover, another chamber has been made for long dog boned specimens.
- A heating chamber has been designed and tested for creep experiments.
- New dial gauges with stand are prepared and tested for four and three points bending of SCC and pitting corrosion experiments.

Task 3: This task involves modification, advancement and use of the WinBUGs' Bayesian formalism for model validation using experimental data and integration of the field data and information including sensor-based data (acoustics and/or optical) to update the empirical models and estimate the remaining life of oil pipelines and structures. (100% Complete)

- The WinBUGs' Bayesian formalism for model estimation and validation was developed as part of M. Chookah's work. This formalism is being updated and new applications of the formalism have been performed using past experimental data and new data of corrosion and fatigue obtained since departure of Dr. Chookah. Further work with this software for integration the experimental data has already be done.

Task 4: Dissemination of Results
Two papers planned for submission to conferences and journals will be developed to report the results of Tasks 1-3. (50% Complete).

Schedule/Milestones/Deliverables

Tasks 1.1-1.3 (5/1/09-12/15/09); Task 1.4 (12/15/09-3/1/10); Task 2.1 (completed 7/1/09); Task2.2 (7/1/09-12/15/09); Task 2.3 (12/15/09 – 6/1/10); Task 2.4 (6/1/10-2/1/11); Task 3 (12/15/09-1/15/12), Task 4 (1/1/12-3/30/12).

The Cortest rig was boxed and shipped to the Cortest Corporation to test and send to **PI.**

The project is on schedules and there is no issue or delay at this point.

Dr. Seibi was appointed as a Co-Advisor of Mr. Nuhi.

Visits

- Dr. A.Seibi visited UMD in July 2009
- Dr. A.Seibi visited UMD in July 2010

- Two PI students Abdullah Al Tamimi, and Mohammad Abu Daghah took parts at summer internship (2009).
- A PI student Taher Abu Seer took parts at summer internship (2010).
- Prof. Modarres attended the 1st Annual PI Partner Schools Research Workshop. The Petroleum Institute, Abu Dhabi, U.A.E. January 6-7, 2010.